

**The effects of biological crowders on the structure, diffusion, and conformational dynamics  
of  $\alpha$ -synuclein**

By  
Sina Heravi

A thesis submitted to the School of Graduate Studies in partial fulfillment of the requirements for  
the degree of

**Master of Science**

In the  
Department of Biochemistry, Faculty of Science

Memorial University of Newfoundland

June 2023

St. John's, Newfoundland, Canada

## Abstract

$\alpha$ -synuclein is an intrinsically disordered protein (IDP) whose spontaneous aggregation in presynaptic neuronal cells is a pathological hallmark of Lewy body formation and Parkinson's disease. This aggregation process is likely affected by the crowded cellular environment. In this study,  $\alpha$ -synuclein was studied in the presence of a synthetic crowder, Ficoll70, and biological crowdiers composed of lysed cells that better mimic the biocomplexity of the cellular environment.  $^{15}\text{N}$ - $^1\text{H}$  HSQC NMR results from freshly prepared samples show similar  $\alpha$ -synuclein chemical shifts in non-crowded and all crowded conditions implying that its structure remains disordered in all conditions. Nevertheless, both HSQC NMR and fluorescence measurements indicate that, only in the cell lysate,  $\alpha$ -synuclein forms aggregates at timescales of 48 hours.  $^{15}\text{N}$ -edited diffusion measurements indicated that all crowdiers slow down the IDP diffusivity; however, at high concentrations,  $\alpha$ -synuclein diffuses faster in cell lysate than in Ficoll70, possibly due to additional soft (e.g. electrostatic or hydrophobic) interactions.  $^{15}\text{N}$ -edited relaxation measurements show that some residues are more mobile in cell lysate than in Ficoll70; the most strongly different rates are predominantly in hydrophobic residues. I thus examined cell lysates with reduced hydrophobicity and found higher relaxation rates (slower dynamics) in several  $\alpha$ -synuclein residues. Taken together, these experiments suggest that while cell lysate does not substantially affect  $\alpha$ -synuclein structure (HSQC spectra), it does affect chain dynamics (transverse relaxation rates) and translational motion (diffusion), and strongly affects aggregation over a timescale of days, in a manner that is different from either no crowder or an artificial crowder: soft hydrophobic interactions are implicated.

## **Acknowledgments**

I would like to express my sincere gratitude to my supervisor, Dr. Valerie Booth. Your invaluable guidance, knowledge, enthusiasm, and patience helped me throughout my research. I am so glad that I had such a remarkable mentor. Thanks for being so helpful in all aspects of my life.

I would also like to thank my co-supervisor, Dr. Anand Yethiraj. Your profound multidisciplinary knowledge and continuous support enriched my perspective on science. You are a great motivational mentor for my personal and scientific life. Thank you for everything.

Thank Dr. Jaeok Park, my supervisor committee, for all your advice and inspiration. Thanks to my former and current labmates, Drs. Sarika Kumari and Yanitza Trosel, whose friendship and scientific help made my master's journey much more enjoyable.

Lastly, I would like to thank my incredible parents and family, whose constant support always pushes me forward to reach my goals.

Thanks for choosing my M.Sc. thesis to read. I hope it will be helpful for your research.

# Table of Contents

Abstract.....	I
Acknowledgements.....	II
Table of Contents.....	III
List of tables.....	VII
List of Figures.....	VIII
List of Abbreviations.....	XI
1. Introduction	
1.1. Intrinsically Disordered Protein (IDP) .....	1
1.1.1. A brief history of the discovery of disordered protein.....	1
1.1.2. Characteristics of IDPs.....	3
1.1.3. IDPs in cell function and diseases.....	4
1.2. $\alpha$ -synuclein.....	6
1.2.1. Characteristics of $\alpha$ -synuclein.....	8
1.2.2. Functions of $\alpha$ -synuclein.....	11
1.3. Macromolecular crowding.....	12
1.3.1. Macromolecular crowding in biological environment.....	12
1.3.2. Macromolecular crowding effects on proteins.....	14
1.3.3. Ficoll and Bacterial cell lysate.....	16
1.4. Aggregation of protein.....	18
1.4.1. How does a protein aggregate?.....	18

1.4.2.	Aggregation of $\alpha$ -synuclein.....	19
1.4.3.	Aggregation of $\alpha$ -synuclein in crowded conditions .....	22
1.5.	Nuclear Magnetic Resonance spectroscopy (NMR) .....	23
1.5.1.	Heteronuclear Single Quantum Correlation (HSQC) .....	23
1.5.2.	Diffusion NMR.....	25
1.5.3.	Relaxation NMR.....	27
1.6.	Hypothesis and objectives.....	29
1.6.1.	Hypothesis.....	29
1.6.2.	Objectives.....	29
2.0	Materials and methods	
2.1.	Vector design.....	30
2.2.	Transformation.....	32
2.3.	Expression of $\alpha$ -synuclein.....	33
2.4.	Purification and preparation of $\alpha$ -synuclein.....	37
2.5.	Preparation of Ficoll70 .....	41
2.6.	Preparation of bacterial cell lysate .....	42
2.7.	Preparation of less hydrophobic bacterial cell lysate.....	43
2.8.	Hydrophobicity measurement of bacterial cell lysate.....	44
2.8.2	Weight.....	44
2.8.2	Bligh and Dyer.....	45
2.8.3	Dynamic light scattering.....	46
2.9.	NMR spectroscopy.....	46
2.9.1	1D $^1\text{H}$ .....	47

2.9.2	1D $^1\text{H}$ with water suppression.....	47
2.9.3	2D $^{15}\text{N}^1\text{H}$ HSQC.....	48
2.9.4	2D $^1\text{H}$ DOSY.....	49
2.9.5	Pseudo 2D $^{15}\text{N}^1\text{H}$ HSQC-DOSY.....	50
2.9.6	Pseudo 2D $^{15}\text{N}^1\text{H}$ HSQC- $T_2$ .....	52
2.10 Microscopy		
2.10.1	Confocal fluorescence microscopy.....	53
2.10.2	Scanning electron microscopy.....	54
3.0 Results		
3.1	$^{15}\text{N}$ $\alpha$ -synuclein expression and purification.....	55
3.2	Manipulating the hydrophobicity of the cell lysate and ultracentrifuged cell lysate..	60
3.3	Structure of $\alpha$ -synuclein with and without crowder.....	65
3.4	$^{15}\text{N}$ - $^1\text{H}$ Diffusion of $\alpha$ -synuclein.....	73
3.5	$\alpha$ -synuclein $^{15}\text{N}$ - $^1\text{H}$ HSQC spectrum peak assignment.....	76
3.6	$\alpha$ -synuclein $^{15}\text{N}$ - $^1\text{H}$ $R_2$ relaxation in the absence and presence of Ficoll70 and bacterial cell lysate.....	78
3.7	$\alpha$ -synuclein structure and $^{15}\text{N}$ - $^1\text{H}$ $R_2$ relaxation in the absence and presence of less hydrophobic cell lysate.....	83
3.8	$\alpha$ -synuclein structure in the absence and presence of ultracentrifuged less hydrophobic cell lysate.....	84
4.0 Discussion		
4.1	Structure of $\alpha$ -synuclein in the absence and presence of macromolecular crowding.....	86

4.2 Diffusion of $\alpha$ -synuclein in the absence and presence of macromolecular crowding.....	90
4.3 Backbone internal dynamics of $\alpha$ -synuclein in the absence and presence of macromolecular crowding.....	93
5.0 Conclusion.....	96
Future directions.....	98
Bibliography.....	99
Appendix I: Supplemental information.....	121
Appendix II: BioRender publication license.....	125

# List of Tables

Table 2.1) The directory of Bradford Assay.

Table 2.2)  $^1\text{H}$  DOSY gradient strengths with sinusoidal gradient pulses.

Table 2.3)  $^{15}\text{N}$ - $^1\text{H}$  HSQC-DOSY gradient strength.

Table 3.1) Comparing the characteristics of the unmanipulated bacterial cell lysate and ultracentrifuged bacterial cell lysate before and after the HIC column.

Table 3.2) Quantification of peaks chemical shift in  $^{15}\text{N}$ - $^1\text{H}$  HSQC spectra of  $\alpha$ -synuclein in the absence presence of Ficoll70 and bacterial cell lysate.

Table 3.3) The diffusion coefficient of 0.2 mM  $\alpha$ -synuclein in the absence and presence of crowders.

Table 3.4) Average of  $R_2$  values in different regions of  $\alpha$ -synuclein in the Ficoll70 and Bacterial Cell Lysate.

Table 3.5)  $\alpha$ -synuclein's residues with different  $R_2$  values in the presence of crowders.

Table S1) Characteristics of  $\alpha$ -synuclein sequence.

# List of Figures

Figure 1.1)  $\alpha$ -synuclein's aggregations potentially lead to Lewy bodies in neuron cells, which disrupt dopamine release.

Figure 1.2)  $\alpha$ -synuclein's structure.

Figure 1.3) Macromolecular crowding in the cell lysate and Ficoll.

Figure 1.4)  $\alpha$ -synuclein's aggregation pathways.

Figure 1.5)  $^{15}\text{N}$ - $^1\text{H}$ -HSQC spectrum of  $\alpha$ -synuclein.

Figure 1.6) Diffusion NMR experiment: Attenuated  $^1\text{H}$  signal decay versus gradient strength.

Figure 2.1) Expressed protein construct, and the amino acids sequence of His-tag, GB-, and  $\alpha$ -synuclein.

Figure 2.2) pET-21 vector used for expression of the  $\alpha$ -synuclein fusion protein.

Figure 2.3) Recombinant  $^{15}\text{N}$   $\alpha$ -synuclein expression and purification.

Figure 2.4) Preparation of less hydrophobic bacterial cell lysate.

Figure 3.1) Gel electrophoresis showing  $\alpha$ -synuclein's purification.

Figure 3.2) The Bradford standard curve of BSA.

Figure 3.3) The size distribution of macromolecules in the bacterial cell lysate crowder.

Figure 3.4)  $^{15}\text{N}$ - $^1\text{H}$  HSQC spectra of  $\alpha$ -synuclein in the absence and presence Ficoll70 and bacterial cell lysate.

Figure 3.5) Confocal microscopy of  $\alpha$ -synuclein and ThT fluorescence.

Figure 3.6) Scanning electron microscopy of 0.2 mM  $\alpha$ -synuclein.

Figure 3.7)  $^{15}\text{N}$ - $^1\text{H}$  HSQC spectra of 0.2 mM  $\alpha$ -synuclein in the presence of unmanipulated cell lysate and less hydrophobic cell lysate.

Figure 3.8) Translational diffusion of  $\alpha$ -synuclein in absence and presence of unmanipulated bacterial cell lysate and Ficoll70.

Figure 3.9) Assigned residues of  $^{15}\text{N}$ - $^1\text{H}$  HSQC spectrum of 0.2 mM  $\alpha$ -synuclein.

Figure 3.10)  $T_2$  decay of  $\alpha$ -synuclein's residues.

Figure 3.11)  $^{15}\text{N}$ - $^1\text{H}$  HSQC transverse relaxation rate ( $R_2$ ) of 0.2 mM  $\alpha$ -synuclein.

Figure 3.12)  $^{15}\text{N}$ - $^1\text{H}$  HSQC spectra of 0.2 mM  $\alpha$ -synuclein in the absence and presence of less hydrophobic ultracentrifuged cell lysate.

Figure S1)  $1\text{D}^1\text{H}$  with water suppression spectrum of  $\alpha$ -synuclein on NMR 600 MHz.

Figure S2)  $1\text{D}^1\text{H}$  with water suppression spectrum of  $\alpha$ -synuclein in the cell lysate.

Figure S3)  $1\text{D}^1\text{H}$  with water suppression spectrum of  $\alpha$ -synuclein in Ficoll70.

Figure S4) Publication permission for Figure 1.1.

Figure S5) Publication permission for Figure 1.2.

Figure S6) Publication permission for Figure 1.3.

Figure S7) Publication permission for Figure 1.4.

# List of Abbreviations

IDP	Intrinsically Disordered Protein
IDPR	Intrinsically Disordered Protein Region
$^{15}\text{N}$	Nitrogen-15
$^1\text{H}$	Proton
NMR	Nuclear Magnetic Resonance
TBS	Tris Buffered Saline
EDTA	Ethylenediaminetetraacetic acid
MITF	Microphthalmia-Associated Transcription Factor
PD	Parkinson's Disease
NAC	Non-Amyloid Component
A $\beta$	Amyloid-Beta
PTM	Post Translation Modification
DNA	Deoxyribonucleic Acid
RNA	Ribonucleic Acid
PEG	Polyethylene Glycol
BSA	Bovine Serum Albumin
HSQC	Heteronuclear Single Quantum Coherence
DOSY	Diffusion Ordered Spectroscopy
CSA	Chemical Shift Anisotropy
T <sub>1</sub>	Longitudinal Relaxation Time

## List of Abbreviations

---

R <sub>1</sub>	Longitudinal Relaxation Rate
T <sub>2</sub>	Transverse Relaxation Time
R <sub>2</sub>	Transverse Relaxation Rate
IPTG	Isopropyl β D Thiogalactoside
IMAC	Immobilized Metal Affinity Chromatography
TEV	Tobacco Etch Virus
GB-1	Guanine Nucleotide-Binding Protein Subunit Beta
LB	Lysogeny Broth
DLS	Dynamic Light Scattering
TXI	Triple X Inverse
DSS	Sodium 2,2-Dimethyl-2Silapentane-5-Sulfonate
TD	Time Domain
NS	Number of Scan
HIC	Hydrophobic Interaction Chromatography
ThT	Thioflavin T
SEM	Scanning Electron Microscopy
SSP	Secondary Structure Propensity
FID	Free Induction Decay
PVP	Polyvinylpyrrolidone

# 1 Introduction

## 1.1 Intrinsically Disordered Protein (IDP)

### 1.1.1 A brief history of the discovery of disordered proteins

In the 20th century, it was thought that proteins could be functional only if they had a well-ordered 3D structure. However, further protein studies have changed this point of view and showed that there are other critical functional proteins than just well-ordered ones. The concept of the protein's function based on its 3D structure started in 1894 when Emil Fischer proposed the lock-and-key theory or the structure-function paradigm (Fischer 1894). He suggested that the lock-and-key behavior is crucial for the function of the protein (Fischer 1894; Lemieux and Spohr 1994). In 1936, Mirsky and Pauling supported the idea when they found out that the pepsin activity is dependent on the native form of the protein and denatured protein loses its enzyme activity (Mirsky and Pauling 1936). However, Hsien Wu proposed later that ordered structure plays an important role in protein function, but probably for the first time did not accept the lock-and-key proposal (Edsall 1953; Wu 1995).

In 1950 Karush brought up the configurational adaptability proposal. He realized that albumin's binding site takes different configurations with slow rates of conversion between structures upon binding typically to hydrophobic and anionic molecules (Karush 1950). Koshland

also supported this configurational adaptability, but by a different name of “induced fit.” He suggested that the protein synthesis process needs some kind of conformational flexibility to accommodate various shapes of the side chains in the growing chain (Koshland 1958). These two are the first proposals about protein production depending on conformational changes. After introducing the conformational flexibility, many mechanisms could be explained, such as reversible oxygen and carbon dioxide binding to hemoglobin, which needs hemoglobin structural shifts to absorb the gases, transfer, and release them (Dunker et al. 2001).

The above history of the controversy about the function and structure of the protein was mainly focused on ordered proteins and their various conformations. However, about 40 years ago, scientists found some protein fragments that produced no electron density when they used x-ray crystallography, even though they were functioning well. They realized the missing electron density was from atoms that were invisible due to their failure to scatter the X-ray coherently. The incoherent scattering was due to variation in the atoms’ position from one protein copy to another (Bloomer et al. 1978; Bode, Schwager, and Huber 1978). The concept of intrinsically disordered proteins (IDPs) probably tracks back to this work on incoherent scattering. In 1978, NMR along with X-ray crystallography, uncovered that the histone H5 tail is disordered, but still functional (Aviles et al. 1978). Thereafter, NMR played an important role in characterizing disordered proteins (Wright and Dyson 1999). Since then, an explosion of analogous studies combined to come up with the disorder-function paradigm. The disorder-function paradigm, unlike the first mentioned structure-function paradigm, states that proteins can play pivotal roles in cellular functions without stable 3D structure (Pinet, Assrir, and van Heijenoort 2021). In the following, I will explain in more depth the characteristics and functions of IDPs.

### 1.1.2 Characteristics of IDPs

Intrinsically disordered proteins and intrinsically disordered protein regions (IDPRs) rule out proteins' structure-independent function since they play critical role in cellular mechanisms. Research has revealed that IDPs are present in all living organisms, and their abundance increases with genome complexity. For example, there are more IDPs in eukaryotes than in prokaryotes (Peng et al. 2014; Uversky 2010; Ward et al. 2004; Xue, Dunker, and Uversky 2012). Around 33%, 4.2%, and 2% of eukaryotic, prokaryotic, and archaean proteins have at least one IDPR, respectively (Ward et al. 2004).

The term “intrinsically disordered protein” describes proteins with unfolded, disordered, unstructured, and non-globular structure conformations at the secondary or tertiary structural level (Dunker et al. 2001; Tompa 2003; Uversky, Gillespie, and Fink 2000; Wang et al. 2010). It can also be defined as a form of a protein that interconverts between different structures on a fast time scale (Trivedi and Nagarajaram 2022). Most proteins in the Protein Data Bank (PDB) have some kind of disorder (Oldfield et al. 2005; Uversky 2010, 2019; Xue, Dunker, and Uversky 2012). In many cases IDPs/IDPRs become more ordered upon binding to small ligands or large biomolecules, post-translational modifications, or macromolecular crowding (Oldfield and Dunker 2014).

The primary reason for the propensity of a protein to either fold or remain disordered is based on its amino acid composition. Sequence determines 3D structure; however, overall composition of IDPs/IDPRs is more determinant in their 3D structure than their sequence. Protein

segments with residues including Ala, Arg, Gly, Gln, Glu, Lys, Pro, and Ser are more common in disordered proteins. However, Asn, Cys, Ile, Leu, Phe, Val, Trp, and Tyr were more abundant in ordered and folded proteins (Dunker et al. 2001; Radivojac et al. 2007; Romero et al. 2001; Williams et al. 2001). Strong repulsive forces or lack of attraction due to loss of driving forces for compaction may keep the protein unfolded (Dunker et al. 2001; Nelson 2008). Loss of driving forces can occur due to high hydrophobicity or a high net charge. However, IDPs mostly contain uncharged, polar, and less hydrophobic amino acids. The degree of structure varies based on their foldability potency or whether the whole protein is disordered or if there is a smaller region of disorder (Crick et al. 2006; Walter and Murphy 2009).

The second reason for the propensity of a protein to fold or not is its interactions with other biomolecules. Proteins undergo a range of unfolded to folded conformational exchanges upon reaction with macromolecules (Trivedi and Nagarajaram 2022). Therefore, interaction with other macromolecules inside cells can also determine whether the protein is ordered or disordered. I will delve into this more in section 1.3.2.

### **1.1.3 IDPs in cell function and diseases**

IDPs can interact with other cell components with more freedom (multiple binding partners) due to their lack of 3D and stable structure. This enables them to conduct many biological processes, including cell signalling and regulation (Dunker et al. 2001). IDP functions are categorized into eight classes: entropic chains, modification sites, disordered chaperones,

molecular effectors, molecular recognition assemblers, molecular recognition scavengers, metal sponges, and unknown (Sickmeier et al. 2007).

IDPs, like ordered proteins, can lose their normal function and cause diseases. There are many examples of the dysfunction of IDPs causing serious health problems. For example, P53,  $\alpha$ -synuclein, Mdm2, PTEN, c-Myc, AF4, BRCA1, EWS, Bcl-2, C-Fos, nupr1, and HPV oncoproteins have important roles in many diseases, including diabetes, cancer, neurodegenerative diseases, amyloidosis, and cardiovascular diseases (Chang et al. 1997; Langella et al. 2021; Lee et al. 2000; Uversky, Oldfield, and Dunker 2008). In the last two decades, many studies focused on the mechanism, behavior, and characteristics of IDPs in diseases. Many IDPs act as tumor suppressors; for example, p53 regulates cell cycling and nupr1 acts as a transcriptional regulator, and their dysfunction may subsequently lead to cancer or tumor growth. Microphthalmia-associated transcription factor (MITF) is another IDP that has a major role in gene expression regulation, and its dysfunction can bring about melanoma (Chen and Kriwacki 2018; Kulkarni and Uversky 2019).  $\alpha$ -synuclein normally regulates the neuronal signalling and regulation, and its abnormality may cause neurodegenerative diseases (Mehra, Sahay, and Maji 2019). The focus of this study is on  $\alpha$ -synuclein and how its behavior would differ in various conditions, which will be discussed in the following sections.

## 1.2 $\alpha$ -synuclein

$\alpha$ -synuclein is an intrinsically disordered protein and is expressed throughout the brain in presynaptic neuronal cells (Iwai et al. 1995). It has a leading role in vesicle formation and

neurotransmitter release and regulation (Iwai et al. 1995).  $\alpha$ -synuclein can spontaneously aggregate inside cells, which has a pivotal role in the formation of amyloid fibrils and Lewy Bodies. The deposition of Lewy bodies in neuronal cells disrupts the normal regulation of neurotransmitter (mainly dopamine) release and causes Parkinson's disease (PD) (Figure 1.1) (Mehra, Sahay, and Maji 2019). PD is the second most common neurodegenerative disorder and most common movement disorder (Tysnes and Storstein 2017).

$\alpha$ -synuclein was originally discovered while using an antibody against cholinergic vesicles from *Torpedo* electric organ (*Torpedo californica*). This was the first evidence of its role in presynaptic cells (Maroteaux, Campanelli, and Scheller 1988). They found three proteins with different molecular weights (17.5, 18.5, and 20 kDa), but the 17.5 kDa protein was the most abundant one. Researchers extracted this protein from *Torpedo* and rats, and they found seven series of conserved amino acids repeats. The presence of these conserved sequences in different species might explain their functions (Maroteaux, Campanelli, and Scheller 1988). Later in 1990, researchers extracted a 14 kDa protein from a bovine brain. They stated that this protein that exists in humans and rats is mostly located in nerve cells, and is analogous to the proteins explored in *Torpedo* (Nakajo et al. 1990, 1993). Subsequent studies confirmed its nuclear and synaptic role, so it was called "synuclein" (Clayton and George 1998; Maroteaux, Campanelli, and Scheller 1988). The involvement of synucleins in diseases was identified when non-A $\beta$  components in senile plaques were studied in Alzheimer's disease (Ueda et al. 1993). They realized that the protein in senile plaques is homologous to human, rat and *Torpedo* synuclein, which we know it as  $\alpha$ -synuclein today (Jakes, Spillantini, and Goedert 1994; Maroteaux, Campanelli, and Scheller

1988; Maroteaux and Scheller 1991). Thereafter many researchers focused on this protein to discover its role in neurodegenerative diseases.

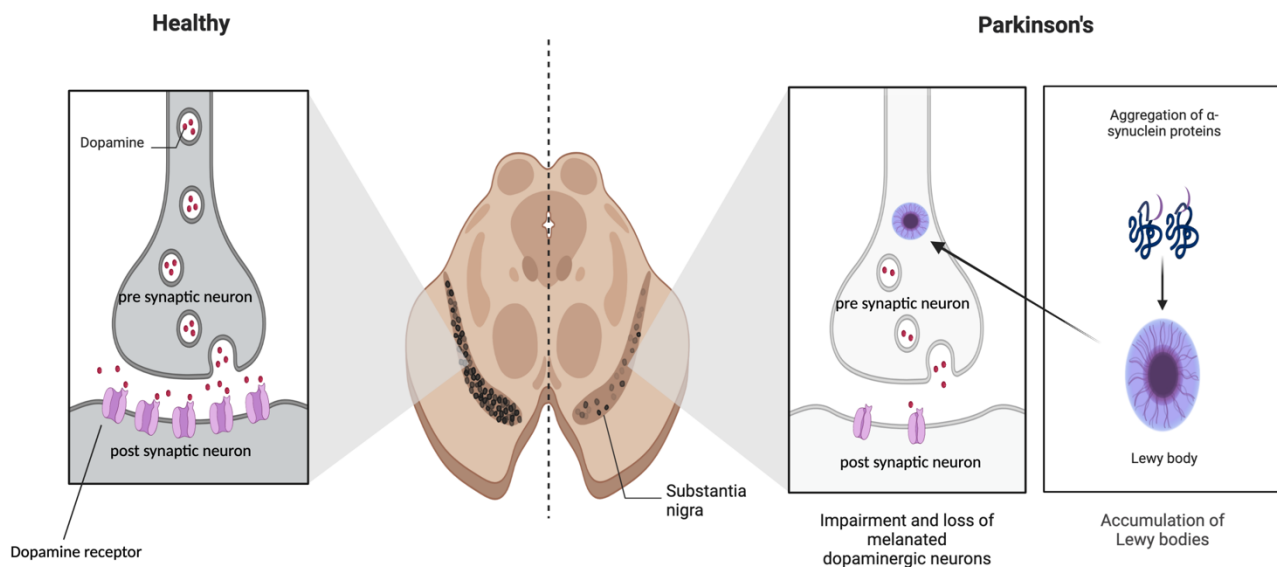


Figure 1.1)  $\alpha$ -synuclein's aggregations potentially lead to Lewy bodies in neuron cells, which disrupt dopamine release. Adapted from "Progression of Parkinson's Disease in the Substantia Nigra", by BioRender.com (2023). Retrieved from [https://app.biorender.com/biorender-templates\(Figure S4\)](https://app.biorender.com/biorender-templates(Figure S4))

### 1.2.1 Characteristics of $\alpha$ -synuclein

$\alpha$ -Synuclein consists of 140 amino acids (14kDa) and is composed of three main regions in its structure: the N terminal, the non-A $\beta$  component (NAC), and the C terminal regions. The N terminal region (residues 1-60) has an overall positive charge and seven repeated hexamer motifs of KTKEGV. This repeated motif induces stable amphipathic  $\alpha$ -helical structure when it binds to

the lipid in the cell membrane (Clayton and George 1998; George et al. 1995). The NAC region, which derived the name from its initial characterization in Alzheimer disease, is made of a hydrophobic sequence (residues 61-95) that can take on a random coil or  $\beta$ -sheet configuration depending on the aggregation progress (Ueda et al. 1993; Uversky et al. 2007). The C terminal region (residues 96-140) is highly negatively charged and enriched in prolines and entirely disordered. It contributes to function by interacting with proteins inside the cell (Chandra et al. 2003a).

As  $\alpha$ -synuclein is intrinsically disordered, it does not have a stable structure, and it interchanges between different conformations. Studies postulate that  $\alpha$ -synuclein when is in contact with a cell membrane in intact cells exists as a tetramer and adopts an  $\alpha$ -helical structure in its N terminal and NAC regions (Bartels, Choi, and Selkoe 2011; Wang et al. 2011). However, it is still unclear whether the native form of  $\alpha$ -synuclein is tetramer or not (Dettmer et al. 2013; Roberts, Wade-Martins, and Alegre-Abarrategui 2015). Non-denaturing  $\alpha$ -synuclein purification from mammalian cells at the native level of expression resulted in the tetrameric (non-water soluble) form of the protein, but purified protein from bacterial cells was observed in monomeric disordered states (water soluble) (Villar-Piqué, Lopes da Fonseca, and Outeiro 2016). Later, studies showed that adding micelles to  $\alpha$ -synuclein, as well as its N terminal acetylation, can induce the formation of stable tetramers of  $\alpha$ -synuclein (Meade, Fairlie, and Mason 2019). It was suggested that the hydrophobic core and hydrophilic exterior of  $\alpha$ -synuclein tetramer make it stable (Meade, Fairlie, and Mason 2019; Wang et al. 2011).

There are two states of  $\alpha$ -synuclein in neurons: the soluble state and the membrane-bound state. The secondary structure of  $\alpha$ -synuclein is dependent on its state (Chandra et al. 2003; Fauvet, Mbefo, et al. 2012; Kim 1997; Weinreb et al. 1996). The soluble cytosolic  $\alpha$ -synuclein is entirely disordered and unfolded. However, the membrane-bound state becomes more compact by changing the disordered N terminal region to a single elongated helical structure or two  $\alpha$ -helices based on the membrane curvature (Figure 1.2) (Chandra et al. 2003; Davidson et al. 1998; Dettmer et al. 2013; Fauvet et al. 2012; Fortin et al. 2004; Kim 1997; Nuscher et al. 2004; Roberts, Wade-Martins, and Alegre-Abarategui 2015; Weinreb et al. 1996). Lower membrane curvature promotes an elongated  $\alpha$ -helical structure (Burré, Sharma, and Südhof 2018; Bussell and Eliezer 2003), and interaction with highly curved membranes induces two smaller helices (Chandra et al. 2003b; Georgieva et al. 2008). In the normal physiological condition, when  $\alpha$ -synuclein binds to synaptic vesicles with small and highly curved membranes, it exhibits two helices (Davidson et al. 1998).

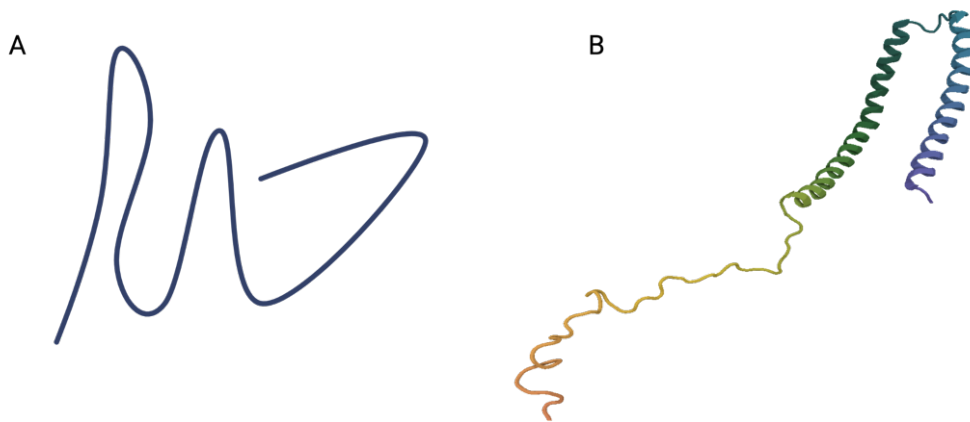


Figure 1.2)  $\alpha$ -synuclein's structure. A. Soluble or cytosolic state: the whole protein is disordered; B. Micelle-bound state: with  $\alpha$ -helix in the N terminal and NAC regions (PDB ID: 1XQ8)(Ulmer et al. 2005). Created with BioRender.com (Figure S5).

$\alpha$ -Synuclein undergoes multiple post translational modifications (PTMs), mostly in the C-terminal region, including phosphorylation, oxidation, acetylation, ubiquitination, glycation, glycosylation, nitration, and proteolysis. These lead to different conformations (e.g. the secondary structure changes) and modifications in the properties of the protein (Burré, Sharma, and Südhof 2018).

$\alpha$ -Synuclein has been suggested to be degraded by several pathways, including ubiquitin proteasome, autophagy-lysosome, and extracellular metalloproteases, which help keep its concentration under control (Burré, Sharma, and Südhof 2018). The normal level of  $\alpha$ -synuclein inside cells can participate in many cell signalling pathways, and its dysregulation can turn down the pathways (Burré, Sharma, and Südhof 2018).

### 1.2.2 Functions of $\alpha$ -synuclein

$\alpha$ -synuclein's functions still are not clear and are under investigation (Sulzer and Edwards 2019). However, the main known features of  $\alpha$ -synuclein are as follows.  $\alpha$ -synuclein regulates function in the pre-synaptic terminal, including neurotransmitter release (Maroteaux, Campanelli, and Scheller 1988). Also,  $\alpha$ -synuclein carries out several cellular functions by interacting with other proteins as well as negatively charged phospholipids. However, the physiological consequences of most of these interactions still are unclear.  $\alpha$ -synuclein can bind and inhibit phospholipase D in lipid transport, packing, and membrane biogenesis (Jenco et al. 1998), regulate small GTP-binding protein rab3 interactions with membranes, regulate tyrosine hydroxylase (Lou et al. 2010), and bind to the SNARE-protein synaptobrevin-2 to facilitate synaptic exocytosis and induce SNARE-complex assembly via the N terminal of the protein (Burré et al. 2010). It also can bind to synphilin and regulate dopamine release (Masliah et al. 2000), microtubule synthesis (Lee et al. 2006), and tau phosphorylation (Jensen et al. 1999).

$\alpha$ -synuclein also acts in the nucleus, but its role is yet unclear. Familial mutations, oxidative stress, and PTMs can localize more  $\alpha$ -synuclein in the nucleus (Kontopoulos, Parvin, and Feany 2006; Schell et al. 2009; Xu et al. 2006). It has been suggested that  $\alpha$ -synuclein influences transcription by either interacting with DNA or transcription factors (Villar-Piqué, Lopes da Fonseca, and Outeiro 2016). It has been shown that  $\alpha$ -synuclein interacts with histones via acetylation-deacetylation cycles (Kontopoulos, Parvin, and Feany 2006; Liu et al. 2011).

All these observations point to the importance of  $\alpha$ -synuclein and of understanding its behavior. Understanding what causes  $\alpha$ -synuclein's dysfunction is a crucial issue that still is under investigation and needs further studies. As mentioned before, macromolecular crowding is an environmental factor that can impact  $\alpha$ -synuclein aggregation and dysfunction. In the following, I will explain why we study the behavior of  $\alpha$ -synuclein in crowded conditions.

### **1.3 Macromolecular crowding**

Macromolecular crowding refers to a high concentration of macromolecules in a solution which restricts the amount of water and affects many aspects of biochemistry (Rivas and Minton 2016).

#### **1.3.1 Macromolecular crowding in biological environment**

The intracellular environment likely has a high concentration of biomolecules that acts as macromolecular crowders either through a high concentration of a single macromolecule such as hemoglobin in red blood cells or through a variety of macromolecules in most cells (Zimmerman and Minton 1993). The total concentration of cellular macromolecules is between 80-400 g/L, including nucleic acids, proteins, carbohydrate, lipids and other biopolymers (Munishkina, Fink, and Uversky 2008; Zimmerman and Trach 1991), and the intracellular crowding occupies 5%-40% of cytoplasmic volume (Gershon, Portert, and Trust 1985; Zimmerman and Trach 1991). Macromolecular crowding enhances non-specific interactions, such as hydrophobic, electrostatic, Van der Waals, and hydrogen bonds termed "soft interactions," between biomacromolecules and

might affect the structure and properties of the molecules. Therefore, studying the biomolecules under crowding conditions would clarify their complex behavior in the intracellular environment. The ideal condition for studying the weakly non-specific interactions is when the interactions are identical, and we know what type of interactions is happening between molecules such as between water and solute. However, the cellular environment is far from the ideal condition, and its heterogeneous crowded environment makes the study complex. In the cellular milieu, solutes interact with water and also with other cosolutes. For example, a protein inside a cell can interact with other proteins, as well as a variety of other biomolecules (Sarkar, Li, and Pielak 2013). Therefore, it might be a challenge to study protein interactions with crowders in an intracellular milieu.

A fundamental aspect of macromolecular crowding is volume exclusion (Smith et al. 2015). The excluded-volume or hard interaction phenomenon refers to the concept that two molecules cannot occupy the same space, and each of them excludes the other one from its environment (Ralston 1990). By increasing the concentration of particles in the solution, the available space is progressively limited, and molecules or macromolecules are more restricted to the part of the space from which they occupy (Ralston 1990). As a result, volume exclusion substantially decreases the entropy of a group of particles by decreasing the space they can occupy (Ralston 1990). Therefore, excluded volume can affect the kinetic and thermodynamic effects of biochemical reactions in cells as it restricts the available space for the reactions (Ellis 2001; Minton 2000). For instance, crowding effects of PEG stabilize double stranded DNA. Also, the size and shape of the crowding agents can define the extent of excluded volume (Minton 2005).

### 1.3.2 Macromolecular crowding effects on protein

Understanding the impact of molecular crowding on IDPs is important in fundamental research and has the potential to aid in the better management of misfolding diseases. Macromolecular crowding may impact various biological processes and chemical reaction rates, including protein folding, enzymatic activity, and the strength of macromolecule interactions like protein-protein or RNA-protein interactions (Minton 2000). Consideration of macromolecular crowding helps to understand protein interaction roles in cellular mechanisms, mutations, and maintaining homeostasis (Cong et al. 2019). As mentioned, macromolecular crowding also plays a major role in protein aggregation in many neurodegenerative diseases (Sahni et al. 2015).

Macromolecular crowding is able to change the excluded volume of the whole system by either changing the hydrodynamic radius of a protein or changing its oligomerization or aggregation/fibrilization states (Kuznetsova, Turoverov, and Uversky 2014). In other words, macromolecular crowding tends to stabilize proteins by compacting the unfolded state. However, the idea of protein stabilization in the presence of crowders is still under investigation, and many studies focus on it. For example, it has been shown that macromolecular crowding pushes the equilibrium towards the folded state of cytochrome-c (Sasahara, McPhie, and Minton 2003). Also, lysozyme refolding rate can be increased 5-fold in the presence of macromolecular crowding compared to in the dilute condition (Van Den Berg et al. 2000). On the other hand, it has been shown that crowding does not affect the folding of oxidized lysozyme or aggregation of the reduced lysozyme (Van Den Berg, Ellis, and Dobson 1999).

Macromolecular crowding can increase the protein propensity to either aggregate or fold. In other words, there is always a competition between the folding and aggregation of the protein; however, the presence of macromolecular crowding can take the competition to the next level and make the aggregation faster (Zhou et al. 2009). Since IDPs do not fold, in the presence of crowding, aggregation often is dominant than folding (Dhar et al. 2010; Kinjo and Takada 2003; Munishkina, Fink, and Uversky 2008). Therefore, more aggregation is seen in IDPs in the presence of crowding.

Studies suggested that interactions between the crowders and proteins can dramatically affect more dynamic proteins such as IDPs and molten globule form of proteins (Uversky 2013). IDP's malleability might make them more prone to be affected in crowded conditions. Also, IDPs can interact non-specifically with the crowders, which might impact their conformational ensembles (Kuznetsova, Turoverov, and Uversky 2014; Miklos et al. 2011; Senske et al. 2014). Studies so far have focused on the steric repulsion effects of crowders and how they can alter the thermodynamics and kinetics of IDP binding (Kuznetsova, Turoverov, and Uversky 2014; Miklos et al. 2011; Senske et al. 2014; Zhou, Rivas, and Minton 2008). Recently, studies, including my thesis, have also probed on the effects of weak or soft interactions between crowders and IDPs (Banks et al. 2018; Breydo et al. 2015).

Research on the impact of crowding on IDPs has traditionally been carried out with *in vitro* or *in vivo* crowded conditions. Crowded conditions have often been emulated by adding artificial crowders such as polyethylene glycol (PEG), Dextran, or Ficoll (Bai et al. 2017; Wang et al. 2012). Also, biological crowders have been used, such as proteins like Bovine Serum Albumin (BSA), to mimic the complexity of the cellular environment, but adding a single protein certainly does not

mimic the full complexity of crowding in real cells with many sizes, shapes, and charges of crowders. The development of techniques in studying proteins enabled researchers to study proteins in living cells such as mammalian cells, *E.coli* or *Xenopus laevis* oocytes (Hubbard et al. 2003; McCully, Beck, and Daggett 2012; Predeus et al. 2012; Sakai et al. 2006; Selenko et al. 2006; Serber, Keatinge-Clay, et al. 2001; Serber, Ledwidge, et al. 2001; Serber and Dtsch 2001; Waudby et al. 2013). However, the downside of in-cell studies is we cannot simply manipulate the crowding environment, and that makes it much harder to tease out what the important interactions, e.g. soft interactions, in driving a process are. I will discuss this more in the next section by explaining the two types of crowders I used in my research. The effects of crowders on  $\alpha$ -synuclein will be explained in the section 1.4.3.

### 1.3.3 Ficoll and Bacterial Cell Lysate

In this study, I decided to use bacterial cell lysate as a biological crowder and Ficoll as a synthetic crowder. The reason for the two types of crowders is to compare the effects of crowders on  $\alpha$ -synuclein under different crowding conditions, for example, in the presence or absence of soft interactions. In the following, I will define my reasons for choosing these two crowders.

Ficoll (Figure 1.3) is an inert highly branched cross-linked polysucrose, a copolymer of sucrose and epichlorohydrin (Minton 2005; Ranganathan et al. 2022). Ficoll is a homogeneous crowder in terms of size and provides a simple means to study the impact of crowding on protein-protein interactions (Ranganathan et al. 2022). Earlier studies used Ficoll 70 or 400 kDa to study the impact of crowding on protein folding and aggregation (Bai et al. 2017; Horvath, Kumar, and

Wittung-Stafshede 2021; Munishkina et al. 2004). However, the complexity of the crowded environment inside cells is beyond the properties of synthetic polymers. One factor that differentiates intracellular crowding from synthetic crowders is that there are various types of soft interactions (hydrophobic, electrostatic, Van der Waals forces, and hydrogen bonds) inside cells, some of which do not exist between proteins and synthetic crowders. Therefore, it is better to study the effects of crowding on proteins in an environment that more closely mimics the intracellular milieu.

I used bacterial cell lysate (Figure 1.3) as the biological crowded environment, because of the following reasons. First, bacterial cell lysate is composed of nucleic acids, proteins, carbohydrate, and lipids which mimics the biocomplexity of the intracellular crowding. The macromolecular concentration in *E.coli* cytoplasm is estimated to be around 300-400 g/L, and it occupies 30% of the volume (Zimmerman and Trach 1991). Second, bacterial cell lysate enables us to manipulate its properties. Manipulating the cell lysate (e.g. the hydrophobicity or the distribution of particle sizes) can focus the study on a particular interaction or crowding effect of the cell lysate.

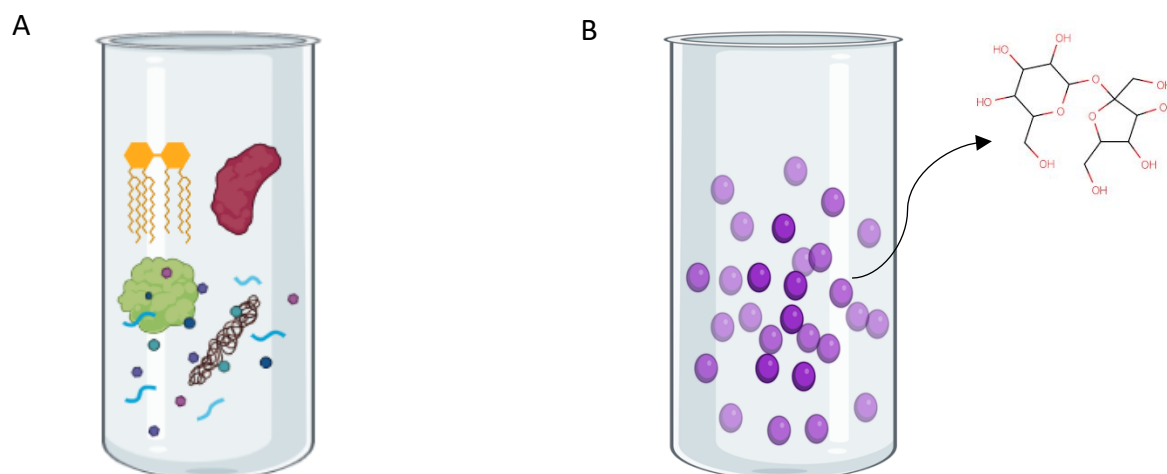


Figure 1.3) Macromolecular crowding in A) Bacterial cell lysate: including proteins, carbohydrates, nucleic acids, lipids B) Ficoll. Created with BioRender.com (Figure S6).

## 1.4 Aggregation of proteins

### 1.4.1 How does a protein aggregate?

Protein aggregation is a pathological hallmark of many protein deposition-derived disorders, including Parkinson's disease, Down's syndrome, Alzheimer's disease, Huntington's disease, and transmissible encephalopathies (Carrell and Lomas 1997; Fink 1998; Sipe 1992; Uversky 2008; Uversky and Fink 2004). Protein aggregation is considered a series of events starting from internal structural changes that make the initial pre-oligomeric form of the protein. Then it progresses with oligomerization and polymerization, which eventually lead to the visible particles based on the level of the aggregation (Alam et al. 2017; Ow and Dunstan 2014; Roberts 2014). The initial oligomerization usually starts with a local structural perturbation. The structural perturbation can occur due to altered pH, temperature, or environmental stress, which allow aggregation-prone sequences to be exposed. These sequences can interact with another protein to

make a monomer into an oligomer. This event is often called nucleation, which might promote further protein aggregation (Wang and Roberts 2018). Protein oligomerization as an aggregation nucleating event can be induced by hydrophobic interactions and created via bond exchange (e.g. disulphide bonds) through inter-residues cross-links, and oligomers can be varied from dimers to several monomers (Cabra et al. 2008; Zhai et al. 2012).

In cellular conditions, there is an equilibrium between the native form of the protein and some of its aggregation-prone forms, and normally this equilibrium is shifted toward the native form. However, under environmental stress and pathological conditions, this equilibrium is shifted toward enhanced aggregation propensity (Turoverov, Kuznetsova, and Uversky 2010). Since I study  $\alpha$ -synuclein, in the following section, I will discuss the aggregation of  $\alpha$ -synuclein.

#### **1.4.2 Aggregation of $\alpha$ -synuclein**

A variety of conditions can induce  $\alpha$ -synuclein's aggregation, including macromolecular crowding, temperature, acidic pH, metal ions such as aluminum, copper (II), iron (III), cobalt (III), and manganese (II), lipids and short hydrocarbon chains, glycosaminoglycans,  $\alpha$ -synuclein binding partners, polycations, and pesticides (Jan et al. 2021).  $\alpha$ -synuclein aggregation growth is not a linear process with respect to the time and shape of oligomerization, and usually the aggregation growth is exponential, and initially it increases the amount of  $\alpha$ -synuclein seeds or nuclei, which speeds up the additional growth of the aggregates (Kayser et al. 2011; Saluja et al. 2014). It was suggested that the aggregation growth can be controlled in two ways: First is the

conformational stability of a protein and second is the colloidal stability or protein-protein interactions (Wang and Roberts 2018).

The aggregation process of  $\alpha$ -synuclein is quite an elaborate process that I classify into two pathways. The first is a non-fibrillar pathway which makes amorphous aggregates directly from the monomer of  $\alpha$ -synuclein. The second is the fibrillar pathway with many intermediate oligomeric states composed of multiple steps (Mehra, Sahay, and Maji 2019) (Figure 1.4), which will be explained in the following paragraph.

The fibrillar pathway starts from the monomer of  $\alpha$ -synuclein, then develops into small aggregates,  $\beta$ -sheet rich oligomers, protofibrils and finally fibrils (Li, Uversky, and Fink 2001; Shtilerman, Ding, and Lansbury 2002). Small aggregates of  $\alpha$ -synuclein by an unknown mechanism might act as seeds to promote further aggregation of  $\alpha$ -synuclein. Therefore, oligomerized or pre-oligomerized forms of  $\alpha$ -synuclein might act as its cytotoxic form, causing more aggregation of  $\alpha$ -synuclein and affecting overall cellular mechanisms by reducing the amount of functional  $\alpha$ -synuclein. Although the  $\alpha$ -synuclein's oligomeric/pre-oligomeric form is toxic and causes disease pathogenesis, the fibrillar form of the  $\alpha$ -synuclein can transfer from one cell to another and spread out the disease. In this way,  $\alpha$ -synuclein fibrils act prion-like and can spread disease between neurons (Desplats et al. 2009; Levin et al. 2016; Luk et al. 2012; Mehra, Sahay, and Maji 2019).

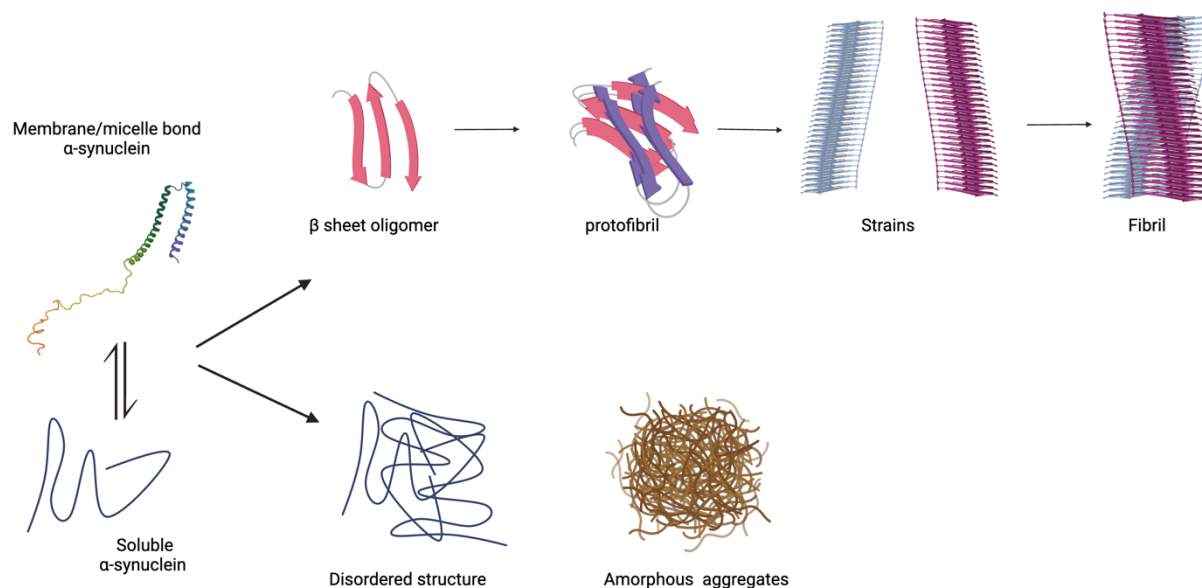


Figure 1.4)  $\alpha$ -synuclein's aggregation pathways: fibrillar versus non-fibrillar. Created with BioRender.com (Figure S7).

Familial PD mutations of  $\alpha$ -synuclein can also vary its aggregation process. It has been found that A53T, A53V, E46K, and H50Q accelerate aggregation (Conway, Harper, and Lansbury 1998; Ghosh et al. 2013; Greenbaum et al. 2005), whereas A30P, A53E, and G51D slow it down (Ghosh et al. 2014; Lesage et al. 2013; Li, Uversky, and Fink 2001). Researchers realized that E46K (Zarranz et al. 2004) and A53T (Polymeropoulos et al. 1997) mutations tend to aggregate more rapidly than the wild type and cause early onset familial PD. However, the mutations' effects are influenced by other factors like age, dopamine level, colloidal condition, etc. It was also shown that  $\alpha$ -synuclein gene (SNCA) duplication and tripling bring about increased  $\alpha$ -synuclein expression and high concentration which typically enhances  $\alpha$ -synuclein's propensity to aggregate (Chartier-Harlin et al. 2004; Singleton et al. 2003).  $\alpha$ -synuclein nucleation occurs above a certain concentration of  $\alpha$ -synuclein, because of higher levels of protein-protein interactions it has more

chances of structural perturbation (Shirai and Kikuchi 2016). The normal concentration of  $\alpha$ -synuclein in neuronal cells is estimated to be less than 60  $\mu$ M (Minton 2005).

### 1.4.3 Aggregation of $\alpha$ -synuclein in crowded conditions

$\alpha$ -synuclein's monomer is natively unfolded and unstable in the cytoplasm. It has been suggested that macromolecular crowding can induce the folding of the protein into a pre-molten globule state. Macromolecular crowding tends to stabilize proteins' conformation by either facilitating protein folding or pushing them toward the aggregation (Breydo et al. 2014). The compaction force that comes from hard interaction effects would make no distinction between the different compact forms (aggregated or folded) of proteins and reduces their conformational entropy (Elcock 2010; Minton 2005).

Macromolecular crowding also alters the diffusivity of proteins. It slows down the diffusion of proteins and decreases their translational entropy, and it induces partial folding of the protein (Laganowsky et al. 2012; Liu et al. 2012; Ralston 1990; Tycko 2006). The diffusion of a model polymer (PEG) (Trosel et al. 2023) and  $\alpha$ -synuclein in the presence of crowders was studied in the lab by Yanitza Trosel; however, it was performed in low concentrations of crowders.

By knowing how macromolecular crowding might induce  $\alpha$ -synuclein's aggregation, in the following sections, I will explain the main techniques that I used to study the aggregation process.

## 1.5 Nuclear Magnetic Resonance spectroscopy (NMR)

To understand the behavior and structure of a protein, we need to study it on different length scales. The dominant technique in studying the structure of a protein is X-ray crystallography. However, it is not useful in studying the dynamics of the protein in solutions. In my study I use Nuclear Magnetic Resonance (NMR), which is a well-developed technique in studying structure, diffusion, and dynamics of proteins (Smith et al. 2015). Indeed, the development of NMR techniques, including multidimensional NMR experiments, have been helping to have a better understanding of protein characteristics. In this study, I used HSQC, diffusion, and relaxation techniques, which I will explain in the following.

### 1.5.1 Heteronuclear Single Quantum Coherence (HSQC)

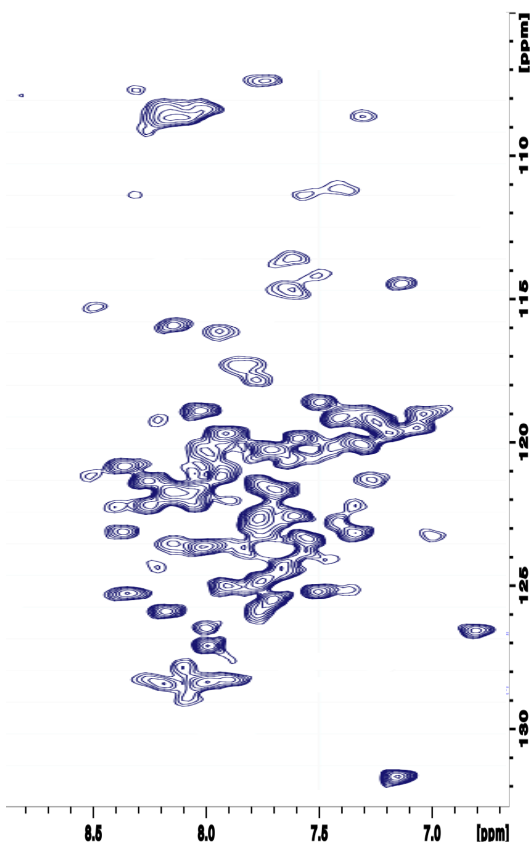
HSQC is a two-dimensional NMR technique that utilizes the coherent transfer of excitation between two nuclei that are connected covalently (e.g. nitrogen and hydrogen). A HSQC spectrum plots the chemical shift of  $^1\text{H}$  plotted versus  $^{15}\text{N}$  or  $^{13}\text{C}$ . In this study as I focus on the backbone of the protein, I label the backbone residues with  $^{15}\text{N}$ . Thus, I can focus on  $^1\text{H}$  and  $^{15}\text{N}$  correlation via  $^{15}\text{N}$ - $^1\text{H}$ -HSQC experiments in which each contour (peak) corresponds to one amino acid in the protein (Figure 1.5).

IDPs' structure can be affected easily by their environment, and any change in the environment might change the structure of the protein. Therefore, each amino acid in the structure of a protein has a particular chemical shift, and if I observe any change in their chemical shift

(nitrogen or proton frequency) by changing the environment (e.g. adding macromolecular crowding), it indicates a change in the electronic environment around the nucleus, normally from a change in structure or direct interaction with a binding partner.

As mentioned above, HSQC is a 2D experiment, but it also can be combined with other techniques to make it a 3D or 4D technique. In this study, I also performed pseudo-3D experiments, including relaxation-HSQC and diffusion-HSQC. The third dimension refers to the 2D experiment carried out at various values of a third parameter (mixing/delay times for relaxation and gradient strength for diffusion) and then further analyzed by characterizing the exponential dependence of the signal as a function of this parameter.

Figure 1.5)  $^{15}\text{N}$ - $^1\text{H}$ -HSQC spectrum of  $\alpha$ -synuclein. Y axis:  $^{15}\text{N}$  chemical shift (ppm), X axis:  $^1\text{H}$  chemical shift (ppm). Each peak represents one amino acid.



### 1.5.2 Diffusion NMR

Diffusion is a major mode of molecular transportation inside cells, and it gives us information about the characteristics of molecules, including shape, size, aggregation, and binding. Diffusion NMR is often referred to as Diffusion Ordered Spectroscopy (DOSY). DOSY is based on the applied field gradient combined with regular radiofrequency pulses to find the location of a molecule in the direction of the applied gradient, which can in turn indicate the diffusion of the molecule by providing a measure of how far it travels (Claridge 2009).

DOSY measurements are carried out as a series of 1D  $^1\text{H}$  spectra (Figure 1.6). However, to probe the diffusion of a protein in crowded conditions or a mixture of molecules, it is important to focus on the labelled isotope to separate it from the crowded background. So, I labelled the backbone of  $\alpha$ -synuclein with a  $^{15}\text{N}$  isotope to get the signal only from the protein's backbone and separate it from the crowded environment.  $^{15}\text{N}$ - $^1\text{H}$  HSQC-DOSY is a 3D technique in which I can focus on the intensity of the signal of either  $^{15}\text{N}$  or  $^1\text{H}$  (NH group) in different gradient fields. Then I can measure the diffusion by plotting the attenuated signal decay versus the gradient strength parameter (Vitorge and Jeannerat 2006).

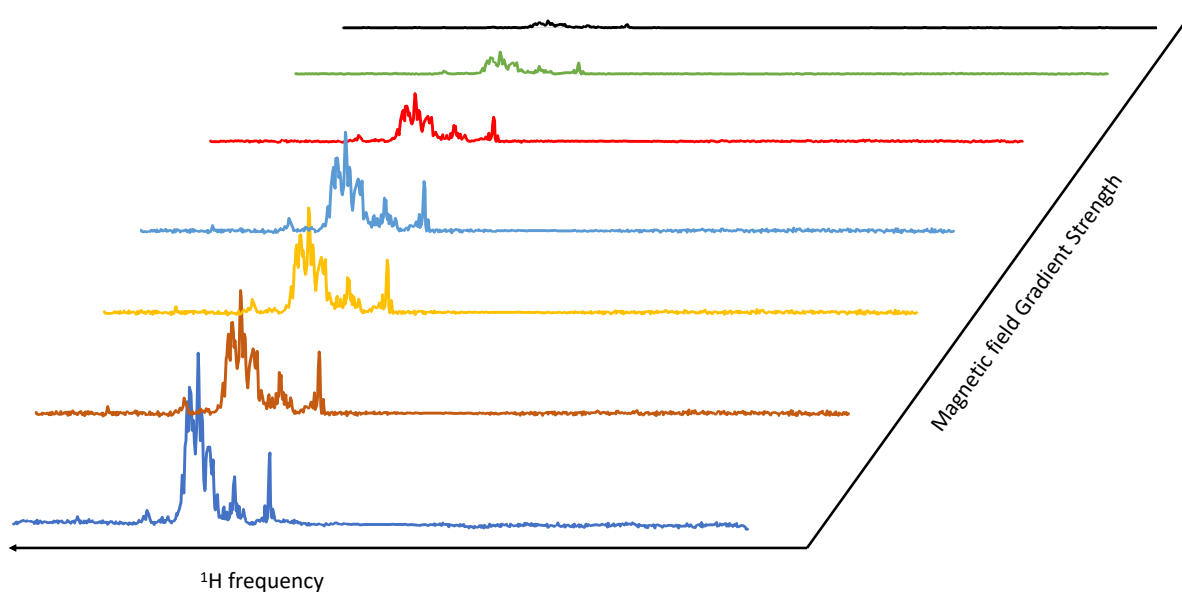


Figure 1.6) Diffusion NMR experiment: Attenuated  $^1\text{H}$  signal decay versus gradient strength.

### 1.5.3 Relaxation NMR

Proteins, especially IDPs, exist in a complex ensemble of structural states that continuously interconvert between different conformations due to changes in their internal molecular structure. Studying the internal molecular dynamics of proteins can provide information about residues' interactions or conformations. In other words, “dynamics” to some extent can be described as the interconversion between various conformations (Jarymowycz and Stone 2006).

Macromolecular crowding, apart from changing the translational diffusion of the protein, might also change the internal dynamics of the protein through soft interactions. Macromolecular crowding might alter the dynamics of the protein by electrostatic interactions, hydrogen bonds,

dispersion and Van der Waals forces (Jarymowycz and Stone 2006; Ohta-Lino et al. 2001; Williams et al. 1991). Therefore, the interactions between the protein and crowders might influence the internal motion of each residue in the structure of the protein. From Andy Garnier's honors thesis with MD simulations (Garnier 2021) we also see that there is likely competition between  $\alpha$ -synuclein to  $\alpha$ -synuclein interactions and  $\alpha$ -synuclein to crowder interactions. Consequently,  $\alpha$ -synuclein's motion might slow down or speed up due to attractive or repulsive interactions.

There has been an explosion of research on protein dynamics over the last two decades by doing relaxation NMR (Barchi et al. 1994; Charlier, Cousin, and Ferrage 2016; Cino, Karttunen, and Choy 2012; Jarymowycz and Stone 2006). Relaxation NMR is an experiment that perturbs the equilibrium of a spin state by radio frequency pulses, and the way they relax back to their resting position relates to their molecular mobility. Thus, relaxation is exclusively sensitive to molecular dynamics (Jarymowycz and Stone 2006). There are two main interactions that can impact on the fast dynamics scale (picoseconds to nanoseconds). First, dipole-dipole interactions between a pair of magnetic nuclei. Second, chemical shift anisotropy (CSA) (Jarymowycz and Stone 2006; Wagner 1993). The two main types of relaxation NMR are longitudinal ( $T_1=1/R_1$ ) and transverse ( $T_2=1/R_2$ ) relaxation. The purpose of this study is to focus on the transverse relaxation time ( $T_2$ ), the characteristic time frame over which the transverse magnetisation disappears, since it is more sensitive to IDP's internal backbone motion than longitudinal relaxation time ( $T_1$ ) (Jarymowycz and Stone 2006). Also,  $T_2$  is often much shorter than  $T_1$  for large molecules, like proteins, that tumble slowly. Therefore, it is better to measure the  $T_2$  since it gives us more information about the fast dynamics of residues.

The  $^1\text{H}$   $T_2$  experiment represent the loss of coherence in the xy plane as a function of several delay times, which can vary from microseconds to many seconds. However, just as for the same idea as the diffusion measurements, in order to separate the protein intensity from the crowders and other molecules in the solution, I use the  $^{15}\text{N}$ - $^1\text{H}$  HSQC- $T_2$  experiment, which allows us to only measure the relaxation of the  $^{15}\text{N}$ - $^1\text{H}$  group in the backbone of the protein. In other words, it enables measurement of the intensity of exact cross peaks in a series of HSQC plots versus the delay times. Therefore, I can understand the relaxation rate of each residue in the structure of the protein and consequently learn about the mobility of the part of the chain it is in.

## 1.6 Hypothesis and Objectives

### 1.6.1 Hypothesis

Unlike synthetic crowders, biological crowders may interact with  $\alpha$ -synuclein via soft interactions. Thus, I hypothesize that biological crowders will affect  $\alpha$ -synuclein's aggregation, translational diffusion, and internal dynamics differently than Ficoll.

### 1.6.2 Objectives

I will assess how the presence of biological crowders affects the aggregation of  $\alpha$ -synuclein via NMR and confocal microscopy. Also, I will measure the diffusion and internal dynamics of  $\alpha$ -synuclein in the presence and absence of crowders by pulsed field gradient NMR and transverse relaxation NMR experiments.

## 2. Materials and Methods

### 2.1 Vector design

A recombinant plasmid was designed and prepared by Liam Gregory (Liam Gregory 2020). The expressed protein construct is composed of  $\alpha$ -synuclein and polyhistidine tagged guanosine nucleotide protein beta subunit (GB-1) coding sequences. A tobacco etch virus (TEV) protease cleavage site was designed between  $\alpha$ -synuclein and GB-1. The designed sequence (Figure 2.1) was inserted into a pET21 expression vector (Figure 2.2). The designed vector was ordered from Genscript Biotech. The transcription of the sequence was engineered under the control of a T7 promoter, which is inhibited by the lac protein. Therefore, by adding isopropyl  $\beta$  D thiogalactoside (IPTG)(GoldBio) to the culture, the inhibitor leaves the promoter and transcription begins.



MSGSHHHHHH GMQYKLALNG KTLKGETTTE AVDAATAEKV FKQYANDNGV DGEWTYDDAT  
 KTFTVTEPGG PASENLYFQG MDVFMKGLSK AKEGVVAAAE KTKQGVAEAA GKTKEGVLYV  
 GSKTKEGVVH GVATVAEKTQ EQVTNVGGAV VTGVTAVAQK TVEGAGSIAA ATGFVKKDQL  
 GKNEEGAPQE GILEDMPVDP DNEAYEMPSE EGYQDYEPEA

Figure 2.1) Expressed protein construct, and the amino acids sequence of His-tag (purple), GB-1 (blue), EZCut TEV (red), and  $\alpha$ -synuclein (green).

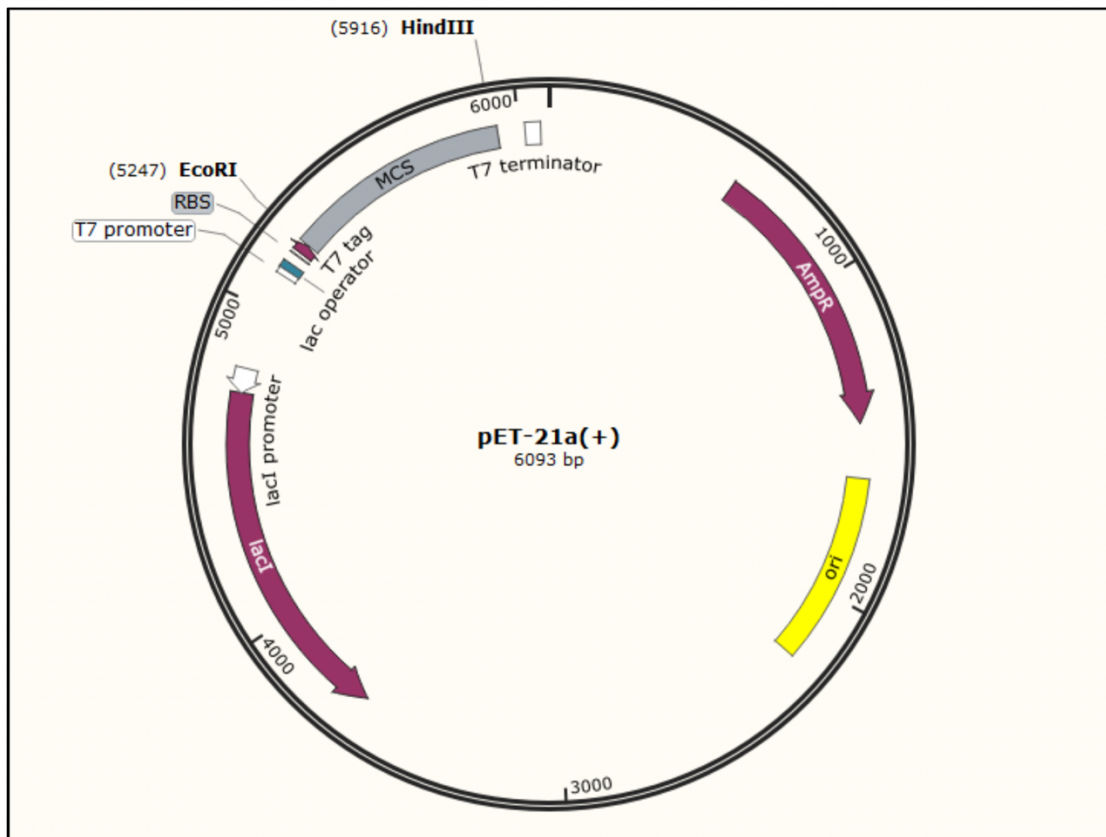


Figure 2.2) pET-21 vector used for expression of the  $\alpha$ -synuclein fusion protein. Figure prepared by Grace Kong (Genscript).

## 2.2 Transformation

The transformation process was performed by Liam Gregory. The designed vector was transformed to *E. coli* BL21(DE3). Two microliters of pET21 vectors were combined with *E. coli* BL21(DE3) cells. The tubes containing them were heat shocked at 42 °C in a water bath for 20 seconds and the tubes were then put on ice for 2 minutes. Next, 450 µL of super optimal broth with catabolite repression (SOC) recovery medium, including 20 g/L tryptone (Fisher), 5 g/L yeast extract (Fisher), 0.5 g/L NaCl (Fisher), 0.19 g/L KCl (Fisher), 0.92 g/L MgCl<sub>2</sub> (Sigma), 1.2 g/L MgSO<sub>4</sub> (Sigma), 3.6 g/L glucose (Sigma), was added to the tubes. The tubes were incubated at 37 °C using an incubator (Thermo Scientific Max Q 5000) for 60 minutes and shaking at 225 RPM.

A plate containing 2X yeast-tryptone agar (16 g/L tryptone (Sigma), 10 g/L yeast extract (Fisher), 5 g/L NaCl (Fisher), 12 g/L agar (Fisher), 100 mg/mL ampicillin (Fisher), 35 mg/mL chloramphenicol (Sigma)) was prepared. Ninety µL of the SOC recovery medium was transferred to the plate. 10 µL of transformed culture was pipetted onto the plate with SOC recovery medium. The plate was incubated overnight at 37 °C using an incubator (Fisher Scientific Isotemp). After 22 hours, tubes containing 5 mL and 10 mL aliquots of lysogen broth (LB) media were inoculated with a colony harvested from the plate. These tubes were incubated at 30 °C and at 150 RPM overnight. After that, cell stocks were aliquoted in microtubes containing 500 µL of the overnight culture and 500 µL of sterile glycerol (Sigma), then stored at -80 °C.

### 2.3 Expression of $\alpha$ -synuclein

$\alpha$ -synuclein's expression starts with growing *E. coli* BL21(DE3) in 75 mL of LB media and then transferring the grown bacteria to M9 media. The M9 media is enriched with  $^{15}\text{N}$ -labelled ammonium chloride ( $^{15}\text{NH}_4\text{Cl}$ ) (Cambridge Isotope Laboratories, Inc) to label the protein's backbone and inducing them to express the labelled  $\alpha$ -synuclein with IPTG treatment. A brief description of the expression and purification of  $\alpha$ -synuclein is shown in Figure 2.3.

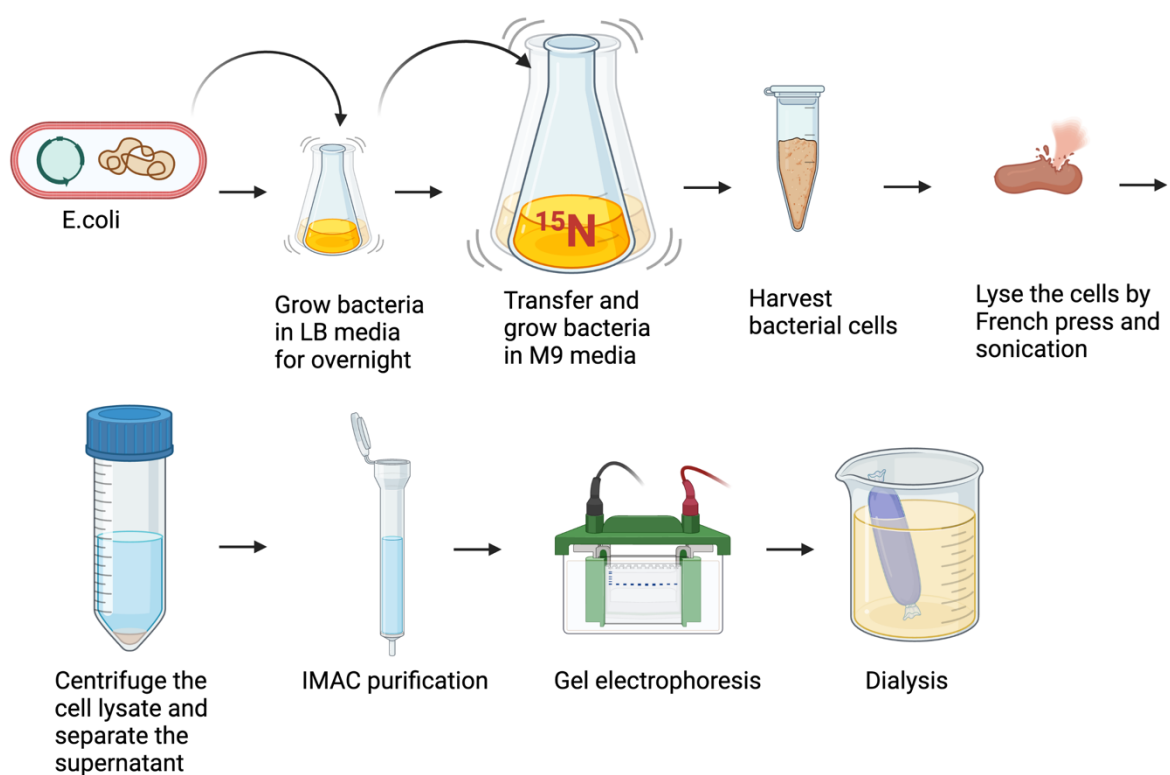


Figure 2.3) Recombinant  $^{15}\text{N}$   $\alpha$ -synuclein expression and purification.

The 75 mL LB medium was made up of 10 g/L tryptone (Sigma), 10 g/L sodium chloride (Fisher), and 5 g/L yeast extract (Fisher). The LB medium was autoclaved before use. Following that, 100 mg/mL of ampicillin and 35 mg/mL of chloramphenicol were added to the medium. Both chloramphenicol and ampicillin are selective antibiotics that cover many ranges of gram positive and negative bacteria. However, the vector is ampicillin resistant and the *E. coli* BL21 is chloramphenicol resistant which ensures selection of the desired bacteria. Chloramphenicol was dissolved in ethanol, and ampicillin was dissolved in deionized water, and since ampicillin was dissolved in water, it was filtered by a 0.22  $\mu\text{m}$  Sartorius filter. A sample of *E. coli* BL21 was added to the media, then it was kept in an incubator (Geneq Inc SI) at 30 °C while shaking at 150 RPM overnight (around 16-18 hours). The next day the media was taken out of the incubator and transferred to M9 media.

Preparing M9 is necessary to produce  $^{15}\text{N}$  labelled protein.  $^{15}\text{N}$  labelling is achieved by feeding bacteria with M9 media that has one nitrogen source,  $^{15}\text{N}$  labelled. M9 media was composed of salts, antibiotics, trace elements, and vitamins. First, a 6 L solution was prepared of 6 g/L sodium phosphate dibasic (Sigma), 3 g/L potassium phosphate monobasic (Sigma), and 0.5 g/L sodium chloride (Fisher). Then the pH was adjusted to 7.4. Second, two antibiotic stocks were prepared, 100 mg/mL ampicillin (Fisher) and 35 mg/mL chloramphenicol (Sigma). Third, four stocks were prepared, 1 M magnesium sulfate heptahydrate (Sigma), 1 M calcium chloride dihydrate (Sigma), 10 mM iron (II) sulfate heptahydrate (Fisher), and 5 mg/mL thiamine hydrochloride (Sigma). All these stocks were filtered by 0.22  $\mu\text{m}$  Sartorius filters. Fourth, a stock of 400X trace elements was prepared using 27 mg/mL iron (II) chloride hexahydrate (Sigma), 2 mg/mL manganese (II) chloride tetrahydrate (Sigma), 2 mg/mL cobalt (II) chloride hexahydrate

(Fisher), 2 mg/mL sodium molybdate dihydrate (Sigma), 1 mg/mL calcium chloride dihydrate (Sigma), 1.3 mg/mL copper (II) chloride dihydrate (Sigma), and 0.5 mg/mL boric acid (Sigma). Finally, a 1000X vitamin supplement was prepared composed of 1 mg/mL D-biotin (Novabiochem), 0.5 mg/mL choline chloride (Sigma), 0.5 mg/mL folic acid (Sigma), 1 mg/mL myoinositol (Sigma), 0.5 mg/mL nicotinamide (Sigma), 0.5 mg/mL pantothenic acid (Sigma), 0.5 mg/mL pyridoxal hydrochloride (Sigma), 0.05 mg/mL riboflavin (Sigma), and 0.05 mg/mL thiamine hydrochloride (Sigma). This was then filtered by a 0.22  $\mu\text{m}$  Sartorius filter.

After dissolving the salts (sodium phosphate dibasic, potassium phosphate monobasic, sodium chloride) in 6 L deionized water. 1 L of salt solution was transferred to a 4 L flask and autoclaved (in total six 4 L flasks). Following that, the flasks were preincubated in an incubator (Thermo Scientific MaxQ 5000) at 37 °C and shaken at 175 RPM overnight. The next day before transferring the bacteria from the 75 mL overnight culture to the 4 L flasks, the rest of the materials were added to the flasks from the stocks prepared before as above. Thus, other ingredients were added to final concentrations of 2 mM magnesium sulfate heptahydrate, 0.1  $\mu\text{M}$  calcium chloride, 0.01 mM iron (II) sulfate, 5  $\mu\text{g/mL}$  thiamine hydrochloride, 2.5 mL of the 400x trace elements, 1 mL of the 1000X vitamin supplement, 100  $\mu\text{g/mL}$  ampicillin, and 35  $\mu\text{g/ml}$  chloramphenicol were added to the flasks. Then 4 g glucose (Sigma) and 1 g ammonium chloride ( $^{15}\text{NH}_4\text{Cl}$ ) (Cambridge isotope Laboratories, Inc) were added to each flask.  $^{15}\text{NH}_4\text{Cl}$  is the source of  $^{15}\text{N}$  isotope and, as mentioned before, replaces the  $^{14}\text{N}$  in the backbone of the protein.

The growth of bacteria in M9 media normally takes longer than in LB media, and it took 20 hours to reach the specific OD. The growth of bacteria was monitored by measuring the

absorbance of the media using a Genesys 10X UV-VIS spectrophotometer. The spectrophotometer was calibrated against the autoclaved M9 media without any bacteria. The absorbance was measured at OD 600 nm. Incubation continued at 37 °C with shaking at 175 RPM until the absorbance of the media reached 0.6. This was the moment to induce the bacteria to express the protein. To induce the expression, a final concentration of 0.01 M IPTG was added to each flask. The incubation continued under the same conditions until the absorbance reached 1.0 (around 5 hours after induction), then the media were taken out of the incubator.

The bacterial cultures were centrifuged at 4690 g for 15 minutes at 4 °C using a Sorvall RC6+ centrifuge to harvest the cells. Afterward, the pellets were scooped and dissolved in TBS buffer (50 mM Tris (Sigma) and 150 mM sodium chloride (Fisher)) containing 1X Halt™ Protease Inhibitor Cocktail (Fisher), and the pH was adjusted to 7.5. The protease inhibitor cocktail was composed of AEBSF\*HCl, aprotinin, bestatin, E-64, leupeptin, and pepstatin A.

The harvested cells in the buffer were lysed by Amico French press three times at 1200 psi. Then the suspension was sonicated three consecutive times for 30 seconds by using a Branson Sonifier Cell Disruptor for further lysing, which breaks up the DNA into smaller fragments so they do not plug the purification column. The sonification and French press processes were done while keeping the sample at 4 °C. Following that, the suspension was centrifuged at 100 000 g for 40 minutes at 4 °C using a Beckman L90K ultracentrifuge. After centrifugation, the supernatant was separated carefully from the pellet. The supernatant is expected to contain the  $\alpha$ -synuclein while the pellet is expected to contain insoluble cell components. It is possible some of the  $\alpha$ -synuclein is associated with the membrane and would have been discarded with the pellet.

## 2.4 Purification and preparation of $\alpha$ -synuclein

Immobilized Metal Affinity Chromatography (IMAC) was used in order to purify the  $\alpha$ -synuclein from the rest of the biomolecules in the supernatant (Figure 2.3) at 4 °C. A GE healthcare PD-10 chromatography column was loaded with 5 mL sepharose fast flow resin (GE Healthcare). Then in order to charge the column 2 mL of 0.2 M nickel (II) sulfate hexahydrate (Sigma) was added to the column. After that the column was washed with 25 mL deionized water and then pre-equilibrated with 25 mL loading buffer (5 mM imidazole (Sigma), 50 mM Trizma base (Sigma), 150 mM sodium chloride (Fisher); pH=7.4). The column preparation was done at room temperature, but the protein purification process was performed at 4 °C.

The supernatant was loaded onto the IMAC column and 1.5 mL fractions were collected in 1.5 mL microtubes. Following that, 20 mL loading buffer was added to the column. Then 20 mL washing buffer (20 mM imidazole (Sigma), 50 mM Trizma base (Sigma), 150 mM sodium chloride (Fisher); pH=7.4), and then the protein was eluted with 20 mL elution buffer (300 mM imidazole (Sigma), 50 mM Trizma base (Sigma), 150 mM sodium chloride (Fisher); pH=7.4). 1.5 mL fractions were collected from all above steps.

The absorbance of the fractions at OD 280 nm was measured using a Genesys 10X UV-Vis spectrophotometer and quartz cuvettes. The spectrophotometer was calibrated against the appropriate buffer for each fraction; for example, washing fractions were calibrated against the washing buffer. As expected, the fractions with the highest absorption values after the flow through, were the elution fractions. The fractions were categorized based on their absorbance from

lowest to highest, and they were run via gel electrophoresis to indicate whether the sample absorbance is from  $\alpha$ -synuclein or other proteins. The fractions were incubated with 2X sample buffer (0.125 M Tris-HCl (Sigma), 4% sodium dodecyl sulfate (Sigma), 0.01% bromophenol blue (Bio-Rad), and 20% glycerol (Sigma)) for 5 minutes at 100 °C in a water bath. The gel electrophoresis was run using a 12% Mini-PROTEAN® TGXTM, 10-well, 30  $\mu$ L volume, precast gel (Bio-Rad). After loading the protein samples, the gel was run at 80 V for 5 minutes and then 155 V for 30 to 60 minutes immersed in 1 X running buffer (10 X running buffer: 250 mM Trizma base (Sigma), 1.92 M glycine (Sigma), 1% SDS (Sigma)). The Precision Plus Protein™ Kaleidoscope™ Prestained Protein Standard was used to obtain the molecular weight of the protein. Electrophoresis gels' images were obtained by ChemiDoc MP System (Bio-Rad) on a white tray. As it was expected, most His-tagged-GB-1 fusion- $\alpha$ -synuclein was found in the elution fractions at around 25 kDa, consistent with the molar mass of 23.19 of these recombinant expressed proteins. The fractions with the most  $\alpha$ - His-tagged-GB-1 fusion- $\alpha$ -synuclein were pooled for cleavage to break the polypeptide chain between the poly His-tagged GB-1 fusion and  $\alpha$ -synuclein.

In order to carry out the cleavage, 1  $\mu$ g/ $\mu$ L EZCut Tobacco Etch Virus (TEV) protease (Biovision) was incubated with the chosen fractions at 34 °C in a water bath for 90 minutes. 19  $\mu$ L of 1  $\mu$ g/ $\mu$ L of the TEV protease was added to the fractions per mg of protein. I obtained the concentration of the protein from its absorbance at OD 280 nm by Beer–Lambert law. For example, we usually obtain 8 mg protein per batch of protein expression. Therefore, I need 152  $\mu$ L EZCut TEV protease to perform the cleavage process.

In the next step, it was necessary to separate the cleaved  $\alpha$ -synuclein from the poly-His tagged GB-1. The cleavage suspension was loaded onto a charged IMAC column, and the fractions were collected. Then the column was washed with TEV washing buffer (50 mM Trizma base and 100 mM NaCl, pH=8) and elution buffer. All the fractions were collected in 1.5 mL microtubes. Afterward, the same process of measuring the absorbance and running a gel were done to confirm the presence of  $\alpha$ -synuclein and separation of the GB-1. The molecular weight of  $\alpha$ -synuclein and GB-1 is 14 and 6.6 kDa, respectively.

Although the purification worked very well, there was a little contamination (mostly at a MW around 45 kDa) in some fractions. To remove the contamination, the fractions were loaded on the IMAC column for a third time. However, this time they were washed with four different concentrations of the imidazole buffer. The column was first washed with buffer #1 (50 mM imidazole (Sigma), 50 mM Trizma base (Sigma), 150 mM sodium chloride (Fisher); pH=7.4) then buffer #2 (100 mM imidazole (Sigma), 50 mM Trizma base (Sigma), 150 mM sodium chloride (Fisher); pH=7.4) then buffer #3 (200 mM imidazole (Sigma), 50 mM Trizma base (Sigma), 150 mM sodium chloride (Fisher); pH=7.4), and elution buffer (300 mM imidazole (Sigma), 50 mM Trizma base (Sigma), 150 mM sodium chloride (Fisher); pH=7.4). Then the absorbances of fractions were measured, and accordingly, gel electrophoresis was performed for the flowthrough fractions and collected washing #3 and elution fractions since they had a high absorbance.

The isolated  $\alpha$ -synuclein was dialyzed to reduce the amount of salts and remove the molecules less than 6-8 kDa. Dialysis tubing with a molecular weight cut off 6-8 kDa (Fisher) was used for the dialysis. The clamped tubing containing purified  $\alpha$ -synuclein was floated in a pool of 4 L milliQ water stirring overnight at 4 °C. The enrichment of the  $\alpha$ -synuclein was assessed by

running a gel after the dialysis and measuring the absorbance by using a Genesys 10X UV-VIS spectrophotometer and quartz cuvettes. The absorbance was confirmed with a Thermo Nanodrop Spectrophotometer blanked against water. The concentration of  $\alpha$ -synuclein was calculated based on the absorbance with Beer–Lambert law at 280 nm ( $A_{280\text{ nm}}$ ) using a molar extinction coefficient of  $5960\text{ M}^{-1}\text{ cm}^{-1}$  (De Oliveira et al. 2016), and it also was confirmed with Bradford Assay.

To perform the Bradford Assay, 1X Bradford reagent from Coomassie brilliant blue G-250 dye (Sigma) is required. A stock of 1 mg/mL of Bovine Serum Albumin (BSA) (Sigma) was prepared as a standard protein. The volumes used for the standard curve and  $\alpha$ -synuclein samples are shown in Table 2.1. All samples were shaken gently for 30 seconds and incubated at room temperature for 20 minutes. The samples were diluted with TBS buffer and the absorbance was measured using a Genesys 10X UV-VIS spectrophotometer at OD 595 nm. The spectrophotometer was calibrated against the TBS buffer.

Finally, to increase the concentration of  $\alpha$ -synuclein, the purified fractions were frozen at a  $-80\text{ }^{\circ}\text{C}$  for 24 hours, and then their water volume was reduced by 80 % using a Labconco Freezone 12 Freeze Dryer. The results of the protein purification are shown in section 3.1.

I also used centrifugal tubes as a second method to increase the  $\alpha$ -synuclein concentration. 5 mL of purified fractions were added to Microsep<sup>TM</sup> advance centrifugal tubes (Pall corporation), 3K MWCO, and centrifuged at 4690 g for 30 minutes at  $4\text{ }^{\circ}\text{C}$  using a Sorvall RC6+ centrifuge. However, this method was not efficient, which will be explained in section 3.1.

Table 2.1) The directory of Bradford Assay

	<b>Protein (<math>\mu\text{L}</math>)</b>	<b>TBS (<math>\mu\text{L}</math>)</b>	<b>Bradford color reagent (<math>\mu\text{L}</math>)</b>
	BSA		
1	0	1600	400
2	4	1596	400
3	8	1592	400
4	12	1588	400
5	16	1584	400
6	20	1580	400
7	24	1576	400
8	28	1572	400
9	32	1568	400
10	36	1564	400
11	40	1560	400
12	44	1556	400
13	48	1552	400
14	52	1548	400
15	56	1544	400
16	60	1540	400
	$\alpha$ -synuclein		
17	-	1600	400
18	-	1600	400
19	3	1597	400
20	3	1597	400

## 2.5 Preparation of Ficoll70

A stock of 400 mg/mL of Ficoll70 (Sigma) was prepared in deionized water, and pH was adjusted to 7. The Ficoll suspension was homogenized with a homogenizer (Fisher homogenizer 850) at 11000 RPM for 3 minutes and 3 consecutive times. Then the Ficoll stock was stored at room temperature.

## 2.6 Preparation of bacterial cell lysate

Bacterial cell lysate preparation starts with preparing LB media to be used in growing JM10 *E.coli*. A 500 mL Erlenmeyer flask was added with 75 mL LB media (10 g/L tryptone (Sigma), 10 g/L sodium chloride (Fisher), and 5 g/L yeast extract (Fisher)). Up to six 4 L Erlenmeyer flasks were filled with 1 L LB media (in total, 6 L LB media). All flasks containing the LB media were autoclaved. Following that, the 75 mL media was inoculated with 1 mL of *E.coli JM109* glycerol stock. The bacterial stock contains 500  $\mu$ L of overnight culture and 500  $\mu$ L of sterile glycerol (Sigma). All the cell stocks were stored at -80 °C. The flask was incubated in an incubator (Geneq Inc SI) at 30 °C while shaking at 150 RPM overnight (16-18 hours). The 4 L flasks containing the 1 L autoclaved media were preincubated in an incubator (Thermo Scientific MaxQ 5000) at 37 °C while shaking at 175 RPM overnight. The next day, after 16 to 18 hours, 10 mL of the overnight bacteria were transferred to each 4 L flask. The flasks were incubated at 37 °C while shaking at 175 RPM. The absorbance was checked every 30 minutes to determine the stage of growth of the bacterial culture. The absorbance was measured using a Genesys 10X UV-VIS spectrophotometer at OD 600 and calibrated against an autoclaved LB media (without bacteria). The flasks were taken out of the incubator when the absorbance reached 0.8. The bacterial culture was centrifuged at 4690 g for 15 minutes at 4 °C using a Sorvall RC6+ centrifuge to harvest the cells. Following that, the pellets containing the cells were resuspended in TBS buffer. The suspension of the harvested cell was lysed by Amico French press for three times at 1200 psi at 4 °C. Then the suspension was sonicated using three cycles for 30 seconds each, using a Branson Sonifier Cell Disruptor to break up the large strands of DNA at 4 °C. Following that, the pH was adjusted to 7. The cell lysate was dried out by using a Labconco Freezone 12 Freeze Dryer and stored at -20 °C. 1X Halt™ Protease

Inhibitor Cocktail (Fisher) was added to the suspension just before all experiments with cell lysate (including unmanipulated and manipulated cell lysate) to prevent the enzymatic proteolysis upon adding the  $\alpha$ -synuclein to the cell lysate.

### **2.7 Preparation of less hydrophobic bacterial cell lysate**

First, a 100 mL suspension of 2 mg/mL of the unmanipulated cell lysate was prepared. The suspension was vortexed for 30 minutes at 4 °C. Second, a PD-10 column was loaded with 3 mL of weakly hydrophobic Macro-Prep Methyl HIC resins (Bio-Rad). The column was washed with 20 mL of deionized water. Then, the cell lysate suspension was loaded onto the column. Two fractions were collected with the same volume ( $2 \times 50$  mL). By this step, the fractions are expected to contain less hydrophobic cell lysate (mostly the first fraction) since the strong hydrophobic particles in the cell lysate stick to the weakly hydrophobic resins in the column (Figure 2.3).

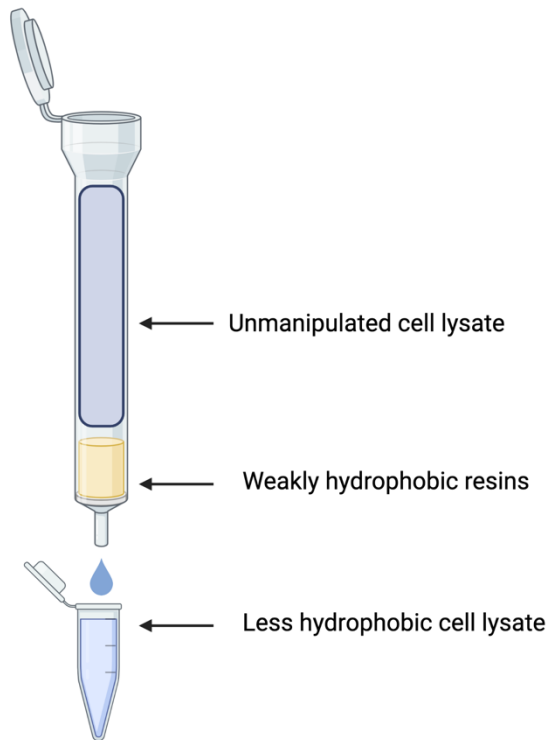


Figure 2.4) Preparation of less hydrophobic bacterial cell lysate.

## 2.8 Hydrophobicity measurements of the cell lysate

### 2.8.1 Weight

One way to understand the effects of weakly hydrophobic resins on cell lysate is to measure the dried weight of the cell lysate before and after applying it to the column. The dried weight of the cell lysate was measured before passing it through the column. After the cell lysate was passed through the weakly hydrophobic resins, the collected fractions were freeze-dried using a Labconco

Freezone 12 Freeze Dryer. Then the weight of the dried cell lysate was measured and compared to the initial weight (before HIC). If some mass was lost due to handling of the material, I still changed the hydrophobicity of the samples as it will be shown in the next section by Bligh and Dyer. The results are shown in section 3.2.

### **2.8.2 Bligh and Dyer analysis**

In order to measure the mass of hydrophobic and hydrophilic particles in our samples, I used a standard method, Bligh and Dyer (Bligh and Dyer 1959). A 30 mL suspension with 0.2 g of unmanipulated cell lysate was prepared. The entire Bligh and Dyer procedure was done in a fume hood. 20 mL of chloroform (Fisher) was added to a borosilicate glass chromatography column. Then the cell lysate suspension was added to the column, and 20 mL methanol (Caledon Laboratories Ltd) was added over the suspension. The column was covered with aluminum foil and parafilm and inverted several times to mix the contents. Then the column was left for 5 minutes until two phases were observed. The lower phase contained chloroform and hydrophobic particles, and the upper phase contains methanol and hydrophilic particles. The hydrophobic phase was separated gently and transferred to aluminum weight boats (VWR). Each weigh boat was filled with 10 mL of the solution. Then the hydrophilic phase was separated carefully and transferred to different aluminum weigh boats. All filled aluminum weigh boats were heated on a hot plate stirrer (Corning hot plate stirrer PC-351) in a fume hood until all solvent was evaporated. Then the dried weight boats were kept in an oven (Fisher Scientific Isotemp) at 105 °C for 10 minutes. After that, the mass of the weigh boats was measured, and the original mass of the dishes were subtracted

from the mass of weigh boats (after the evaporation) to obtain the mass of the hydrophilic and hydrophobic components.

### 2.8.3 Dynamic light scattering (DLS)

DLS is a useful technique to measure the particle size in the cell lysate and understand the effects of the weakly hydrophobic column on the cell lysate. Suspensions of 1 mg/mL of the cell lysate before and after applying it to the column were prepared, and a Malvern Zetasizer Nano-ZS ZEN3600 was used to measure the size of the particles in the suspensions at 25 °C. The size distribution was measured by intensity. The refractive index was 1.330, and the viscosity was 0.8872 cP.

## 2.9 NMR spectroscopy

All NMR experiments were done on three sample compositions: 1)  $\alpha$ -synuclein in the absence of crowders, 2)  $\alpha$ -synuclein in the presence of Ficoll70, and 3)  $\alpha$ -synuclein in the presence of bacterial cell lysate. All NMR experiments were conducted on either a Bruker 500 MHz or 600 MHz spectrometer via a Triple X Inverse (TXI) probe. The  $^1\text{H}$  Larmor frequencies for 500 and 600 spectrometers are  $21.288 \times 10^9$  and  $25.545 \times 10^9$  Hz. The  $^{15}\text{N}$  Larmor frequencies for 500 and 600 spectrometers are  $2.158 \times 10^9$  and  $2.589 \times 10^9$  Hz. All NMR samples contained 0.4 mM sodium 2,2-dimethyl-2-silapentane-5-sulfonate (DSS)(Sigma) to directly calibrate the  $^1\text{H}$  chemical shift and 10%  $\text{D}_2\text{O}$  (Cambridge Isotope Laboratories, Inc) to lock the field frequency. The spectral width of the proton channel was 14 ppm, and the nitrogen channel width was 36 ppm. All NMR

experiments were conducted with precision NMR sample tubes, 7" long and 5 mm in diameter (New Era Enterprises, Inc) at 25 °C or 37 °C. The total volume of all NMR samples was 600  $\mu$ L and the  $\alpha$ -synuclein concentration was 0.2 mM. It is noteworthy to mention that 0.3 mM of  $\alpha$ -synuclein was tried for a few NMR experiments, but aggregation occurred after a few hours. Since most NMR experiments in our study take place for 10 to 24 hours, 0.2 mM of  $\alpha$ -synuclein is an ideal concentration for the study purposes. On the other hand, our initial experiments with NMR showed that less than 0.2 mM  $\alpha$ -synuclein is not a sufficient concentration to obtain appropriate signal intensities by NMR spectroscopy.

### 2.9.1 1D $^1\text{H}$ NMR experiment

A 1D  $^1\text{H}$  single-pulse experiment was performed before each NMR experiments on the NMR 500 and 600 MHz spectrometers. To set up the experiment, proton tuning (atma), lock, topshim, and 90° pulse calibration were performed. The "ZG" pulse program,  $^1\text{H}$  single pulse experiments, was used for the 1D  $^1\text{H}$  experiment. ZG uses a 90° pulse for excitation with one scan. The 1D  $^1\text{H}$  experiment helped to find the transmitter frequency offset (O1) and used the same offset for suppressing the water peak. The data were processed by Fourier transformation in  $^1\text{H}$  dimension (the efp command), phased, and analyzed using Bruker TopSpin 4.1.4.

### 2.9.2 1D $^1\text{H}$ with water suppression

A 1D  $^1\text{H}$  with water-peak suppression pulse program was used on the NMR 500 and 600 MHz spectrometers to suppress the water peak and make the  $\alpha$ -synuclein and the crowders signals

more visible. The “p3919gp”,  $^1\text{H}$  1D experiment using watergate, pulse program (Cavanagh et al. 2007) was used with 128 scans, and the water suppression (uses watergate water suppression) took place at the O1 offset frequency. The size of the time domain signal (TD), known as the free induction decay (FID), was 32000. The FID was processed by Fourier transformation in the  $^1\text{H}$  dimension (the efp command) and analyzed using the Bruker TopSpin 4.1.4.

### 2.9.3 2D $^{15}\text{N}$ - $^1\text{H}$ HSQC

The 2D  $^{15}\text{N}$ - $^1\text{H}$  HSQC experiment was used to obtain signals from all amide H-N groups of  $\alpha$ -synuclein. The positions of chemical shifts are determined by the local structure and conformation of the protein. Therefore, the HSQC gives us a fingerprint of all residues in different conditions. NMR samples used for the  $^{15}\text{N}$ - $^1\text{H}$  HSQC experiment contain  $\alpha$ -synuclein in the absence and presence of the crowders (150 mg/mL and 200 mg/mL of both Ficoll70 and cell lysate). The name of the HSQC pulse program is “invietfpf2gp.mm,” 2D H-1/X correlation via double inept transfer, and it was conducted on the NMR 500 MHz spectrometer at 25°C or 37°C. All the HSQC experiments were run at the same O1 as the 1D experiments with 128 scans, and the TD (number of increments) number was 1024 for the proton channel and 128 for the nitrogen. Nitrogen offset (O2) was 5827.94 Hz and spectral width on proton channel was 14 ppm and on nitrogen channel was 40 ppm.

The HSQC spectra were processed by Fourier transformation in both  $^{15}\text{N}$  and  $^1\text{H}$  dimensions using the TopSpin 4.1.4 software (the xfb command with sine square multiplication

window) and then visualized with CcpNmr software (Skinner et al. 2016) for further analysis, including comparing the peaks frequency and intensity (contour level).

The processed HSQC spectra were also imported to NMRFAM-Sparky (W. Lee, Tonelli, and Markley 2015) to assign the peaks. The  $\alpha$ -synuclein peak assignment was done based on published papers (Wu and Baum 2011; Sivanesam et al. 2015). Since the concentration of  $\alpha$ -synuclein, pH and temperature of these two papers are close to my experimental conditions, I chose them to assign my spectrum.

#### 2.9.4 2D $^1\text{H}$ DOSY

The  $^1\text{H}$  DOSY experiment was used to measure the diffusion coefficient of trace HDO in a  $\text{D}_2\text{O}$  sample ( $\text{H}_2\text{O}$  0.1 %;  $\text{D}_2\text{O}$  99.9 %, because of rapid exchange) on the NMR 500 MHz spectrometer at 25 °C. The HDO in  $\text{D}_2\text{O}$  diffusion coefficient was measured as a standard to calibrate the  $\alpha$ -synuclein diffusion measurements (I considered the diffusion of HDO in  $\text{D}_2\text{O}$  is  $1.905 \times 10^{-9} \text{ m}^2/\text{s}$  at 25 °C). The  $^1\text{H}$  DOSY pulse program (dstegp3s) used a double stimulated echo and LED (longitudinal encode-decode) with 3 spoiler gradients (Jerschow and Müller 1997). The TD number was 16384 and 16 scans at the same O1 frequency as in the 1D  $^1\text{H}$  experiment was used for the measurements. The  $^1\text{H}$  DOSY experiments were performed at 16 gradient strengths (Table 2.2). The duration of the gradient pulse ( $\delta$ ) was  $2.4 \times 10^{-3}$  seconds, and the delay between gradient pulses ( $\Delta$ ) was  $100 \times 10^{-3}$  seconds.

$^1\text{H}$  DOSY spectra were processed (the `xf2` command with sine multiplication window for F1 and Lorentzian broadening factor (`em`) for F2) and analyzed using TopSpin 4.1.4 software. The  $^1\text{H}$  DOSY data, including the proton signal intensity and gradient strengths, were imported to the Igor Pro 8.04 software to calculate the diffusion coefficient values. The natural logarithmic scale of the attenuated signal decay,  $\ln(S(k))$ , was plotted versus the gradient strength ( $k = (\gamma\delta g)^2 \left(\Delta - \frac{\delta}{3}\right) \left(\frac{s}{m^2}\right)$ );  $\gamma$  is the gyromagnetic ratio,  $\delta$  is the duration of the gradient pulse,  $g$  is the gradient strength, and  $\Delta$  is the delay between gradient pulses), and the plots were fit to the linear function  $\ln(S(k)) = \ln(S(0)) - Dk$ . The slope of the plots indicates the diffusion coefficient  $D$  of water.

Table 2.2)  $^1\text{H}$  DOSY gradient strengths with sinusoidal gradient pulses stepped from 2 to 95% of the maximum strength.

Gradient plane	Gradient strength (G/cm)
1	0.705
2	2.889
3	5.073
4	7.257
5	9.441
6	11.62
7	13.81
8	15.99
9	18.18
10	20.36
11	22.55
12	24.73
13	26.91
14	29.1
15	31.28
16	33.47

### 2.9.5 Pseudo 2D $^{15}\text{N}$ - $^1\text{H}$ HSQC-DOSY

The pseudo 2D  $^{15}\text{N}$ - $^1\text{H}$  HSQC-DOSY experiments were conducted on NMR 500 MHz spectrometer at 25 °C to obtain the translational diffusion coefficient of  $\alpha$ -synuclein. This experiment can help to obtain the diffusion coefficient of  $\alpha$ -synuclein even in a crowded condition and in the presence of other molecules since it focuses on  $^{15}\text{N}$ - $^1\text{H}$  in the backbone of the protein. The “led1dhsqc2d.jkr\_modified,” Coupling of ledbpgp2s1d with hsqcetfpgpsi2, pulse program was used for this experiment, which was adapted from Shin et al. (2017). The experiment was run at the same O1 as the 1D  $^1\text{H}$  experiment with 2560 scans. The TD for the proton channel was 2048 and for the  $^{15}\text{N}$  channel was 128. The gradient strength used was composed of 1%, 10%, 20%, 30%, 40%, 50%, 60%, 70%, 80%, 90%, and 95% of the maximum gradient strength. The variation of the strength of the magnetic gradient strength is shown in Table 2.3. Here the gradients were trapezoidal (nearly square) and thus the mean gradient- squared was 95% of 45.74 G/cm. The duration of the gradient pulse ( $\delta$ ) was  $2.4 \times 10^{-3}$  seconds, and the delay between gradient pulses ( $\Delta$ ) was  $100 \times 10^{-3}$  seconds. The main downside of the TXI probe is the gradient field strength only goes up to 45.74 G/cm in this experiment and so may not be sensitive to more slowly diffusing species.

The  $^{15}\text{N}$ - $^1\text{H}$  HSQC-DOSY experiment was processed in 1D with the efp command which Fourier transformed with an exponential line broadening function, command with sine square multiplication window and analyzed using TopSpin 4.1.4. All process spectra were phased manually. Auto-correct baseline correction was performed using polynomial by “bas” command. The degree of polynomial ABSG was 3. The water peak was removed by changing the BC\_MOD

to “qfill” and choosing 0.2 Hz correction offset for BC\_MOD. Then, the chosen peaks and certain regions (7.73-8.70 ppm) that is related to  $\alpha$ -synuclein’s signals were integrated to obtain the intensity of the peak. From the second gradient (10%) the last scale was used to calibrate the integration. Then all the intensities and gradient strengths were imported to the Igor pro 8.04 software to calculate the diffusion coefficient values. The logarithmic scale of the attenuated signal decay was plotted versus the gradient strength ( $k = (\gamma\delta g)^2(\Delta - \frac{\delta}{3})(\frac{s}{m^2})$ ). The value for the plots were fit to a bi-exponential function,  $S(k)/S(0) = f \exp(-D_{fast}k) + (1 - f) \exp(-D_{slow}k)$ ;  $f$  was allowed to vary. The slope of the plots indicates the two diffusion coefficients. The fast component potentially is fragments of  $\alpha$ -synuclein or  $^{15}\text{N}$ -labelled metabolites, and the slow component shows the diffusion coefficient of  $\alpha$ -synuclein. An important factor in calculating the diffusion coefficient is considering which type of gradient shape I use. I used SMSQ10.100 (smoothed rectangular shape) for the HSQC-DOSY experiment and SINE.100 (sine wave shape) for the proton DOSY.

Table 2.3)  $^{15}\text{N}$ - $^1\text{H}$  HSQC-DOSY gradient strength.

<b>Gradient percentage (%)</b>	<b>Gradient strength (G/cm)</b>
1	0.4815
10	4.815
20	9.63
30	14.445
40	19.26
50	24.075
60	28.89
70	33.705
80	38.52
90	43.335
95	45.7425

### 2.9.6 Pseudo 2D $^{15}\text{N}$ - $^1\text{H}$ HSQC- $R_2$

An HSQC-edited transverse relaxation (or  $^{15}\text{N}$ - $^1\text{H}$  HSQC- $R_2$ ) experiment was used to obtain the transverse relaxation rate of the  $^{15}\text{N}$  nuclei in the backbone of  $\alpha$ -synuclein. The 3D H/N correlation via double INEPT transfer (hsqct2etf3gpsi3d) pulse program was used on an NMR 600 MHz spectrometer at 25 °C. The experiments were run with the same O1 value as the 1D experiments and with 44 scans. The TD for the proton channel was 2048 and for the  $^{15}\text{N}$  channel was 128. The experiment was conducted at 8 variable delays. The relaxation delay times were 16, 32, 64, 96, 128, 160, 240, and 320 milliseconds.

The data were Fourier-transformed in 2D (xfb with squared sine multiplication window) into 8 HSQC spectra using TopSpin 4.1.4. The processed data were imported to NMRFAM-Sparky Software to assign the peaks and calculate the  $R_2$  values of each peak. In Sparky, the intensities of each peak were plotted against the delay times and fit to an exponential function.  $h = A \times \exp(-R \times t)$  where  $h$  is height, and  $t$  is the spectrum time delays. The best fit time constant  $T$  (rate constant  $R = 1/T$ ) was obtained, and  $R$  reported.

## 2.10 Microscopy

### 2.10.1 Confocal Fluorescence Microscopy

A buffer of Thioflavin T (ThT) fluorescence was prepared composed of 20  $\mu\text{M}$  ThT (Fisher), 20 mM Tris-HCl (Fisher), and 0.1 M NaCl at pH=7. Then three slides were prepared: 10

$\mu\text{L}$  of 0.2 mM  $\alpha$ -synuclein in the absence of crowders; 10  $\mu\text{L}$  of 0.2 mM  $\alpha$ -synuclein in the presence of 200 mg/mL Ficoll70; and 10  $\mu\text{L}$  of 0.2 mM  $\alpha$ -synuclein in the 200 mg/mL cell lysate after 72 hours incubation at 37 °C. 5  $\mu\text{L}$  of the ThT buffer was added to each slide and mixed with the samples. Each sample was sealed between a microscope slide and a coverslip using a SecureSeal™ imaging spacer. Images were captured by a Nikon C1 confocal microscope using a 100X (NA=1.4) oil-immersion objective and a 488 nm (blue) laser for excitation and dichroic filter that selected for green emission.

### **2.10.2 Scanning Electron Microscopy**

To obtain SEM images, three samples were prepared: 20  $\mu\text{L}$  of 0.2 mM  $\alpha$ -synuclein in the absence of crowders; 20  $\mu\text{L}$  of 0.2 mM  $\alpha$ -synuclein in the presence of 200 mg/mL Ficoll70; and 20  $\mu\text{L}$  of 0.2 mM  $\alpha$ -synuclein in the 200 mg/mL cell lysate after 72 hours incubation at 37 °C. The samples were loaded on carbon discs on SEM pin stubs. Then the samples were incubated at room temperature for 72 hours to be dried. The images were captured at the Micro Analysis Facility at Memorial University using a FEI MLA 650FEG scanning electron microscope.

## 3.0 Results

### 3.1. $^{15}\text{N}$ $\alpha$ -synuclein expression and purification

After expressing the recombinant  $\alpha$ -synuclein, the harvested *E. coli* cells were lysed and ultracentrifuged. The supernatant obtained from the ultracentrifuged cell lysate was added to the IMAC nickel column. The histag-GB1- $\alpha$ -synuclein construct should bind the resin while contaminants should pass through. Figure 3.1A shows the results of this purification step. As can be seen in the lanes marked "W1" and "W2" it appears that some of the  $\alpha$ -synuclein did not bind tightly to the column, likely because there was an insufficient amount of resin to bind all the  $\alpha$ -synuclein in the supernatant. Histag-GB-1- $\alpha$ -synuclein was eluted with 300 mM imidazole, and a large amount can be seen in the first two elution fractions (Lanes "E1" and "E2" in Figure 3.1A). The elution fractions also contained some contaminating proteins, but these were mostly removed in a subsequent purification step (Figure 3.1B).

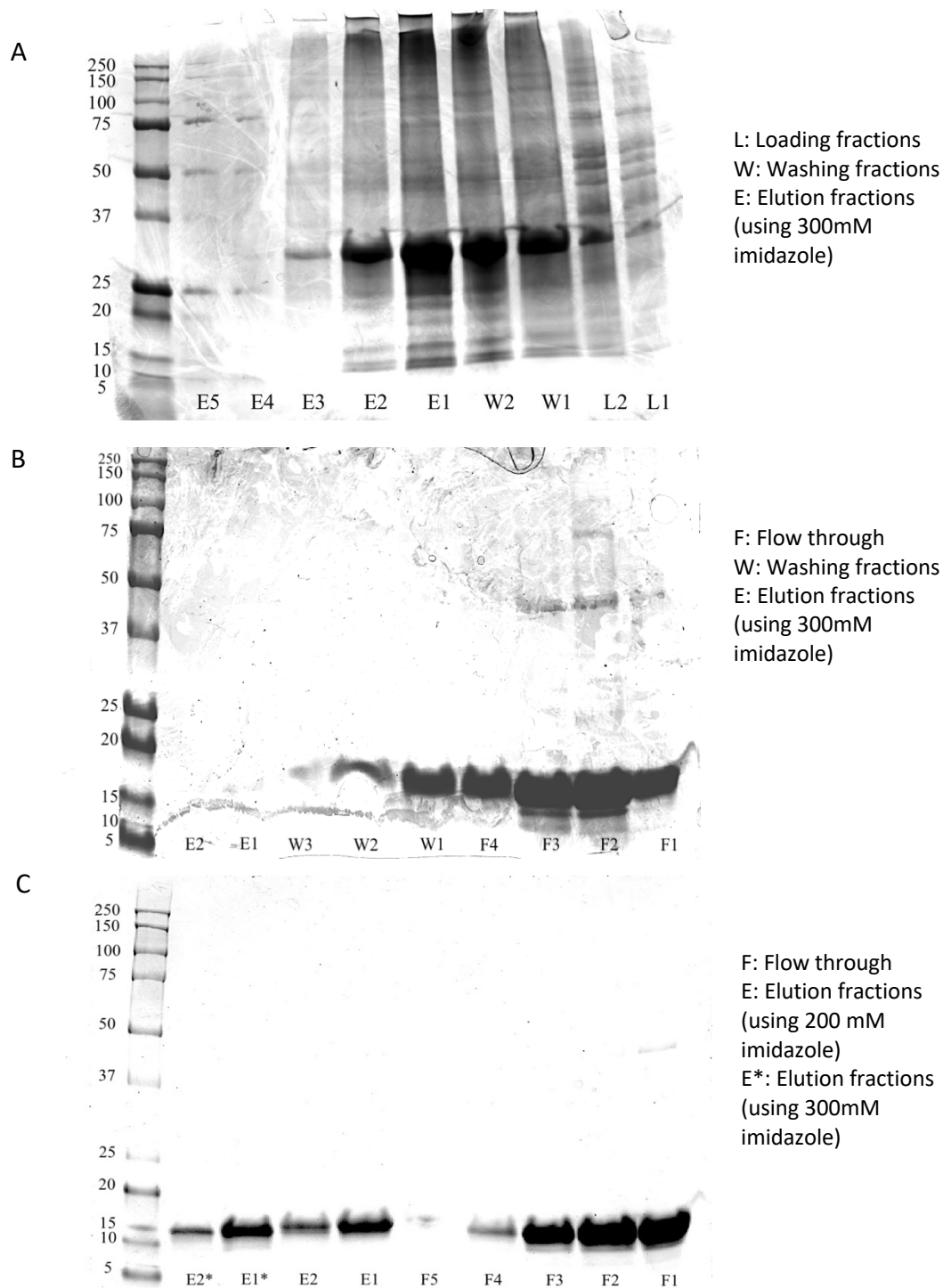


Figure 3.1) Gel electrophoresis showing  $\alpha$ -synuclein's purification: A) After first IMAC purification, B) After cleavage and second IMAC, C) after third IMAC. The molecular weight of  $\alpha$ -synuclein and GB-1 is 14 and 6.6 kDa, respectively. 12% precast polyacrylamide denaturing SDS gel was used for the gel electrophoresis. First lane (from left) is a molecular weight marker. After adding the protein suspension and collecting the flowthrough, loading buffer was added and then loading fractions were collected.

The histag-GB-1- $\alpha$ -synuclein that came off the column during the wash of the IMAC column was rescued by applying it to a fresh IMAC column. Therefore, the purest his-tag-GB-1- $\alpha$ -synuclein fractions from both IMACs were pooled and used in the next step. In the next step,  $\alpha$ -synuclein was enzymatically cleaved from the histag-GB-1 fusion protein. Next, the resulting material was applied to a new IMAC column and analyzed by SDS-PAGE (Figure 3.1B). The cleavage produced two products of the expected sizes, 14 kDa for  $\alpha$ -synuclein and 6.6 kDa GB-1, indicating cleavage was successfully performed (Figure 3.1B shows that  $\alpha$ -synuclein is observable in Flow through 1, 2, 3, and 4). In Figure 3.1B the elution fractions do not show any  $\alpha$ -synuclein's band because it doesn't have his-tag, and all  $\alpha$ -synuclein was washed into the flow-through and washing fractions.

The fractions (Flow through 1, 2, and 3 in Figure 3.1B) with  $\alpha$ -synuclein but contaminated by GB-1 were repurified with IMAC column to get pure  $\alpha$ -synuclein as much as possible. Considering the fact that we never can obtain 100% purified protein, I tried to get the purest sample as much as I could. Figure 3.1C shows that  $\alpha$ -synuclein after the third IMAC purification was isolated successfully, and because there were too much expressed  $\alpha$ -synuclein in the column we could see the protein's band even in the elution fractions. Figure 3.1C also shows that His-tag-TEV band is observable at E1, less than 10 kDa. In the fourth IMAC purification, I used different imidazole concentration steps (50, 150, 200, and 300 mM) to separate the GB-1 from the column. The purified  $\alpha$ -synuclein was dialyzed to reduce the amount of salts in their solution. Regarding the location of  $\alpha$ -synuclein's band in panel B and C, I should mention that there is no difference in size of these two bands, and because there is more protein in panel B, we see a thicker band

with a little different MW. It is a crucial step to reduce the amount of salts in the sample if we want to do NMR experiments; otherwise, tuning the NMR probe will be challenging.

In the next step, the concentration of  $\alpha$ -synuclein was measured by two different methods: absorbance at 280 nm and Bradford assay. As described below, both measurement techniques showed the same concentration of  $\alpha$ -synuclein.

The concentration of  $\alpha$ -synuclein derived from UV spectrophotometer absorbance measurement at OD 280 nm was 0.161 mM and from the nanodrop spectrophotometer absorbance measurement at OD 280 was 0.158 mM. The Bradford assay also agreed with the other values, indicating a concentration of 0.164 mM for  $\alpha$ -synuclein (Figure 3.2). However, this concentration was low for NMR spectrometry, and I used the protein concentrations of 0.2 mM. I tried different concentration of  $\alpha$ -synuclein, from 0.1 mM to 0.3 mM, and the best concentration that I obtain a high resolution NMR spectrum was 0.2 mM. Although given  $\alpha$ -synuclein's propensity to aggregate I did not want a concentration above 0.2 mM. Therefore, to increase the concentration, I tried to reduce the volume of water by two approaches: 1) using centrifugal filtration, 2) using a freeze dryer. The centrifugal filtered tubes did not work since most of the protein visibly stuck to the filter. It seems likely that since  $\alpha$ -synuclein is a disordered protein, it could stick to the filter's surface easily. However, the second approach was more successful, and I could increase the concentration of  $\alpha$ -synuclein up to 0.8 mM, but it is a very high concentration and can facilitate  $\alpha$ -synuclein's aggregation. Therefore, I increased the concentration up to 0.8 mM by Freeze-drying but immediately after that I dilute the concentration to 0.2 mM. Then  $\alpha$ -synuclein's structure was checked with HSQC experiments for samples before and after the freeze drying at the same concentration, both samples diluted to a concentration of 0.13 mM (a concentration that I can compare the structure of  $\alpha$ -synuclein before and after the freeze-drying), and pH 7 and 25 °C, and

no changes in chemical shifts were observed. Therefore, it implies that freeze drying does not change the structure of  $\alpha$ -synuclein. A key point here is after increasing the concentration of  $\alpha$ -synuclein up to 0.8 mM, it needs to be stored at  $-80\text{ }^{\circ}\text{C}$  or immediately dilute it to 0.2 mM since  $\alpha$ -synuclein above 0.2 mM concentration is more prone to aggregation at higher concentrations (Shtilerman, Ding, and Lansbury 2002).

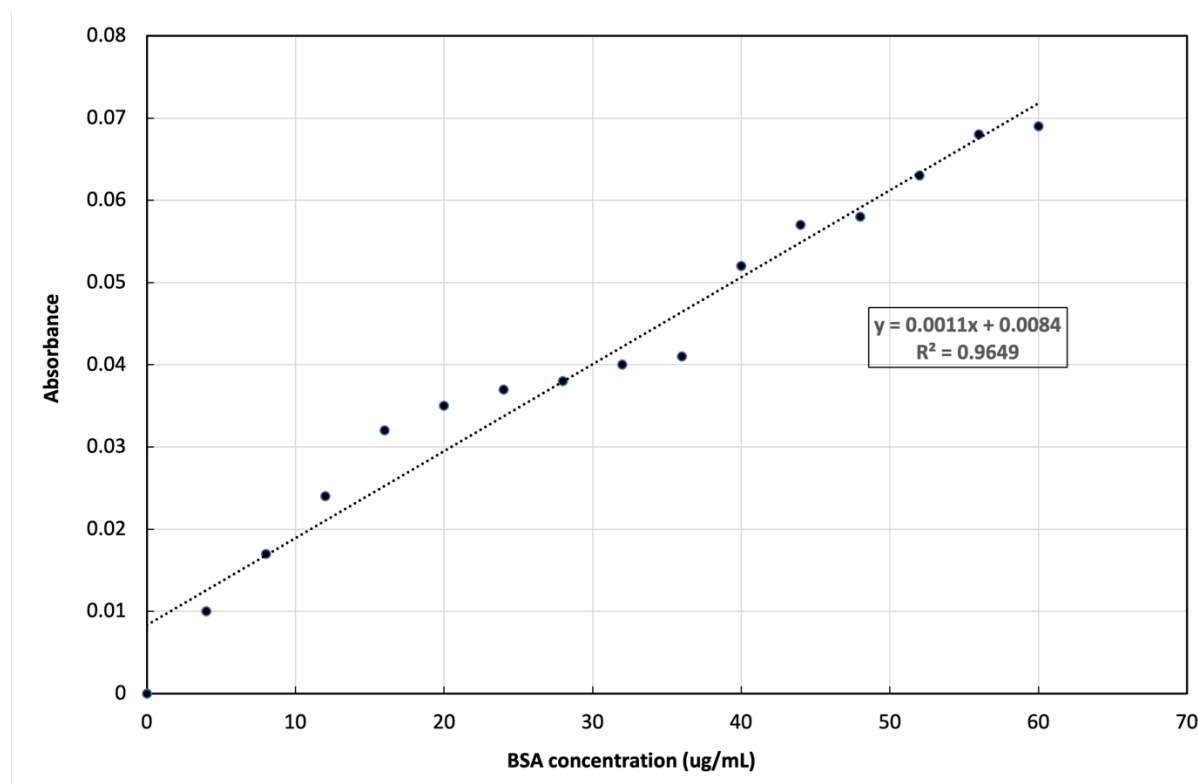


Figure 3.2) The Bradford standard curve for BSA used to obtain the concentration of  $\alpha$ -synuclein. The absorbance of  $\alpha$ -synuclein was 0.016, which based on the slope equation, it gives a concentration of 2.3 mg/mL (0.164 mM).

Increasing the concentration of  $\alpha$ -synuclein was done successfully, but eventually I adjusted its concentration to 0.2 mM for all experiments. I tried to perform an NMR experiment with 0.1 mM of  $\alpha$ -synuclein in the presence of crowders, but I couldn't obtain proper signals. I

also tried 0.3 mM  $\alpha$ -synuclein, but its signals were lost after a few hours, and I could see the cluster of  $\alpha$ -synuclein aggregations in my NMR tube. However, 0.2 mM of  $\alpha$ -synuclein worked well in both the absence and presence of crowders, and I could obtain appropriate NMR signal intensity and also keep the protein for many days without any aggregation. Therefore, after several trials of NMR experiments on  $\alpha$ -synuclein, I decided that 0.2 mM was an appropriate concentration and also is comparable to other studies.

### **3.2. Manipulating the hydrophobicity of the cell lysate and ultracentrifuged cell lysate**

First, I present the development of a novel means of manipulating the crowder to obtain crowder with altered hydrophobicity. Then in following sections I will indicate the results of different types of crowders on  $\alpha$ -synuclein. In order to probe the role of hydrophobic interactions in  $\alpha$ -synuclein conformation, I prepared cell lysate as a crowder and then modified its hydrophobicity by a hydrophobic interaction chromatography (HIC). The unmanipulated cell lysate was passed through a weakly hydrophobic HIC column, and highly hydrophobic particles of the cell lysate were expected to stick to the HIC resins; then I collected the less hydrophobic cell lysate. The important downside of this is it might also change the size distribution of the particles. After manipulating the hydrophobicity of the cell lysate, it was important to examine what actual properties of cell lysate were modified. Three approaches were picked to understand the effects of this manipulation on the cell lysate: 1) dry weight of the cell lysate before and after the manipulation, 2) hydrophobicity (by Bligh & Dyer), and 3) size distribution (by dynamic light scattering).

The mass of the cell lysate before and after the manipulation indicates how the cell lysate was modified by the manipulation. Table 3.1 shows that the cell lysate at totally lost approximately 18 % of its mass by passing through the HIC column. The mass for unmanipulated cell lysate before HIC was 200 mg. After the HIC, two fractions (two fractions were collected to compare the effects of column on them) were collected from the column. The first fraction has a higher weight ( $\approx 88$  mg), and the second fraction has a lower weight ( $\approx 75.7$  mg).

Table 3.1) Comparing the characteristics of the unmanipulated bacterial cell lysate and ultracentrifuged bacterial cell lysate before and after the HIC column.

Samples		Weight	Bligh & Dyer			Size of particles*
Unmanipulated cell lysate			Hydrophilic	Hydrophobic	Hydrophobic/ (Hydrophobic + Hydrophilic)	
Before HIC		200 mg	129.1 $\pm$ 27 mg	39.6 $\pm$ 13.6 mg	23 %	Peak 1: 711.5 $\pm$ 152.9 d.nm Peak 2: 68.68 $\pm$ 10.71 d.nm
After HIC	Fraction 1 (less hydrophobic)	88 $\pm$ 11.4 mg	61.8 $\pm$ 16.6 mg	11.7 $\pm$ 2.5 mg	16 %	Peak 1: 497 $\pm$ 95.47 d.nm Peak 2: 44.67 $\pm$ 6.618 d.nm
	Fraction 2 (More hydrophobic)	75.7 $\pm$ 22.2 mg	53.5 $\pm$ 19.2 mg	13.4 $\pm$ 4.8 mg	20 %	Peak: 357 $\pm$ 30.11 d.nm
Ultracentrifuged cell lysate			Hydrophilic	Hydrophobic		
Before HIC		200 mg	133.5 $\pm$ 5 mg	38.2 $\pm$ 11.7mg	22 %	Peak 1: 314.3 $\pm$ 142.8 d.nm Peak 2: 70.75 $\pm$ 25.18 d.nm Peak 3: 4.84 $\pm$ 7.03 d.nm
After HIC	Fraction 1 (less hydrophobic)	82.8 $\pm$ 3.9 mg	54.5 $\pm$ 1.5 mg	10.3 $\pm$ 0.5 mg	16 %	Peak 1: 377.5 $\pm$ 83.93 d.nm Peak 2: 42.36 $\pm$ 6.322 d.nm
	Fraction 2 (More hydrophobic)	80.5 $\pm$ 0.7 mg	48.9 $\pm$ 0.4 mg	12.8 $\pm$ 3.9 mg	21 %	Peak 1: 214.6 $\pm$ 41.97 d.nm Peak 2: 26.15 $\pm$ 3.641 d.nm

The size of particles was measured by Dynamic Light Scattering (DLS). Data were replicated two times and are provided as mean  $\pm$  standard deviation.\*For more information about particles' size distribution, refer to Figure 3.3.

The Bligh & Dyer technique, which is a standard method to measure the hydrophobicity of solution, indicated that around 23 % of the whole unmanipulated cell lysate is hydrophobic particles (top row of table 3.1), and 16 % and 20 % of the first and second collected fractions from HIC column is hydrophobic, respectively (row 2 and 3 of Table 3.1). The second fraction is more hydrophobic potentially because the capacity of column for keeping hydrophobic particles became lower for the second fraction. This implies that the first fraction's hydrophobicity had been reduced by 7 % compared to the unmanipulated cell lysate, and the second fraction's hydrophobicity had been reduced by 3 %. Therefore, as expected the hydrophobicity of the first fraction was reduced more than the second fraction. Perhaps the presence of large components and the high viscosity of the cell lysate decreased the ability of the column to separate more hydrophobic particles. The hydrophobicity's change might not be very considerable, but even this small manipulation affected our protein's dynamics substantially that will be shown in section 3.7.

The DLS data (Figure 3.3) showed that the size distribution for the unmanipulated cell lysate is a broad distribution with two peaks at 711.5 and 68.68 nm. After passing through the HIC column, the fraction 1 has a somewhat narrower distribution with two peaks at 497 and 44.67 nm, and the fraction 2 has a peak at 357 nm (Table 3.1). The size of the particles was reduced by 40% and 50% in the fraction 1 and 2, respectively. It is concluded that the size of both fractions was affected substantially by passing through the weakly hydrophobic HIC column. However, based on the DLS data, the fraction 2 lost more of its big particles than the fraction 1. Because the aim was to change only the hydrophobicity of the cell lysate, not the size of particles, the fraction 1, in terms of size, was closer to the unmanipulated cell lysate. Therefore, since the fraction 1 is less

hydrophobic and has a closer size of particles to the unmanipulated cell lysate, it was chosen as a “less hydrophobic bacterial cell lysate”, for this study.

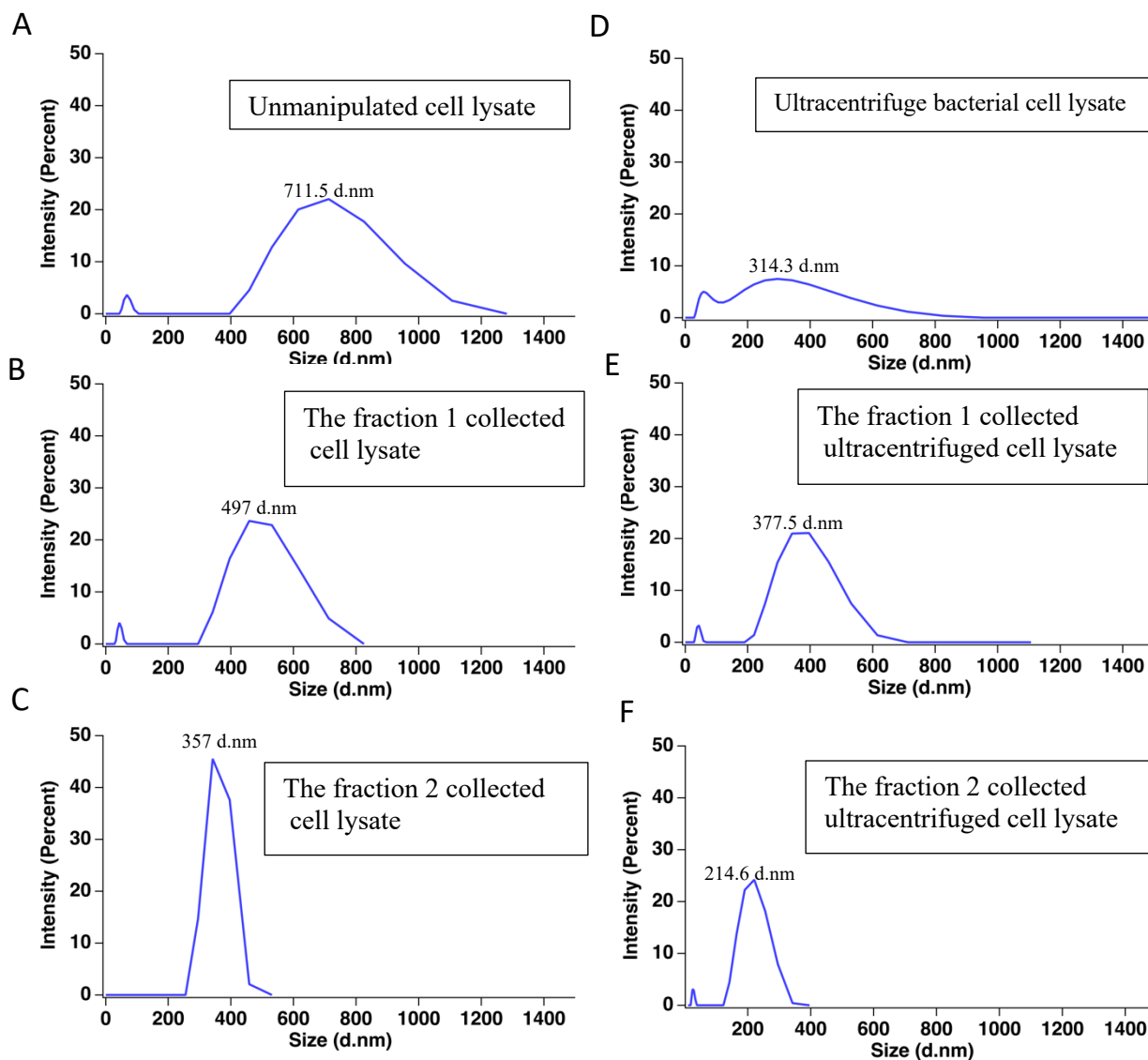


Figure 3.3) The size distribution (by intensity) of macromolecules in the bacterial cell lysate crowder. A) Unmanipulated cell lysate. B) The fraction 1 collected bacterial cell lysate from HIC. C) The fraction 2 collected bacterial cell lysate from HIC. D) Ultracentrifuged bacterial cell lysate. E) The fraction 1 collected ultracentrifuged bacterial cell lysate from HIC. F) The fraction 2 collected ultracentrifuged bacterial cell lysate from HIC.

The second manipulation that was performed on the cell lysate was ultracentrifuging the cell lysate and manipulating the hydrophobicity of the ultracentrifuged cell lysate by passing it through a weakly hydrophobic HIC column. In this way, by removing the large particles via ultracentrifugation, it is possible to reduce the change in size before and after HIC. Therefore, all three approaches mentioned above, weight, Bligh & Dyer, and DLS, were re-performed on the ultracentrifuged cell lysate before and after passing through a HIC column.

The data (Table 3.1) shows the size distribution for the ultracentrifuged cell lysate is a broad distribution with three peaks at 341.3, 70.75, and 4.84 nm. By passing the ultracentrifuged cell lysate through the HIC column the first fraction has two peaks at 377.5 and 42.36 nm. The second collected fraction has two peaks at 241.6 and 26.15 nm. The ultracentrifuged cell lysate lost 18.5% of its weight after passing through the HIC column, and there is no substantial difference in the weight of the first and second fractions. The Bligh and Dyer data showed that 22 % of the ultracentrifuged cell lysate comprises hydrophobic particles. The first and second collected fractions of the HIC column contained 16 % and 21 % hydrophobic particles. The DLS data (Table 3.1 & Figure 3.3) indicates that the size of particles in the first collected fraction ( $377.5 \pm 83.93$  d.nm) was closer to the ultracentrifuged cell lysate ( $314.3 \pm 142.8$  d.nm), and the size of the particles in the second fraction ( $214.6 \pm 41.97$  d.nm) was reduced by 30%. Thus, the first fraction has lower hydrophobicity and is more similar to the ultracentrifuged cell lysate in terms of particle size. As I only want to change the hydrophobicity of the ultracentrifuged cell lysate, the first fraction was chosen for the experiments in this study. The weight and Bligh & Dyer measurements were performed two times for all samples to indicate the reproducibility of the data.

### 3.3 Structure of $\alpha$ -synuclein with and without crowder

Three samples with 0.2 mM  $\alpha$ -synuclein were prepared: in the absence of crowders; in the presence of 200 mg/mL Ficoll70; and in the presence of 200 mg/mL cell lysate. The pH of all samples was adjusted to 7.  $^{15}\text{N}$ - $^1\text{H}$  HSQC experiments were performed at 37 °C immediately after preparing the samples. 1D  $^1\text{H}$  of these  $\alpha$ -synuclein in no crowding condition (Figure S1), in the presence of cell lysate (Figure S2), in the presence of Ficoll (Figure S3) are shown in the Appendix I.  $^{15}\text{N}$ - $^1\text{H}$  HSQC measurements were also performed again at 48 and 72 hours after the first experiment to assess how the samples changed over time. Samples were kept in an incubator at 37 °C between the HSQC measurements.

Figure 3.4A is the HSQC spectrum for  $\alpha$ -synuclein in the absence and presence of crowders at 0 hours. The  $^{15}\text{N}$ - $^1\text{H}$  HSQC results (Fig 3.4A) and quantification of the HSQC peaks (Table 3.2) indicate that the freshly made-up  $\alpha$ -synuclein samples are similar in the absence and in the presence of both Ficoll and cell lysate in both their  $^{15}\text{N}$  chemical shifts shown in Figure 3.4B (The details of the peak assignment are explained in section 3.5) as a function of residue number ( $^{15}\text{N}$  r.m.s chemical shift difference  $\sim 0.5$  ppm), and their  $^1\text{H}$  chemical shifts shown in Figure 3.4C ( $^1\text{H}$  r.m.s chemical shift difference  $\sim 0.02$  ppm). The r.m.s chemical shift difference for the  $\alpha$ -synuclein residues in the cell lysate when compared to Ficoll70 is also  $\sim 0.02$  ppm. Therefore, there were no large changes in chemical shift, and most residues had a change in chemical shift less than 0.02 ppm for  $^1\text{H}$  and less than 0.5 ppm for  $^{15}\text{N}$  indicating no large structural changes. However, there are several peaks, K34, V37, K45, and Q79, that experience small displacement in their proton chemical shift in the presence of crowders. They change enough ( $^1\text{H}$  chemical shift difference  $> 0.02$  ppm;  $^{15}\text{N}$  chemical shift difference  $> 0.5$  ppm) to indicate an alteration in their

electronic environment which could be either a change in the structure of  $\alpha$ -synuclein or its proximity to crowder.

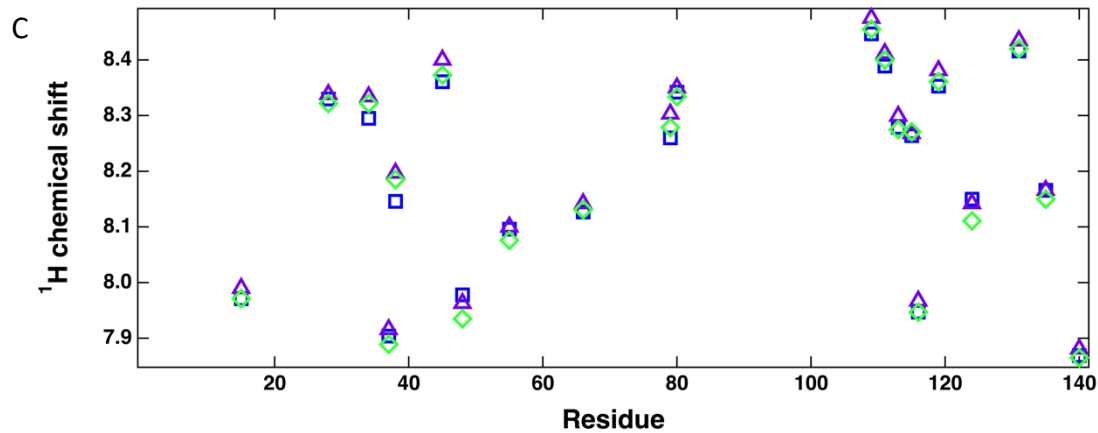
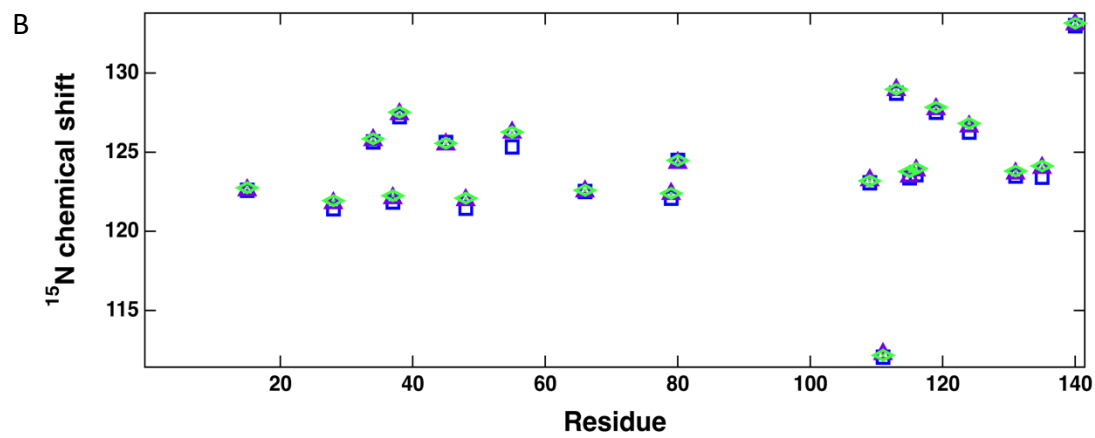
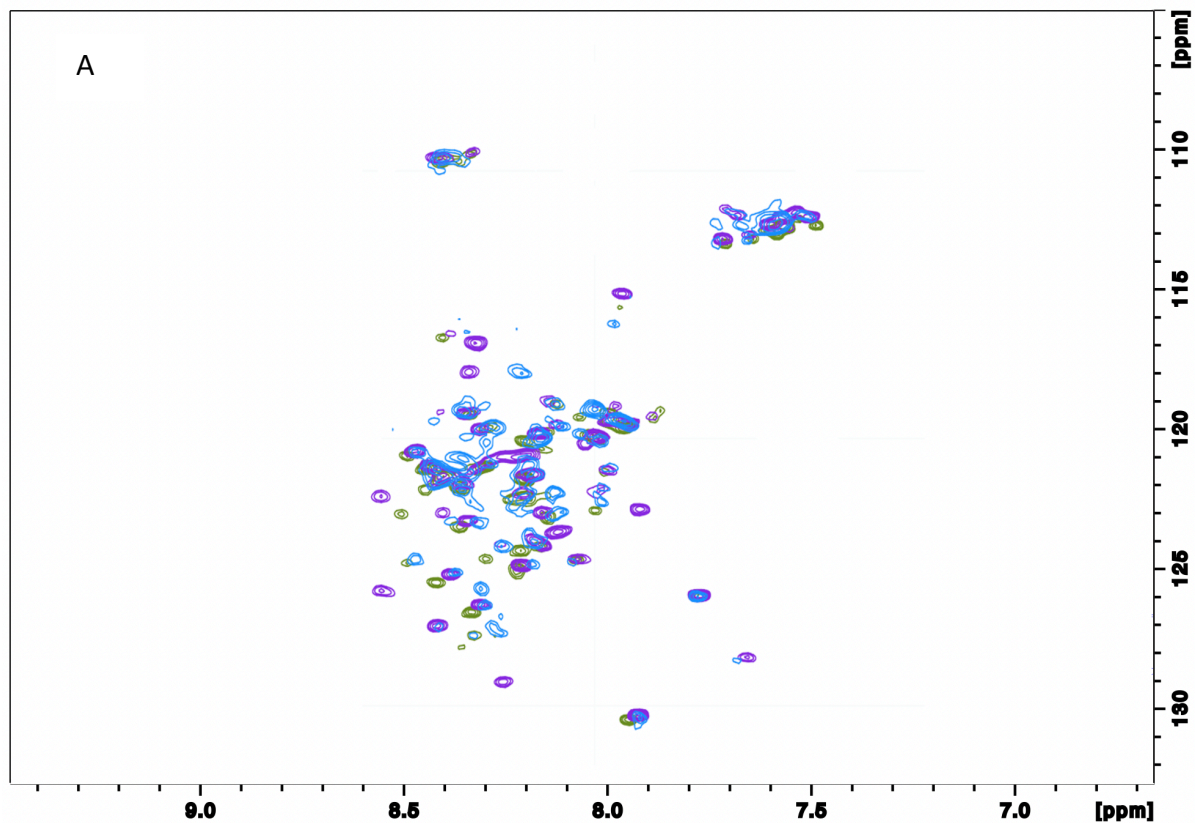


Figure 3.4) A)  $^{15}\text{N}$ - $^1\text{H}$  HSQC spectra of 0.2 mM  $\alpha$ -synuclein in the absence (green) and presence of 200 mg/ml Ficoll70 (purple) and bacterial cell lysate (blue) at 0 hours, 37 °C, and pH 7. The contour levels are the same in all spectra, and the spectra are obtained at a  $^1\text{H}$  frequency of 500 MHz with 128 scans. B)  $^{15}\text{N}$  chemical shift of residues in three conditions: no-crowders (green), in the presence of Ficoll70 (purple), and in the presence of cell lysate (blue). C)  $^1\text{H}$  chemical shift of residues in three conditions: no-crowders (green), in the presence of Ficoll70 (purple), and in the presence of cell lysate (blue). Some peaks in A could not be assigned.

Table 3.2) Chemical shift in  $^{15}\text{N}$ - $^1\text{H}$  HSQC spectra of 0.2 mM  $\alpha$ -synuclein in the absence of crowders, presence of 200 mg/mL Ficoll70, and presence of 200 mg/mL bacterial cell lysate at 37 °C and pH 7.

Residue	No crowder		Cell lysate		Ficoll	
	$^1\text{H}$ (ppm)	$^{15}\text{N}$ (ppm)	$^1\text{H}$ (ppm)	$^{15}\text{N}$ (ppm)	$^1\text{H}$ (ppm)	$^{15}\text{N}$ (ppm)
Y15	7.971	122.761	7.971	122.605	7.99	122.605
E28	8.322	121.941	8.33	121.433	8.338	121.784
K34	8.322	125.847	8.295	125.652	8.334	125.769
V37	7.889	122.253	7.904	121.862	7.916	122.097
L38	8.185	127.527	8.146	127.254	8.197	127.41
K45	8.373	125.574	8.361	125.613	8.4	125.496
V48	7.935	122.097	7.978	121.472	7.963	121.98
V55	8.076	126.277	8.096	125.339	8.1	126.238
V66	8.131	122.605	8.127	122.527	8.142	122.527
Q79	8.279	122.409	8.26	122.097	8.303	122.37
K80	8.334	124.48	8.342	124.48	8.35	124.324
Q109	8.455	123.191	8.447	123.074	8.475	123.23
G111	8.4	112.174	8.389	112.057	8.412	112.252
L113	8.275	128.973	8.279	128.738	8.299	128.934
D115	8.271	123.777	8.264	123.386	8.268	123.464
M116	7.947	123.972	7.947	123.581	7.967	123.855
D119	8.361	127.84	8.353	127.527	8.381	127.722
A124	8.111	126.824	8.15	126.277	8.142	126.629
E131	8.42	123.816	8.416	123.503	8.435	123.66
D135	8.15	124.128	8.166	123.425	8.166	124.011
A140	7.865	133.153	7.869	132.997	7.881	133.075

Chemical shift differences are considered significant if they are greater than  $\pm 0.5$  ppm for  $^{15}\text{N}$  and  $\pm 0.02$  ppm for  $^1\text{H}$ .

$\alpha$ -synuclein's HSQC spectra in the absence and presence of Ficoll70 remained the same after 48 and 72 hours of incubation at 37 °C (Figure 3.4). However, unlike in Ficoll, in cell lysate all peaks were lost after 48 hours, most likely due to aggregation.

To look for direct evidence of aggregation, the NMR samples were examined by fluorescent confocal microscopy for any possible aggregations. Thioflavin T (ThT) fluorescent (Fisher) stain was added to the samples to indicate amyloid fibrillation. Fig 3.5 shows confocal microscopy images of  $\alpha$ -synuclein in the absence of crowders using a 488 nm (blue) laser for excitation and dichroic filter that selected for green emission (Fig 3.5A), in the presence of 200 mg/mL Ficoll70 (Fig 3.5B), and in the presence of 200 mg/mL bacterial cell lysate (Fig 3.5C) after 72 hours incubation at 37 °C and pH 7. No considerable aggregation was observed either in no-crowding conditions (Fig 3.5A) or in the presence of Ficoll70 (Fig 3.5B). Fig 3.5C shows, however, that in the presence of cell lysate there is an abundance of fluorescent signal which come from the cell lysate, but also some clusters of aggregates around 3  $\mu$ m in size were observed which is possibly a sign of  $\alpha$ -synuclein's cluster.

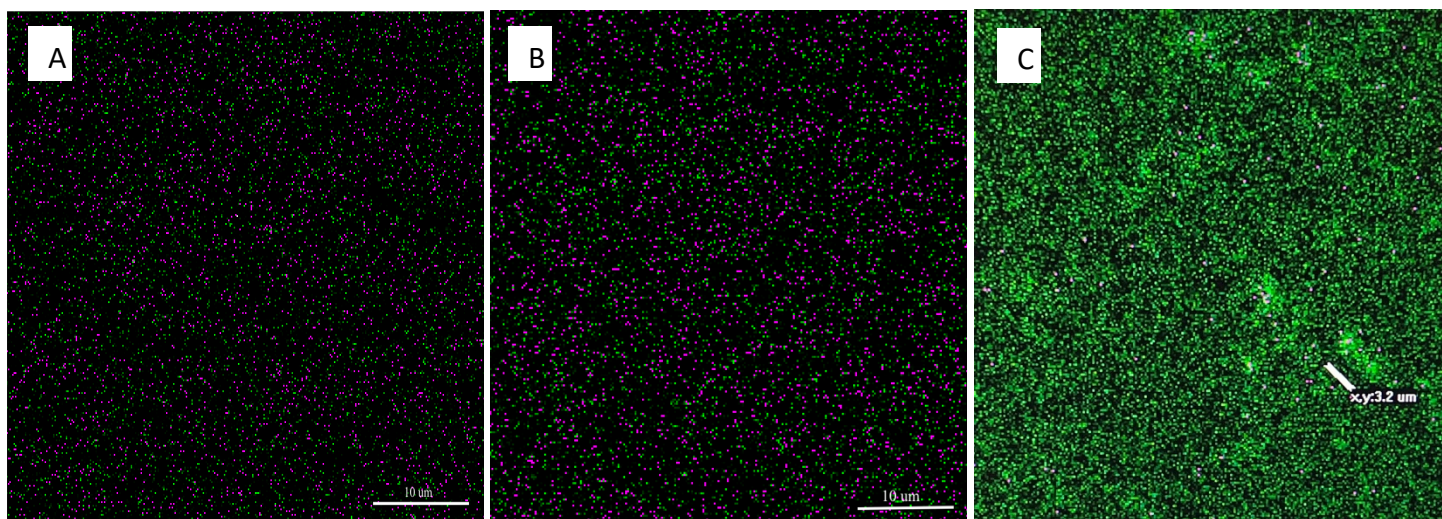


Figure 3.5) Confocal microscopy of  $\alpha$ -synuclein and ThT fluorescence A) in the absence of crowders, B) in the presence of 200 mg/mL Ficoll70, and C) in the presence of 200 mg/mL bacterial cell lysate after 72 hours incubation at 37 °C and pH 7. Samples were prepared immediately after 72 hours NMR experiments. Thioflavin T fluorescent dyes were used as a stain.

In an attempt to get a better resolution of  $\alpha$ -synuclein's aggregates in the cell lysate, Ficoll70, and no-crowding conditions, Scanning Electron Microscopy (SEM) was used on these three samples after 72 hours of incubation at 37 °C. Figure 3.6 shows that SEM was not an ideal method to look at the aggregation since the salt concentration, Tris buffer, in the samples was relatively high so that I could not recognize fibrils in the samples.

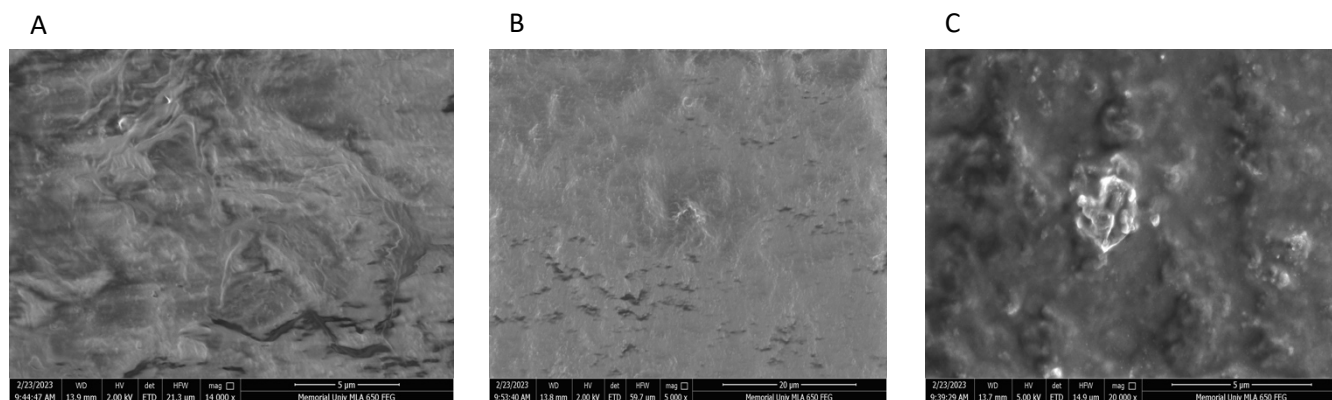


Figure 3.6) Scanning electron microscopy of 0.2 mM  $\alpha$ -synuclein in the A) in the absence of crowders B) in the presence of 200 mg/mL Ficoll70, C) in the presence of 200 mg/mL bacterial cell lysate after 72 hours incubation at 37 °C and pH 7. Samples were prepared immediately after 72 hours NMR experiments.

I also reduced the hydrophobicity of the cell lysate and repeated the HSQC experiment with  $\alpha$ -synuclein in the presence of 200 mg/mL less hydrophobic cell lysate at 25 °C and pH 7. The  $^{15}\text{N}$ - $^1\text{H}$  HSQC spectrum of  $\alpha$ -synuclein in the less hydrophobic cell lysate has similar chemical shifts as unmanipulated cell lysate (Figure 3.7). Therefore, the structure of  $\alpha$ -synuclein in the less hydrophobic cell lysate remains the same as the unmanipulated cell lysate.

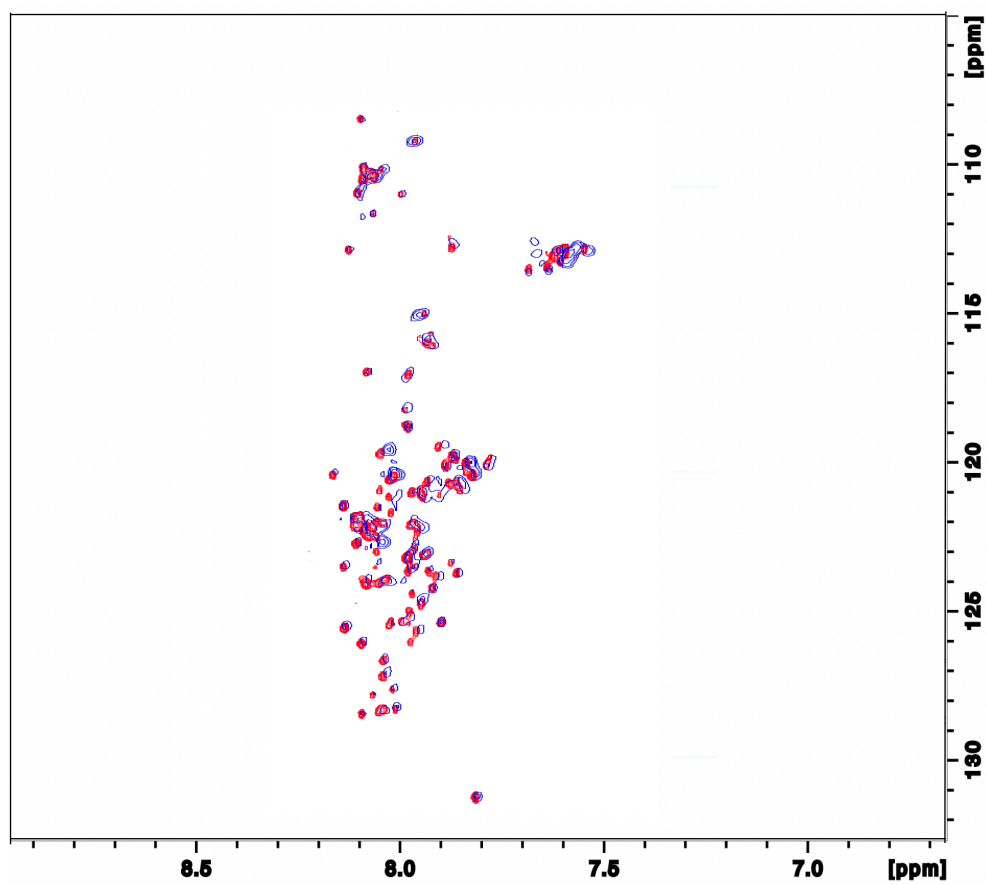


Figure 3.7)  $^{15}\text{N}$ - $^1\text{H}$  HSQC spectra of 0.2 mM  $\alpha$ -synuclein in the presence of 200 mg/mL unmanipulated cell lysate (blue) and 200 mg/mL less hydrophobic cell lysate (red) at 25 °C and pH 7. The contour levels are the same in all spectra, and the spectra are obtained at a  $^1\text{H}$  frequency of 600 MHz with 128 scans.

Now the question is: why does cell lysate cause faster aggregation of  $\alpha$ -synuclein relative to Ficoll70? I hypothesized that various types of soft interactions between the cell lysate and  $\alpha$ -synuclein, which is more than between Ficoll and the protein, accelerate the aggregation process. Next, I examine  $\alpha$ -synuclein's diffusion and internal backbone dynamics in order to understand if there are any plausible soft interaction effects of biological crowders on  $\alpha$ -synuclein.

### 3.4 $^{15}\text{N}$ - $^1\text{H}$ Diffusion of $\alpha$ -synuclein

In this study,  $^{15}\text{N}$ -edited spectra (Figure 3.8A) were used to obtain translational diffusion coefficients for  $^{15}\text{N}$ -labelled  $\alpha$ -synuclein (Figure 3.8B and C) at 25 °C. The reason that I switched from 37 °C to 25 °C is to delay the aggregation process so that I have more time to focus on the diffusivity of  $\alpha$ -synuclein's monomer. The signal attenuations in Figure 3.8B exhibit two exponential decay components: a fast decay at lower gradients that can only be consistent with single  $^{15}\text{N}$ -labelled residues or other  $^{15}\text{N}$ -labelled metabolites, and a slower decay at higher gradients that is consistent with protein diffusion. The protein diffusion coefficient value I obtained for  $\alpha$ -synuclein (Fig 3.8B) without crowder is  $(1.49 \pm 0.06) \times 10^{-10} \text{ m}^2/\text{s}$ .

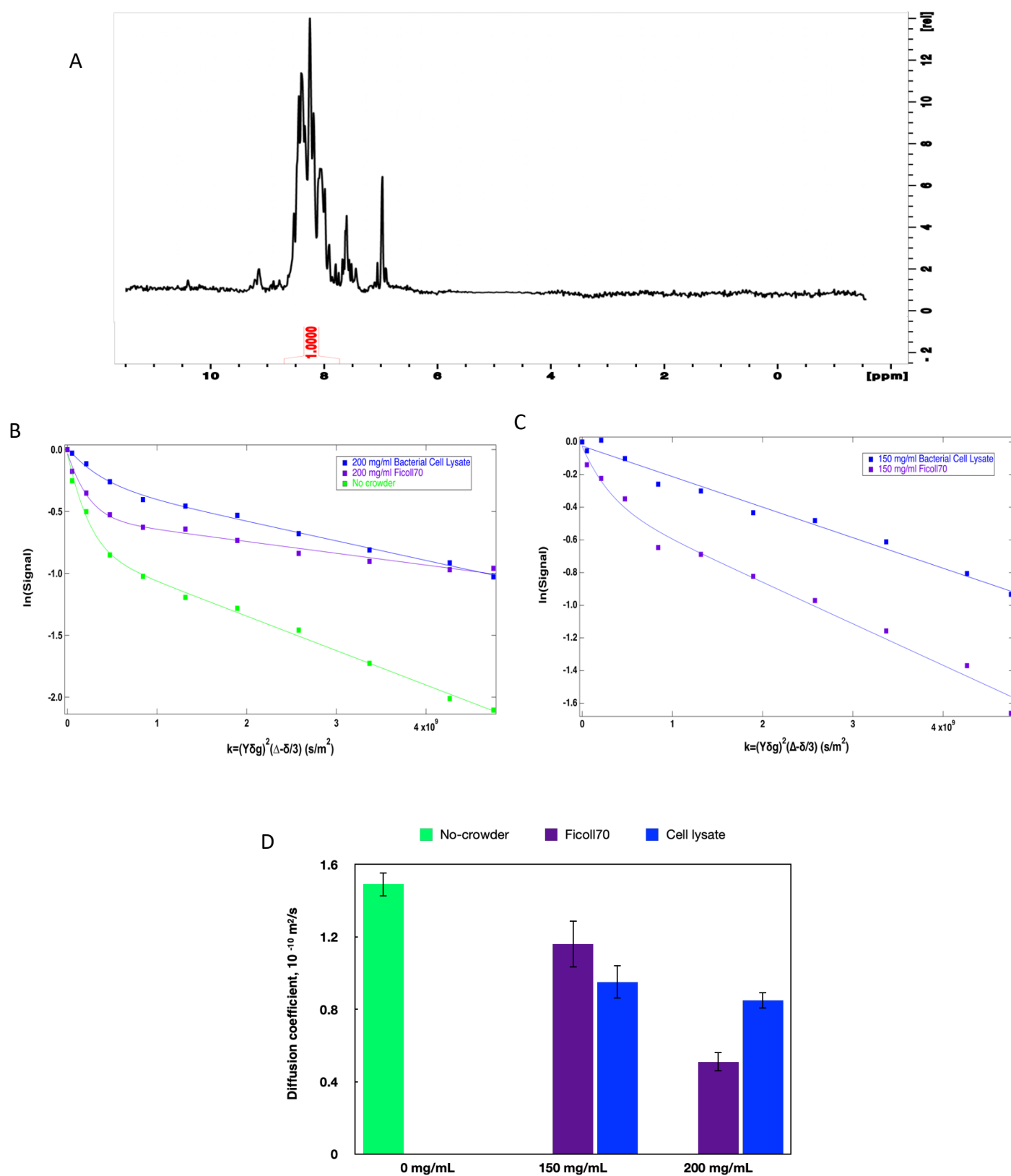


Figure 3.8) Translational diffusion of 0.2 mM  $\alpha$ -synuclein in dilute solution and in the presence of 200 mg/mL unmanipulated bacterial cell lysate and Ficoll70 at 25 °C and pH 7. Diffusion coefficients of  $\alpha$ -

synuclein are obtained by  $^{15}\text{N}$ - $^1\text{H}$  HSQC-DOSY experiments at a  $^1\text{H}$  frequency of 500 MHz NMR with 2560 scans. A) 1D  $^{15}\text{N}$ - $^1\text{H}$  DOSY spectrum of  $^{15}\text{N}$ -enriched  $\alpha$ -synuclein in a no-crowding condition. The integrated intensity between 7.73-8.70 ppm is used to plot the attenuated signal decay on a logarithmic scale versus the gradient strength. Gradient strength ranged from 0.48 to 45.74 G/cm. B) Attenuated signal decay versus the gradient strength parameter with and without 200 mg/mL crowders.  $\gamma$  is the gyromagnetic ratio,  $\delta$  is the duration of the gradient pulse,  $g$  is the gradient strength, and  $\Delta$  is the delay between gradient pulses. The bi-exponential equation,  $S(k)/S(0) = f \exp(-D_{fast}k) + (1 - f) \exp(-D_{slow}k)$ ,  $f$  is allowed to vary, is used to fit the points. C) Attenuated signal decay versus the gradient strength parameter with and without 150 mg/mL crowders. D) Bar graphs depict the comparison of  $\alpha$ -synuclein diffusion value (the slow components of panel B) in different crowded conditions. The error bars represent the standard deviation of the fit to the biexponential.

The diffusion values indicate that  $\alpha$ -synuclein diffuses slower in the presence of crowders compared to the no-crowding condition. At lower concentration (150 mg/mL), it is seen that  $\alpha$ -synuclein has a similar diffusion coefficient in the two crowders,  $(0.95 \pm 0.09) \times 10^{-12} \text{ m}^2/\text{s}$  in the cell lysate and  $(1.16 \pm 0.01) \times 10^{-12} \text{ m}^2/\text{s}$  in the Ficoll70. Because there is no sign of fast component in the presence of 150 mg/mL cell lysate, I fit the plot to a line function. At 200 mg/mL, however,  $\alpha$ -synuclein diffuses faster in bacterial cell lysate,  $(0.85 \pm 0.04) \times 10^{-12} \text{ m}^2/\text{s}$ , than in Ficoll70,  $(0.51 \pm 0.05) \times 10^{-12} \text{ m}^2/\text{s}$  (Figure 3.8D). All diffusion values of  $\alpha$ -synuclein are summarized in Table 3.3.

Figure 3.8B shows a fast component in the sample. The diffusion of fast components is quite similar in no-crowding condition and in the presence of 200 mg/mL Ficoll70. The diffusion of the fast component is  $3.04 \times 10^{-9} \text{ m}^2/\text{s}$  in the absence of crowders and  $2.81 \times 10^{-9} \text{ m}^2/\text{s}$  in the presence of 200 mg/mL Ficoll70. However, in the presence of 200 mg/mL cell lysate it was slowed down to  $1.61 \times 10^{-9} \text{ m}^2/\text{s}$ . Therefore, we can see that the fast component's diffusion decreased substantially in the presence of cell lysate compared to the presence of Ficoll70.

Table 3.3) The diffusion coefficient of 0.2 mM  $\alpha$ -synuclein (the slow component of the signal attenuations, three of which are shown in Figure 3.8B) in the presence and absence of crowders at 25 °C on NMR 500 MHz.

Sample	200 mg/ mL	150 mg/mL
<b>No-crowder</b>	$(1.49 \pm 0.06) \times 10^{-10} \text{ m}^2/\text{s}$	
<b>Cell lysate</b>	$(0.85 \pm 0.04) \times 10^{-12} \text{ m}^2/\text{s}$	$(0.95 \pm 0.09) \times 10^{-12} \text{ m}^2/\text{s}$
<b>Ficoll70</b>	$(0.51 \pm 0.05) \times 10^{-12} \text{ m}^2/\text{s}$	$(1.16 \pm 0.01) \times 10^{-12} \text{ m}^2/\text{s}$

### 3.5 $\alpha$ -synuclein $^{15}\text{N}$ - $^1\text{H}$ HSQC spectrum peak assignment

Peak assignment for  $\alpha$ -synuclein's  $^{15}\text{N}$ - $^1\text{H}$  HSQC spectrum (Figure 3.9) was performed based on previously published data (Sivanesam et al. 2015; Wu and Baum 2011). The approximate frequency and position of the peaks was considered for peak assignment. Peak assignment was performed at both 25 °C and 37 °C. However, peaks were more isolated and distinguishable at 25 °C than in the 37 °C. Thus, I could assign most of the peaks at 25 °C, not most of the residues.

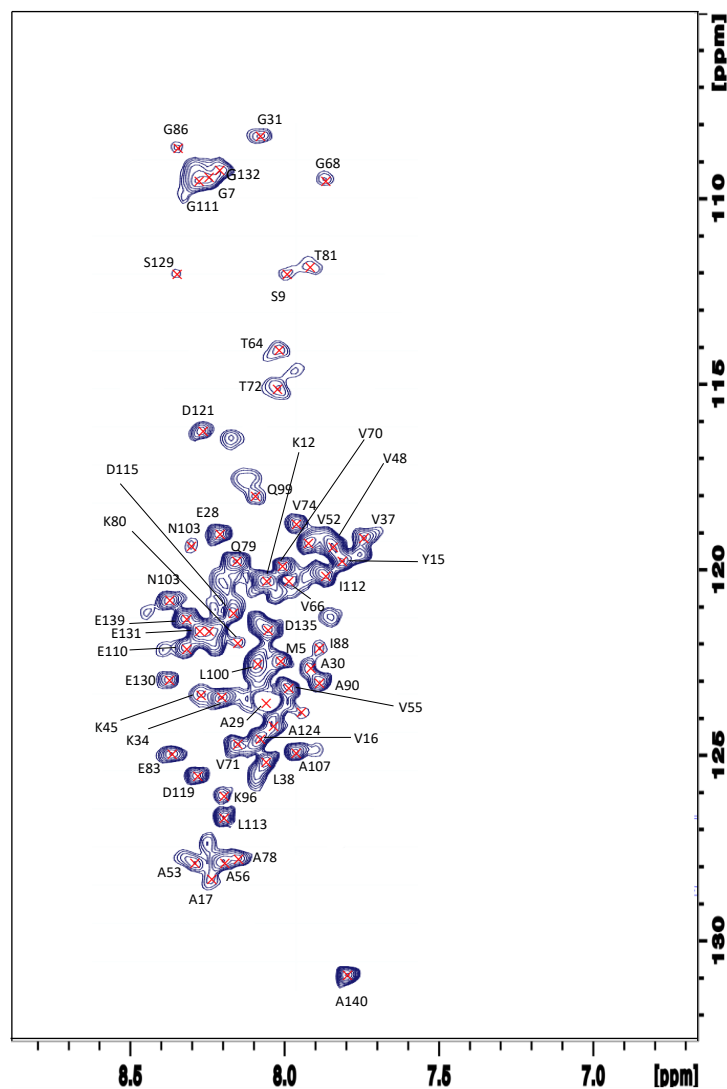


Figure 3.9) Assigned residues of  $^{15}\text{N}$ - $^1\text{H}$  HSQC spectrum of 0.2 mM  $\alpha$ -synuclein at 25 °C and pH 7, and the spectrum is obtained at a  $^1\text{H}$  frequency of 600 MHz. Residues are labelled with the 1-letter amino acid code and based on the published papers (Wu and Baum 2011; Sivanesam et al. 2015). Most peaks on the spectrum (58 peaks) could be assigned.

### **3.6 $\alpha$ -synuclein $^{15}\text{N}$ - $^1\text{H}$ $R_2$ relaxation in the absence and presence of Ficoll70 and bacterial cell lysate**

In this study, the  $R_2$  relaxation rate of  $\alpha$ -synuclein was measured in the absence and presence of the crowders. The  $R_2$  value was obtained from the intensity of each peak at different delay times (16, 32, 64, 96, 128, 160, 240, and 320 milliseconds). Figure 3.10 shows the signal attenuation of selected residues. I selected residues with strong (G7), medium (A90 and D119), and weak (A140) peaks to show the difference in their intensity decays and the fitting.

The intensities all exhibit a good fit to an exponential function versus the delay times. From this fit, I can extract the transverse relaxation time  $T_2$ ; however, I report  $R_2$  ( $R_2=1/T_2$ ).

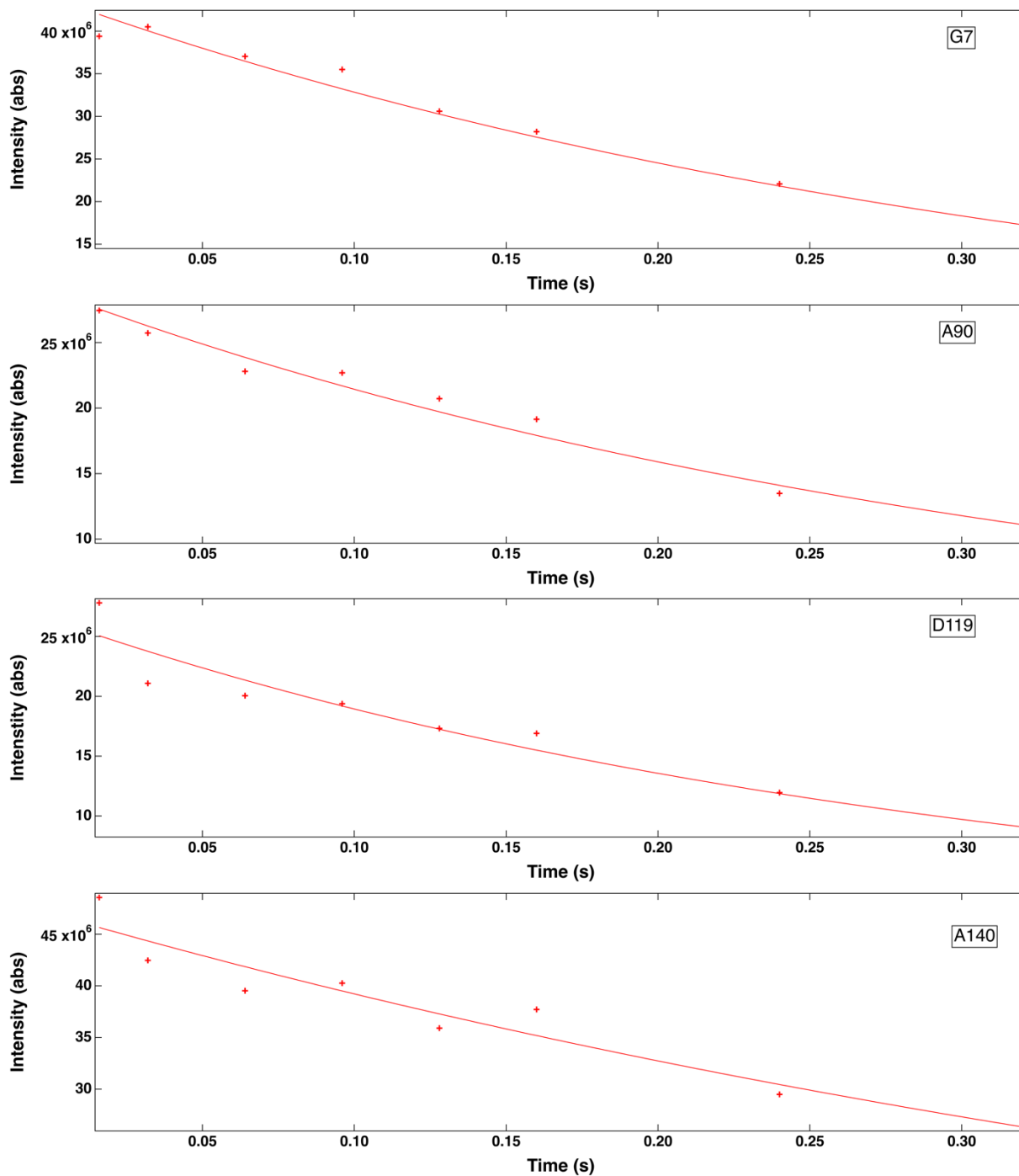


Figure 3.10) T<sub>2</sub> decay of α-synuclein's residues. The variable delay times are 16, 32, 64, 96, and 128, 240, and 320 milliseconds. The fitting results in Igor software is completely compatible with Sparky's fitting results (the difference is  $\sim \pm 0.05$  s). The intensity decay versus time fitted exponentially.

Figure 3.11A plots the  $^{15}\text{N}$ - $^1\text{H}$  transverse relaxation rate  $R_2$  as a function of residue number: the value varies in the range of  $\sim 2$  to  $5 \text{ s}^{-1}$ . It is observed that  $\alpha$ -synuclein has a higher relaxation rate for several residues in the Ficoll70 and cell lysate than in the no-crowding condition, which implies slower rotational mobility of the residues in either crowded condition compared to dilute condition (Figure 3.11C and D). Figure 3.11C and D compares  $\alpha$ -synuclein residues'  $R_2$  in cell lysate and Ficoll, respectively, versus in the absence of crowder, and the blue line is a linear fit. Figure 3.11E compares  $R_2$  in the less hydrophobic cell lysate versus unmanipulated cell lysate. 33% of residues of  $\alpha$ -synuclein in Ficoll70 had a higher  $R_2$  value than in without crowder and 67% were the same (within error bars). 30% of  $\alpha$ -synuclein residues in the cell lysate had a higher relaxation rate than in the no-crowding condition, while 52% and 18% had the same and lower  $R_2$  value, respectively. This higher relaxation rate is more observable in the N terminal region (1-60 residues) (Figure 3.11A) which had an average of  $2.87 \pm 0.22 \text{ s}^{-1}$  without crowding and  $3.54 \pm 0.30$  and  $3.30 \pm 0.27 \text{ s}^{-1}$  in the presence of cell lysate and Ficoll70, respectively (Table 3.4).

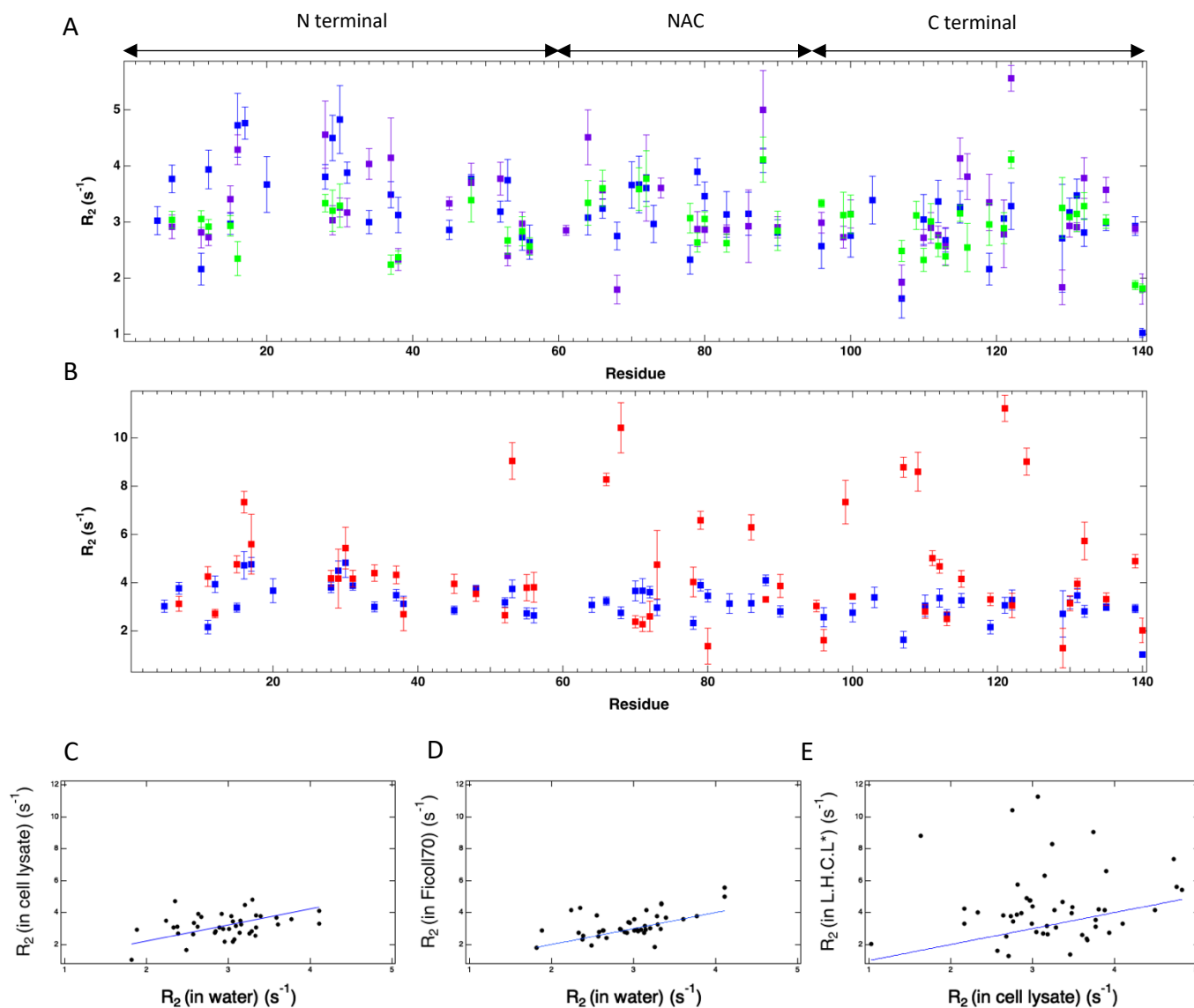


Figure 3.11)  $^{15}\text{N}$ - $^1\text{H}$  transverse relaxation rate ( $R_2$ ) of 0.2 mM  $\alpha$ -synuclein A) in the absence of crowders (green), presence of 200 mg/mL unmanipulated bacterial cell lysate (blue), and Ficoll70 (purple), B) in the presence of 200 mg/mL less hydrophobic cell lysate (red) and unmanipulated bacterial cell lysate (blue) C) in the absence of crowders versus in the 200 mg/mL unmanipulated cell lysate, D) in the absence of crowders versus in the 200 mg/mL Ficoll70, E) in the 200 mg/mL of \* less hydrophobic cell lysate versus 200 mg/mL of unmanipulated cell lysate at 25 °C and pH 7. The  $R_2$  values derived from the peak height (intensity), and the error bar represents the standard deviation of the fit to the exponential of the intensity versus delayed time. The fits for a few of the residues are shown in the supplemental data. The relaxation experiments are done on NMR 600 MHz with 44 scans.

Table 3.4 also shows that the C terminal's average transverse relaxation rate in the cell lysate remains the same as in the no-crowding condition. However, the C terminal's average  $R_2$  value in the presence of Ficoll70 is increased. Therefore, the C terminal moves relatively fast in presence of cell lysate compared to Ficoll70. In the C terminus, 46% residues in the cell lysate had a lower  $R_2$  value than in the Ficoll70 and the rest had the same relaxation rate.

Table 3.4) Average of  $R_2$  values in different regions of  $\alpha$ -synuclein in the Ficoll70 and bacterial cell lysate. Values are presented as mean  $\pm$  standard deviation ( $s^{-1}$ ).

<b><math>\alpha</math>-synuclein's region</b>	<b>No crowder (<math>s^{-1}</math>)</b>	<b>Bacterial Cell lysate (<math>s^{-1}</math>)</b>	<b>Ficoll70 (<math>s^{-1}</math>)</b>	<b>Less hydrophobic bacterial Cell lysate (<math>s^{-1}</math>)</b>
N-terminal (1-60)	2.87 $\pm$ 0.22	3.54 $\pm$ 0.30	3.30 $\pm$ 0.27	4.42 $\pm$ 0.58
NAC (61-95)	3.36 $\pm$ 0.40	3.27 $\pm$ 0.30	3.30 $\pm$ 0.34	4.55 $\pm$ 0.61
C-terminal (96-140)	2.89 $\pm$ 0.26	2.80 $\pm$ 0.33	3.05 $\pm$ 0.27	4.76 $\pm$ 0.44

### 3.7 $\alpha$ -synuclein structure and $^{15}\text{N}$ - $^1\text{H}$ $R_2$ relaxation in the absence and presence of less hydrophobic cell lysate

Figure 3.11A shows that 55% of the residues whose  $R_2$  changed substantially, either higher or lower, with cell lysate compared to in Ficoll are hydrophobic. Table 3.5 shows what types and numbers of residues have different (not within error bar)  $R_2$  in the cell lysate compared to in the Ficoll. Therefore, I reduced the hydrophobicity of the cell lysate and measured the  $R_2$  of  $\alpha$ -synuclein's residues in the presence of less hydrophobic cell lysate (Figure 3.11B). General characteristics of each region of  $\alpha$ -synuclein is shown in Table S1.

Table 3.5)  $\alpha$ -synuclein's residues with different  $R_2$  values in the presence of unmanipulated cell lysate versus Ficoll70 and in the presence of less hydrophobic cell lysate versus the unmanipulated cell lysate.  
\*Total number of the assigned residues.

<b>Amino acid type</b>	<b>Number of residues whose <math>R_2</math> changed substantially with cell lysate compared to in Ficoll</b>	<b>Number of residues with higher <math>R_2</math> in the less hydrophobic cell lysate than in the unmanipulated cell lysate</b>	<b>*Total residues (assigned)</b>
Alanine	5	7	10
Lysine	4	2	5
Valine	2	4	9
Aspartic acid	2	3	4
Glycine	2	4	3
Leucine	1	1	4
Iso leucine	-	2	2
Glutamic acid	1	1	8
Threonine	1	1	2
Glutamine	-	3	3

By manipulating the cell lysate and lowering its hydrophobicity, the transverse relaxation rate  $R_2$  in less hydrophobic cell lysate is compared with that in unmanipulated cell lysate. The relaxation rate for different residues in the N-terminal region of  $\alpha$ -synuclein is almost the same in the presence of less hydrophobic cell lysate as in the unmanipulated lysate. However, the  $R_2$  value has increased considerably for several residues in the NAC region and even more residues in the C terminal region (Figure 3.11B).

### **3.8 $\alpha$ -synuclein structure in the absence and presence of ultracentrifuged less hydrophobic cell lysate**

Centrifuging the cell lysate and removing the big particles might help us if I just want to focus on changing the hydrophobicity, not the size. Therefore, ultracentrifuging the cell lysate first before applying the HIC column might affect less the size distribution of cell lysate particles.

The HSQC results from less hydrophobic ultracentrifuged cell lysate (Figure 3.12) indicates that in the presence of less hydrophobic ultracentrifuged cell lysate, some of the  $\alpha$ -synuclein peaks were lost compared to dilute condition at 25 °C. It is difficult to make any conclusions since the acquisition parameters (number of scans and number of points) are different between these two experiments.

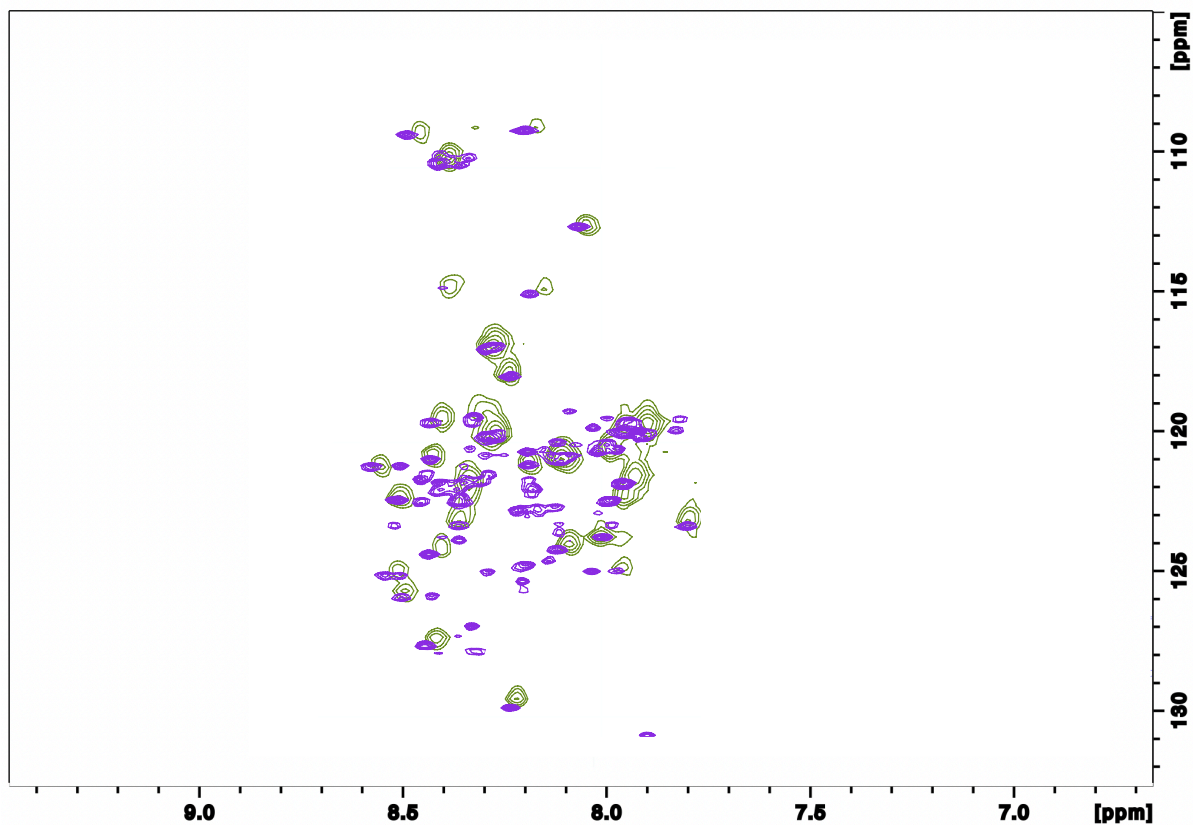


Figure 3.12)  $^{15}\text{N}$ - $^1\text{H}$  HSQC spectra of 0.2 mM  $\alpha$ -synuclein in the absence (purple) and presence of 200 mg/mL less hydrophobic ultracentrifuged cell lysate (green) at 25 °C and pH 7. The contour levels are the same in all spectra, but the acquisition parameters are different (In the presence of less hydrophobic ultracentrifuged cell lysate: 44 scans and for proton channel 1024 points; in the absence of the crowders: 128 scans and for proton channel 2048 points). The spectra are obtained at a  $^1\text{H}$  frequency of 600 MHz.

# 4. Discussion

## 4.1 Structure of $\alpha$ -synuclein in the absence and presence of macromolecular crowding

Does macromolecular crowding accelerate the aggregation of  $\alpha$ -synuclein? This question has always been controversial (Bai et al. 2017; Breydo et al. 2014b; Croke et al. 2008; Kuznetsova, Turoverov, and Uversky 2014) when it comes to intracellular crowding effects on the protein and still needs researchers' attention. There are different scenarios that  $\alpha$ -synuclein might go through before being actually aggregated (Figure 1.4). First,  $\alpha$ -synuclein might experience structural changes in the presence of crowders, and then this structural modification promotes its aggregation. The second scenario is, it might be aggregated directly from the disordered conformation without any structural changes. In either case, perhaps some residues of the protein behave differently in the presence of macromolecular crowding that lead to a direct or step-by-step aggregation process. In this study, we find that various regions of the protein behave differently, in terms of dynamics and motility, in the presence of different types of macromolecular crowding.

Now the second question is, “Is the type of macromolecules, synthetic or biological crowders, important in the aggregation process?” To answer this question of how exactly different crowders can promote the aggregation process, it is important to look at the behavior of each residue in the structure of  $\alpha$ -synuclein. It is worthwhile to study the effects of crowders on the protein while it is in monomeric or pre-oligomeric state and before it actually aggregates. There are many studies that look at the aggregation of  $\alpha$ -synuclein in the presence of crowders, and they mostly focused on the fibrillation of  $\alpha$ -synuclein. However, this study by focusing on the pre-oligomeric behavior of the protein, will try to help to clarify how the transition from a monomer to an oligomer of the protein takes place in the presence of different crowders.

Our results contribute to understanding the effects of macromolecular crowding and also the difference between synthetic and biological crowders' effects. In section 3.3,  $^{15}\text{N}$ - $^1\text{H}$  HSQC data showed that  $\alpha$ -synuclein has some minor changes in its chemical shifts in the presence of either cell lysate or Ficoll. I suggest that the minor changes in  $\alpha$ -synuclein's chemical shifts in crowded conditions come from weak interactions, not a structural change. Therefore,  $\alpha$ -synuclein remains disordered in the presence of Ficoll70 and bacterial cell lysate. In the following paragraphs, I will explain why minor chemical shifts displacement of  $\alpha$ -synuclein is connected to weak interactions.

Previous studies also obtained the same conclusion but for different crowding conditions.  $^{15}\text{N}$ - $^1\text{H}$  HSQC spectrum showed that  $\alpha$ -synuclein's structure within *E. coli* cells did not change relative to dilute condition (Croke et al. 2008; McNulty, Young, and Pielak 2006; Smith et al. 2015). The HSQC spectra and secondary structure propensity (SSP) scores showed no difference

in the secondary structure propensity of  $\alpha$ -synuclein within *E. coli* cells compared to non-crowding conditions. The chemical shifts between these two conditions were similar (Waudby et al. 2013).  $^1\text{H}$ - $^{15}\text{N}$  HSQC spectra of  $\alpha$ -synuclein in human and animal cell lines, including A2780, HeLa, RCSN-3, B65, and SK-N-SH, showed that different intracellular environments did not induce a major conformational change in the monomer of  $\alpha$ -synuclein (Theillet et al. 2016; Waudby et al. 2013).

Individual protein crowders have been also used to mimic the intracellular environment.  $\alpha$ -synuclein in the presence of BSA showed the same spectrum as  $\alpha$ -synuclein in dilute conditions and within *E. coli* cells (McNulty, Young, and Pielak 2006). It was suggested that  $\alpha$ -synuclein in crowded environments, whether complex cellular crowding or protein crowding, did not change its structure, and  $\alpha$ -synuclein remained disordered (McNulty, Young, and Pielak 2006).

Scientists also focused on the effects of synthetic crowders on  $\alpha$ -synuclein. Far-UV CD spectra and  $^1\text{H}$ - $^{15}\text{N}$  HSQC showed that the presence of PEG and Ficoll has minor effects on the structure of  $\alpha$ -synuclein. In the presence of either crowder,  $\alpha$ -synuclein gained negligibly minor amounts of ordered conformation (Bai et al. 2017; Breydo et al. 2015; Cino, Karttunen, and Choy 2012; Horvath, Kumar, and Wittung-Stafshede 2021; Munishkina, Fink, and Uversky 2009).

Therefore, previous studies confirmed that  $\alpha$ -synuclein in the presence of macromolecular crowding experienced small changes in the chemical shifts due to weak interactions compared to no-crowding conditions but still remained disordered (Bai et al. 2017; Cino, Karttunen, and Choy 2012; Li et al. 2008; McNulty, Young, and Pielak 2006; Morar et al. 2008; Wang et al. 2012;

Waudby et al. 2013; Zigoneanu and Pielak 2012). In the current study too, based on the HSQC spectra, the crowding environment using either Ficoll or cell lysate, did not impact on the structure of  $\alpha$ -synuclein. Small changes in the HSQC spectra came from the weak interactions between  $\alpha$ -synuclein and the crowders.

In the current study, I examined the  $\alpha$ -synuclein over long time incubation at 37 °C. Section 3.3 stated that all  $\alpha$ -synuclein's peaks were lost after 48 hours in the cell lysate, which most likely is an indication of its aggregation. Sometimes, the loss of peaks occurs due to fast amide-water proton exchange (McNulty, Young, and Pielak 2006), and sometimes due to aggregation. Since  $\alpha$ -synuclein in the soluble condition is entirely disordered and might have bulk amide-water proton exchange in high temperature, I might lose all its signal at physiological temperature. However, if this was the case, I also would have lost  $\alpha$ -synuclein's signals in the presence of Ficoll at the same temperature, but I lost signals only in the presence of cell lysate. In a study in 2005, McNulty et al. found out that  $\alpha$ -synuclein in non-crowding conditions lost some of its HSQC peaks at 35 °C due to the reversible intermediate conformational exchange. However,  $\alpha$ -synuclein preserved its peaks in crowded conditions, even at high temperatures.  $\alpha$ -synuclein remained disordered in the *E. coli* periplasm and in the presence of 300 mg/mL BSA at 35 °C (McNulty, Young, and Pielak 2006). Therefore, based on this and our observation, fast amide proton exchange should not be the reason for losing  $\alpha$ -synuclein's peaks in the presence of crowders. I therefore suggest that losing  $\alpha$ -synuclein's peaks in the cell lysate at 37 °C after 48 hours is due to its aggregation. In order to further verify this, whether from aggregation or amide proton exchange, fluorescence confocal microscopy was used to check any probable aggregation. The fluorescence data (Figure 3.5)

showed that there are some clusters (Figure 3.5C) in cell lysate (but not in Ficoll and not in the absence of crowder), which potentially is an indication of  $\alpha$ -synuclein's aggregation.

In summary,  $\alpha$ -synuclein in the presence of cell lysate and Ficoll70 at physiological temperature remains disordered. However,  $\alpha$ -synuclein was aggregated after 48 hours of incubation in the cell lysate; whereas, it remained unaggregated in Ficoll70 after 72 hours. The reason for faster aggregation in the cell lysate is not clear, however, I think that soft interactions present in cell lysate but not in Ficoll accelerate  $\alpha$ -synuclein aggregation. Following information will help to improve our understanding to investigate the further impacts of cell lysate on  $\alpha$ -synuclein.

I also examined the structure of  $\alpha$ -synuclein in the presence and absence of ultracentrifuged less hydrophobic cell lysate. Figure 3.12 indicates that some of  $\alpha$ -synuclein's peaks were lost in the presence of the crowder compared with the dilute condition. Perhaps removing the big particles (cell wall, membrane, etc.) by ultracentrifugation boosts the effects of the less hydrophobic macromolecules. Removing the hydrophobic particles from the environment (by HIC) diminishes the hydrophobic interactions and potentially increases the attractive forces. This might push the  $\alpha$ -synuclein into a more compact conformation or its pre-oligomeric/oligomeric form.

#### **4.2 Diffusion of $\alpha$ -synuclein in the absence and presence of macromolecular crowding**

Diffusion is one of the techniques that can give us information about the behavior of the protein and any probable aggregation. Diffusion is the major mode of transportation inside cells and plays a pivotal role in cell signalling. The diffusion behavior for IDPs might be different in

various crowded milieus compared to globular proteins, and they might obtain various conformations to diffuse in different crowding conditions.

In our study, I found that  $\alpha$ -synuclein diffused twice as fast as what has been found previously (Wang et al. 2012). Wang and their colleagues measured the diffusion of  $\alpha$ -synuclein by  $^{19}\text{F}$  NMR, and they found that  $\alpha$ -synuclein diffusion at 25 °C is  $0.78 \times 10^{-10} \text{ m}^2/\text{s}$ . I obtained  $\alpha$ -synuclein diffusion  $1.49 \times 10^{-10} \text{ m}^2/\text{s}$  at 25 °C (Wang et al. 2012). Given this disparity, I confirmed that on the SDS gel, there is a single, strong band at a molecular mass consistent with 14 kDa, the expected molecular mass of  $\alpha$ -synuclein.

Depending on how the diffusion coefficients are converted to hydrodynamic radii, the radii obtained from previous experiments is 3.1 nm and in this work it is 1.6 nm. Uversky suggests for polypeptide chains a series of relations between hydrodynamic radius,  $R_H$ , and molecular mass,  $M$ , of the form  $\log(R_H) = -a + b \log(M)$ , where the values of  $a$  and  $b$  vary depending on how compact or unfolded the protein is (Uversky, 2012). Using this relation, a size of 1.6 nm would indicate a fairly compact  $\alpha$ -synuclein (close to phenomenological Eq.6 in Uversky, 2012). Our experiments were done at the same temperature and comparable pH (7.4 in Wang et al.'s experiments vs 7 in ours), but at different concentrations: 1 mM for Wang et al. and 0.2 mM in this study. We could not increase the concentration of  $\alpha$ -synuclein to more than 0.2 mM since the protein aggregated quickly at higher concentrations. It is possible that  $\alpha$ -synuclein may be prone to clustering at higher concentrations. Due to the potential for clustering (Bülow et al., 2019), and the dependence of  $R_H$  on protein conformation, it is challenging to relate molecular mass to hydrodynamic radius obtained from diffusion measurements.

I found that, the diffusion value in the presence of 200 mg/mL cell lysate decreased by 43 % and in 200 mg/mL Ficoll70 decreased by around 78 % (Table 3.3). It was reported that  $\alpha$ -synuclein diffusion in the presence of 300 mg/mL Ficoll70 reduced by 80 % (Wang et al. 2012). Wang et al also showed that artificial crowders, like 300 mg/mL PVP and Ficoll70, and protein crowders, like 300 mg/ml BSA and lysozyme, slowed down the diffusion of  $\alpha$ -synuclein at 25 °C and pH 7.4. However, it was indicated that  $\alpha$ -synuclein diffuses faster in different individual protein crowders than the synthetic ones. In our study, I found that  $\alpha$ -synuclein diffuses faster in the cell lysate than in the Ficoll, which makes the results consistent with the previous study.

I suggest that the faster diffusion of  $\alpha$ -synuclein in the cell lysate is not because of structural change as  $\alpha$ -synuclein remains disordered in the presence of crowders, discussed in section 4.1 (Li et al. 2008; McNulty, Young, and Pielak 2006; Morar et al. 2008; Wang et al. 2011; Zgoneanu and Pielak 2012). There are at least two explanations for this. First, Ficolls are compact spherical crowders, while the cell lysate is far more heterogenous in molecular shapes and sizes. While Ficolls have been shown to be deformable (Ranganathan et al. 2022) the diversity of molecular shape could make the lysates less obstructive at higher packings. Second,  $\alpha$ -synuclein is negatively charged, as are the majority of bacterial proteins, DNA, and bacterial lipids in the cell lysate. Thus, the faster diffusion of  $\alpha$ -synuclein in the higher concentration of cell lysate could come from the repulsion between cell lysate and  $\alpha$ -synuclein, for example with charged molecules, which does not exist in the Ficoll.

### 4.3 Backbone internal dynamics of $\alpha$ -synuclein in the absence and presence of macromolecular crowding

It has been suggested that  $\alpha$ -synuclein's internal chain motions might be modified by soft interactions with crowders and converted to faster translational motion in biological crowders (Wang et al. 2012). To explore the internal chain motion of  $\alpha$ -synuclein, I measured its  $^{15}\text{N}$ - $^1\text{H}$  HSQC transverse relaxation rate ( $R_2$ ) in the absence and presence of crowders. The dynamical behavior of IDPs is hard to interpret from relaxation data compared to globular proteins as they exchange between different conformations of the proteins (Milles et al. 2018). Because of their flexibility, disordered proteins like  $\alpha$ -synuclein can have different correlation times for different residues (Li et al. 2008). In this study, the  $R_2$  relaxation rate of  $\alpha$ -synuclein was measured in the absence and presence of the crowders to examine  $\alpha$ -synuclein's internal backbone dynamics.

I showed that  $\alpha$ -synuclein's C terminal region moves more in the cell lysate than in the Ficoll as judged by the change in average  $R_2$ . Considering that the C terminal region is governed by electrostatic interactions in intracellular milieu (Theillet et al. 2016), I conjectured that perhaps electrostatic interactions between the C terminal region and cell lysate particles cause  $\alpha$ -synuclein to have faster dynamics in the cell lysate than in the Ficoll. Also, seven residues (non-polar and non-charged) of  $\alpha$ -synuclein, A11, A78, K96, A107, D119, N122, and A140, in the cell lysate move even faster than in the water, which emphasizes the interactions and interplay of repulsive and attractive forces that cause the faster dynamics of the residues in the cell lysate. I note that these faster internal dynamics of different regions of  $\alpha$ -synuclein in the cell lysate concurrent with

faster translational motion and causes the faster translational diffusion of  $\alpha$ -synuclein in the cell lysate compared to Ficoll70.

I find that 55% of the assigned residues that have a different (not within error bar)  $R_2$  value in the cell lysate than in the Ficoll are hydrophobic. Considering the fact that cell lysate preserves the intracellular hydrophobic interactions, it might affect more  $\alpha$ -synuclein's hydrophobic residues. As most previous studies used PEG, Dextran, or Ficoll in their studies (Lee et al. 2012; Munishkina et al. 2004; Munishkina, Fink, and Uversky 2008), which are hydrophilic polymers, it is worthwhile to use a biological crowder with a lower hydrophobicity. To this end, I manipulated the hydrophobicity of the cell lysate and used a less hydrophobic cell lysate (section 3.2).

$^{15}\text{N}$ - $^1\text{H}$  HSQC results showed that the less hydrophobic cell lysate like the unmanipulated cell lysate does not affect the structure of the  $\alpha$ -synuclein. This is consistent with previous indications that the secondary structure of  $\alpha$ -synuclein in a more hydrophobic milieu remains the same as that in hydrophilic milieu at pH 7.5 (Breydo et al. 2015).

However, the  $R_2$  data indicated that the C terminal region of  $\alpha$ -synuclein was affected more by the less hydrophobic cell lysate, and the average relaxation rate increased 1.5 times. By lowering the hydrophobicity of the cell lysate, the residues that have faster dynamics (i.e. lower  $R_2$ ) in the unmanipulated cell lysate than in the water experienced a substantial decrease (i.e. an increase  $R_2$ ) in their dynamics. Looking deeper at the characteristics of the most affected residues in the less hydrophobic cell lysate than in the unmanipulated cell lysate, I find that 64% of the affected residues (residues in the less hydrophobic cell lysate with  $R_2$  not the same, either increase or decrease, as in the unmanipulated cell lysate within the error bars) are hydrophobic amino acids

(Table 3.5). Since lower hydrophobicity can increase the attractive forces, reducing the hydrophobic particles and interactions might reduce the motility of the residues.

Previous studies indicated that longitudinal relaxation rate ( $R_1$ ) did not change substantially in the presence of the synthetic crowder Polyvinylpyrrolidone (PVP). However, the effects of PVP were observable in the  $R_2$  experiment. In the presence of the PVP, the  $R_2$  value increased substantially compared to the buffer (Li et al. 2008). However,  $^{15}\text{N}$   $R_2$  data showed that  $\alpha$ -synuclein in the presence of glucose and Ficoll did not change compared to the dilute condition (Theillet et al. 2016; Wu and Baum 2011). The overall  $R_2$  relaxation rate was increased in the presence of glucose, but the local dynamics did not change relative to the no-crowding condition (Wu and Baum 2011). In the presence of BSA, the N terminal region experienced non-uniform conformational exchange, but in the presence of lysozyme, the C terminal region experienced this conformational exchange (Theillet et al. 2016). In-cell (A2780 and SK-N-SH) data showed that  $\alpha$ -synuclein experienced non-uniform conformational fluctuations for both N and C terminals, and the NAC region experienced less change in the presence of biological crowders (Theillet et al. 2016). Therefore, the outcome of  $\alpha$ -synuclein dynamics in the presence of biological crowders from previous studies is consistent with our results in the presence of the bacterial cell lysate.

## 5. Conclusion

Comparing the effects of biological and artificial crowders gives a better idea of how intracellular crowding affects  $\alpha$ -synuclein. Our results suggest that the  $\alpha$ -synuclein structure remains the same in either Ficoll70 or cell lysate. Our experiments show that  $\alpha$ -synuclein diffuses faster in a high concentration (200 mg/mL) of cell lysate than in Ficoll70. Two regimes of crowding-induced changes in kinetics have been observed by Dhar et al (Dhar et al. 2010) (using Ficoll70 as crowder): a low-concentration regime ( $< \sim 100$  mg/mL) where protein folding timescales are reduced, and a high concentration regime ( $> \sim 100$  mg/mL) where the timescales increase again. In this latter regime, which is physiologically relevant, I find  $\alpha$ -synuclein moves faster in cell lysate than Ficoll70.

In this high-concentration regime, I also evaluated the structure of  $\alpha$ -synuclein over several days in the absence and presence of crowders. I find that  $\alpha$ -synuclein spectrum in cell lysate (but not in Ficoll70 or in the absence of crowder) disappears after 48 hours. These samples were then evaluated by confocal imaging (in the presence of a fluorescent stain that preferentially attaches to aggregates) and indeed, the cell lysate was the only one to show the presence of fluorescent micron-scale aggregates. This would be consistent with their signal disappearing from the NMR spectrum.

I also found that some residues and the C terminal region of  $\alpha$ -synuclein move faster in the cell lysate than in the Ficoll70. The soft interactions between cell lysate and  $\alpha$ -synuclein may cause faster local internal backbone dynamics of the  $\alpha$ -synuclein and then convert it to a faster translational diffusion (Wang et al. 2012). Also, changing the hydrophobicity of the natural crowder caused substantial impacts on  $\alpha$ -synuclein dynamics, especially in its NAC and C terminal regions. This emphasizes the importance of crowder soft interactions with  $\alpha$ -synuclein.

## **Future directions**

As the study has pointed out the effects of biological crowding and its soft interactions, the next level of study will be divided into several parts. First, it is important to realize what kind of soft interactions play a critical role in  $\alpha$ -synuclein aggregation. Examining the dynamics and diffusion of the protein in the ultracentrifuged less hydrophobic cell lysate might provide a better resolution of the interactions between cell lysate and  $\alpha$ -synuclein. Second, focusing on altering the properties of different regions of the protein based on their type of interactions with the crowders might take the study to the next level to prevent the aggregation. Third, using a different biological crowder which is closer to the eukaryotic cells might help us to examine the reproducibility of our data in a closer condition to the human body.

## Bibliography

- Alam, Parvez, Khursheed Siddiqi, Sumit Kumar Chturvedi, and Rizwan Hasan Khan. 2017. "Protein Aggregation: From Background to Inhibition Strategies." *International Journal of Biological Macromolecules* 103: 208–19.
- Aviles, FJ et al. 1978. "The Conformation of Histone H5." *European Journal of Biochemistry* 371(88): 363–71.
- Bai, Jia, Maili Liu, Gary J. Pielak, and Conggang Li. 2017. "Macromolecular and Small Molecular Crowding Have Similar Effects on  $\alpha$ -Synuclein Structure." *ChemPhysChem* 18(1): 55–58.
- Banks, Anthony et al. 2018. "Intrinsically Disordered Protein Exhibits Both Compaction and Expansion under Macromolecular Crowding." *Biophysical Journal* 114(5): 1067–79.
- Barchi, Joseph J., Bruce Grasberger, Angela M. Gronenborn, and G. Marius Clore. 1994. "Investigation of the Backbone Dynamics of the Igg-binding Domain of Streptococcal Protein g by Heteronuclear Two-dimensional  $^1\text{H}$ - $^{15}\text{N}$  Nuclear Magnetic Resonance Spectroscopy." *Protein Science* 3(1): 15–21.
- Bartels, Tim, Joanna G. Choi, and Dennis J. Selkoe. 2011. " $\alpha$ -Synuclein Occurs Physiologically as a Helically Folded Tetramer That Resists Aggregation." *Nature* 477(7362): 107–11.
- Van Den Berg, Bert, R. John Ellis, and Christopher M Dobson. 1999. "Effects of Macromolecular Crowding on the Folding and Aggregation." *EMBO Journal* 18(4): 3870–75.
- Van Den Berg, Bert, Rachel Wain, Christopher M. Dobson, and R. John Ellis. 2000. "Macromolecular Crowding Perturbs Protein Refolding Kinetics: Implications for Folding inside the Cell." *EMBO Journal* 19(15): 3870–75.

- Bligh, E G, and W J Dyer. 1959. "A Rapid Method of Total Lipid Extraction and Purification." *Canadian journal of biochemistry and physiology* 37(8): 911–17.
- Bloomer, A. C. et al. 1978. "Protein Disk of Tobacco Mosaic Virus at 2.8 Resolution Showing the Interactions within and between Subunits." *Nature* 276(5686): 362–68.
- Bode, Wolfram, Peter Schwager, and Robert Huber. 1978. "The Transition of Bovine Trypsinogen to a Trypsin-like State upon Strong Ligand Binding. The Refined Crystal Structures of the Bovine Trypsinogen-Pancreatic Trypsin Inhibitor Complex and of Its Ternary Complex with Ile-Val at 1.9 Å Resolution." *Journal of Molecular Biology* 118(1): 99–112.
- Breydo, Leonid et al. 2014a. "The Crowd You're in with: Effects of Different Types of Crowding Agents on Protein Aggregation." *Biochimica et Biophysica Acta - Proteins and Proteomics* 1844(2): 346–57.
- Breydo, Leonid et al. 2015. "Effects of Polymer Hydrophobicity on Protein Structure and Aggregation Kinetics in Crowded Milieu." *Biochemistry* 54(19): 2957–66.
- Burré, Jacqueline et al. 2010. "α-Synuclein Promotes SNARE-Complex Assembly in Vivo and in Vitro." *Science* 329(5999): 1663–67.
- Burré, Jacqueline, Manu Sharma, and Thomas C. Südhof. 2018. "Cell Biology and Pathophysiology of α-Synuclein." *Cold Spring Harbor Perspectives in Medicine* 8(3).
- Bussell, Robert, and David Eliezer. 2003. "A Structural and Functional Role for 11-Mer Repeats in α-Synuclein and Other Exchangeable Lipid Binding Proteins." *Journal of Molecular Biology* 329(4): 763–78.
- Cabra, Vanessa, Edgar Vázquez-Contreras, Abel Moreno, and Roberto Arreguin-Espinosa. 2008. "The Effect of Sulfhydryl Groups and Disulphide Linkage in the Thermal Aggregation of

- Z19  $\alpha$ -Zein." *Biochimica et Biophysica Acta - Proteins and Proteomics* 1784(7–8): 1028–36.
- Carrell, Robin W., and David A. Lomas. 1997. "Conformational Disease." *Lancet* 350(9071): 134–38.
- Cavanagh, John et al. 2007. "CHAPTER 3 - EXPERIMENTAL ASPECTS OF NMR SPECTROSCOPY." In *Protein NMR Spectroscopy (Second Edition)*, eds. JOHN CAVANAGH et al. Burlington: Academic Press, 114–270.  
<https://www.sciencedirect.com/science/article/pii/B9780121644918500051>.
- Chandra, Sreeganga et al. 2003a. "A Broken  $\alpha$ -Helix in Folded  $\alpha$ -Synuclein." *Journal of Biological Chemistry* 278(17): 15313–18.
- Chang, Brian S. et al. 1997. "Identification of a Novel Regulatory Domain in Bcl-x(L) and Bcl-2." *EMBO Journal* 16(5): 968–77.
- Charlier, Cyril, Samuel F. Cousin, and Fabien Ferrage. 2016. "Protein Dynamics from Nuclear Magnetic Relaxation." *Chemical Society Reviews* 45(9): 2410–22.
- Chartier-Harlin, Marie-Christine et al. 2004. " $\alpha$ -Synuclein Locus Duplication as a Cause of Familial Parkinson's Disease." *Lancet* 364(9440): 1167–69.
- Chen, Jianhan, and Richard W Kriwacki. 2018. "Intrinsically Disordered Proteins: Structure, Function and Therapeutics." *Journal of molecular biology* 430(16): 2275–77.
- Cino, Elio A., Mikko Karttunen, and Wing Yiu Choy. 2012. "Effects of Molecular Crowding on the Dynamics of Intrinsically Disordered Proteins." *PLoS ONE* 7(11).
- Claridge, Timothy D.W. 2009. "Chapter 9 Diffusion NMR Spectroscopy." *Tetrahedron Organic Chemistry Series* 27: 303–34.

- Clayton, David F, and Julia M George. 1998. 21 Trends Neurosci *The Synucleins: A Family of Proteins Involved in Synaptic Function, Plasticity, Neurodegeneration and Disease*. Cambridge University Press.
- Cong, Qian, Ivan Anishchenko, Sergey Ovchinnikov, and David Baker. 2019. "Protein Interaction Networks Revealed by Proteome Coevolution." *Science* 365(6449): 185–89.
- Conway, Kelly A., James D. Harper, and Peter T. Lansbury. 1998. "Accelerated in Vitro Fibril Formation by a Mutant  $\alpha$ -Synuclein Linked to Early-Onset Parkinson Disease." *Nature Medicine* 4(11): 1318–20.
- Crick, Scott L. et al. 2006. "Fluorescence Correlation Spectroscopy Shows That Monomeric Polyglutamine Molecules Form Collapsed Structures in Aqueous Solutions." *Proceedings of the National Academy of Sciences of the United States of America* 103(45): 16764–69.
- Croke, Robyn L. et al. 2008. "Hydrogen Exchange of Monomeric  $\alpha$ -Synuclein Shows Unfolded Structure Persists at Physiological Temperature and Is Independent of Molecular Crowding in Escherichia Coli ." *Protein Science* 17(8): 1434–45.
- Davidson, W Sean, Ana Jonas, David F Clayton, and Julia M George. 1998a. "Stabilization of  $\alpha$ -Synuclein Secondary Structure upon Binding to Synthetic Membranes \*." *Journal of Biological Chemistry* 273(16): 9443–49.
- Davidson, W. Sean, Ana Jonas, David F. Clayton, and Julia M. George. 1998b. "Stabilization of  $\alpha$ -Synuclein Secondary Structure upon Binding to Synthetic Membranes." *Journal of Biological Chemistry* 273(16): 9443–49.
- Desplats, Paula et al. 2009. "Inclusion Formation and Neuronal Cell Death through Neuron-to-Neuron Transmission of  $\alpha$ -Synuclein." *Proceedings of the National Academy of Sciences of the United States of America* 106(31): 13010–15.

- Dettmer, Ulf et al. 2013. “In Vivo Cross-Linking Reveals Principally Oligomeric Forms of  $\alpha$ -Synuclein and  $\beta$ -Synuclein in Neurons and Non-Neural Cells.” *Journal of Biological Chemistry* 288(9): 6371–85.
- Dhar, Apratim et al. 2010. “Structure, Function, and Folding of Phosphoglycerate Kinase Are Strongly Perturbed by Macromolecular Crowding.” *Proceedings of the National Academy of Sciences of the United States of America* 107(41): 17586–91.
- Dunker, A Keith et al. 2001. *Intrinsically Disordered Protein*.
- Edsall, J T. 1953. “Some Comments on Proteins and Protein Structure. Proceedings of the Royal Society of London. Series B, Biological Sciences, 141(902), 97–103.  
<https://doi.org/10.1098/Rspb.1953.0026>.” *Series B, Biological sciences*, 141(902): 97–103.
- Elcock, Adrian H. 2010. “Models of Macromolecular Crowding Effects and the Need for Quantitative Comparisons with Experiment.” *Current opinion in structural biology* 20(2): 196–206.
- Ellis, R J. 2001. “Macromolecular Crowding: An Important but Neglected Aspect of the Intracellular Environment.” *Current opinion in structural biology* 11(1): 114–19.
- Fauvet, Bruno, Mohamed Bilal Fares, et al. 2012. “Characterization of Semisynthetic and Naturally N  $\alpha$ - Acetylated  $\alpha$ -Synuclein in Vitro and in Intact Cells: Implications for Aggregation and Cellular Properties of  $\alpha$ -Synuclein.” *Journal of Biological Chemistry* 287(34): 28243–62.
- Fauvet, Bruno, Martial K. Mbefo, et al. 2012. “ $\alpha$ -Synuclein in Central Nervous System and from Erythrocytes, Mammalian Cells, and Escherichia Coli Exists Predominantly as Disordered Monomer.” *Journal of Biological Chemistry* 287(19): 15345–64.

- Fink, Anthony L. 1998. "Protein Aggregation: Folding Aggregates, Inclusion Bodies and Amyloid." *Folding and Design* 3(1): 9–23.
- Fischer, Emil. 1894. "Einfluss Der Configuration Auf Die Wirkung Der Enzyme." *Ber. Dtsch. Chem. Ges.* 27: 2985–93.
- Fortin, Doris L. et al. 2004. "Lipid Rafts Mediate the Synaptic Localization of  $\alpha$ -Synuclein." *Journal of Neuroscience* 24(30): 6715–23.
- Garnier, Andrew. 2021. "Bringing Order to the Disordered: Molecular Dynamics Simulations of  $\alpha$ -Synuclein with Macromolecular Crowding." *Undergraduate honor thesis*.
- George, Julia M, Hui Jin, Wendy S Woods, and David F Clayton. 1995. 15 Neuron *Characterization of a Novel Protein Regulated during the Critical Period for Song Learning in the Zebra Finch*.
- Georgieva, Elka R., Trudy F. Ramlal, Peter P. Borbat, and Freed H. Freed. 2008. "Membrane-Bound Alpha-Synuclein Forms an Extended Helix: Long-Distance Pulsed ESR Measurements Using Vesicles, Bicelles, and Rod-Like Micelles." *Journal of the American Chemical Society* 130(39): 12856–57.
- Gershon, Nahum D, Keith R Portert, and Benes L Trust. 1985. 82 Cell Biology *The Cytoplasmic Matrix: Its Volume and Surface Area and the Diffusion of Molecules through It (Cytoplasm/Protein Diffusion/Cytoskeleton)*.
- Ghosh, Dhiman et al. 2013. "The Parkinson's Disease-Associated H50Q Mutation Accelerates  $\alpha$ -Synuclein Aggregation in Vitro." *Biochemistry* 52(40): 6925–27.
- Ghosh, Dhiman et al. 2014. "The Newly Discovered Parkinsons Disease Associated Finnish Mutation (A53E) Attenuates  $\alpha$ -Synuclein Aggregation and Membrane Binding." *Biochemistry* 53(41): 6419–21.

- Greenbaum, Eric A. et al. 2005. "The E46K Mutation in  $\alpha$ -Synuclein Increases Amyloid Fibril Formation." *Journal of Biological Chemistry* 280(9): 7800–7807.
- Horvath, Istvan, Ranjeet Kumar, and Pernilla Wittung-Stafshede. 2021. "Macromolecular Crowding Modulates  $\alpha$ -Synuclein Amyloid Fiber Growth." *Biophysical Journal* 120(16): 3374–81. <https://doi.org/10.1016/j.bpj.2021.06.032>.
- Hubbard, Julia A. et al. 2003. "Nuclear Magnetic Resonance Spectroscopy Reveals the Functional State of the Signalling Protein CheY in Vivo in Escherichia Coli." *Molecular Microbiology* 49(5): 1191–1200.
- Iwai, A et al. 1995. "The Precursor Protein of Non-A Beta Component of Alzheimer's Disease Amyloid Is a Presynaptic Protein of the Central Nervous System." *Neuron* 14(2): 467–75.
- Jakes, Ross, Maria Grazia Spillantini, and Michel Goedert. 1994. "Identification of Two Distinct Synucleins from Human Brain." *FEBS Letters* 345(1): 27–32.
- Jan, Asad et al. 2021. "The Prion-like Spreading of Alpha-synuclein in Parkinson's Disease: Update on Models and Hypotheses." *International Journal of Molecular Sciences* 22(15): 1–23.
- Jarymowycz, Virginia A., and Martin J. Stone. 2006. "Fast Time Scale Dynamics of Protein Backbones: NMR Relaxation Methods, Applications, and Functional Consequences." *Chemical Reviews* 106(5): 1624–71.
- Jenco, John M., Andrew Rawlingson, Brenda Daniels, and Andrew J. Morris. 1998. "Regulation of Phospholipase D2: Selective Inhibition of Mammalian Phospholipase D Isoenzymes by  $\alpha$ - and  $\beta$ -Synucleins." *Biochemistry* 37(14): 4901–9.

- Jensen, Poul Henning et al. 1999. "α-Synuclein Binds to Tau and Stimulates the Protein Kinase A-Catalyzed Tau Phosphorylation of Serine Residues 262 and 356." *Journal of Biological Chemistry* 274(36): 25481–89.
- Jerschow, Alex., and N. Müller. 1997. "Suppression of Convection Artifacts in Stimulated-Echo Diffusion Experiments. Double-Stimulated-Echo Experiments." *Journal of Magnetic Resonance* 125(2): 372–75.
- Karush, Fred. 1950. "Heterogeneity of the Binding Sites of Bovine Serum Albumin." *Journal of the American Chemical Society* 72(6): 2705–13.
- Kayser, Veysel et al. 2011. "Molecular Nanomedicine Towards Cancer :". *Journal of pharmaceutical sciences* 101(7): 2271–80.
- Kim, Jongsun. 1997. "Evidence That the Precursor Protein of Non-Aβ Component of Alzheimer's Disease Amyloid (NACP) Has an Extended Structure Primarily Composed of Random-Coil." *Molecules and Cells* 7(1): 78–83.
- Kinjo, Akira R., and Shoji Takada. 2003. "Competition between Protein Folding and Aggregation with Molecular Chaperones in Crowded Solutions: Insight from Mesoscopic Simulations." *Biophysical Journal* 85(6): 3521–31.
- Kontopoulos, Eirene, Jeffrey D. Parvin, and Mel B. Feany. 2006. "A-Synuclein Acts in the Nucleus To Inhibit Histone Acetylation and Promote Neurotoxicity." *Human Molecular Genetics* 15(20): 3012–23.
- Koshland, D. E. 1958. "Application of a Theory of Enzyme Specificity to Protein Synthesis." *Proceedings of the National Academy of Sciences* 44(2): 98–104.
- Kulkarni, Prakash, and Vladimir N. Uversky. 2019. "Intrinsically Disordered Proteins in Chronic Diseases." *Biomolecules* 9(4): 1–6.

- Kuznetsova, Irina M., Konstantin K. Turoverov, and Vladimir N. Uversky. 2014. 15  
International Journal of Molecular Sciences *What Macromolecular Crowding Can Do to a Protein.*
- Laganowsky, Arthur et al. 2012. “Atomic View of a Toxic Amyloid Small Oligomer.” *Science (New York, N.Y.)* 335(6073): 1228–31.
- Langella, Emma, Martina Buonanno, Giuseppina De Simone, and Simona Maria Monti. 2021. “Intrinsically Disordered Features of Carbonic Anhydrase IX Proteoglycan-like Domain.” *Cellular and Molecular Life Sciences* 78(5): 2059–67.
- Lee, Chiu Fan et al. 2012. “Combined Effects of Agitation, Macromolecular Crowding, and Interfaces on Amyloidogenesis.” *Journal of Biological Chemistry* 287(45): 38006–19.
- Lee, He Jin, Farnaz Khoshaghideh, Stephen Lee, and Seung Jae Lee. 2006. “Impairment of Microtubule-Dependent Trafficking by Overexpression of  $\alpha$ -Synuclein.” *European Journal of Neuroscience* 24(11): 3153–62.
- Lee, Hyun et al. 2000. “Local Structural Elements in the Mostly Unstructured Transcriptional Activation Domain of Human P53.” *Journal of Biological Chemistry* 275(38): 29426–32.
- Lee, Woonghee, Marco Tonelli, and John L. Markley. 2015. “NMRFAM-SPARKY: Enhanced Software for Biomolecular NMR Spectroscopy.” *Bioinformatics* 31(8): 1325–27.
- Lemieux, R. U., and U. Spohr. 1994. “How Emil Fischer Was Led to the Lock and Key Concept for Enzyme Specificity.” *Advances in Carbohydrate Chemistry and Biochemistry* 50(2): 1–20.
- Lesage, Suzanne et al. 2013. “G51D  $\alpha$ -Synuclein Mutation Causes a Novel Parkinsonian-Pyramidal Syndrome.” *Annals of Neurology* 73(4): 459–71.

- Levin, Johannes et al. 2016. "Intracellular Formation of  $\alpha$ -Synuclein Oligomers and the Effect of Heat Shock Protein 70 Characterized by Confocal Single Particle Spectroscopy." *Biochemical and Biophysical Research Communications* 477(1): 76–82.
- Li, Conggang et al. 2008. "Differential Dynamical Effects of Macromolecular Crowding on an Intrinsically Disordered Protein and a Globular Protein: Implications for in-Cell NMR Spectroscopy." *Journal of the American Chemical Society* 130(20): 6310–11.
- Li, J., V. N. Uversky, and A. L. Fink. 2001. "Effect of Familial Parkinson's Disease Point Mutations A30P and A53T on the Structural Properties, Aggregation, and Fibrillation of Human  $\alpha$ -Synuclein." *Biochemistry* 40(38): 11604–13.
- Liam Gregory. 2020. "The Effect of Macromolecular Crowding on the Dynamics of Alpha-Synuclein."
- Liu, Cong et al. 2012. "Out-of-Register  $\beta$ -Sheets Suggest a Pathway to Toxic Amyloid Aggregates." *Proceedings of the National Academy of Sciences of the United States of America* 109(51): 20913–18.
- Liu, Xianpeng et al. 2011. "Alpha-Synuclein Functions in the Nucleus to Protect against Hydroxyurea-Induced Replication Stress in Yeast." *Human Molecular Genetics* 20(17): 3401–14.
- Lou, H. et al. 2010. "Serine 129 Phosphorylation Reduces the Ability of Alpha-Synuclein to Regulate Tyrosine Hydroxylase and Protein Phosphatase 2A in Vitro and in Vivo." *The Journal of biological chemistry* 285(23): 17648–61.
- Luk, Kelvin C. et al. 2012. "Pathological  $\alpha$ -Synuclein Transmission Initiates Parkinson-like Neurodegeneration in Non-Transgenic Mice." *Science* 338(6109): 949–53.

- Maroteaux, L., J. T. Campanelli, and R. H. Scheller. 1988. "Synuclein: A Neuron-Specific Protein Localized to the Nucleus and Presynaptic Nerve Terminal." *Journal of Neuroscience* 8(8): 2804–15.
- Maroteaux, L., and R. H. Scheller. 1991. "The Rat Brain Synucleins; Family of Proteins Transiently Associated with Neuronal Membrane." *Molecular Brain Research* 11(3–4): 335–43.
- Maslah, Eliezer et al. 2000. "Dopaminergic Loss and Inclusion Body Formation in  $\alpha$ -Synuclein Mice: Implications for Neurodegenerative Disorders." *Science* 287(5456): 1265–69.
- McCully, Michelle E., David A.C. Beck, and Valerie Daggett. 2012. "Multimolecule Test-Tube Simulations of Protein Unfolding and Aggregation." *Proceedings of the National Academy of Sciences of the United States of America* 109(44): 17851–56.
- McNulty, Brian C., Gregory B. Young, and Gary J. Pielak. 2006. "Macromolecular Crowding in the Escherichia Coli Periplasm Maintains  $\alpha$ -Synuclein Disorder." *Journal of Molecular Biology* 355(5): 893–97.
- Meade, Richard M., David P. Fairlie, and Jody M. Mason. 2019. "Alpha-Synuclein Structure and Parkinson's Disease." *Molecular Neurodegeneration* 14(1): 1–14.
- Mehra, Surabhi, Shruti Sahay, and Samir K. Maji. 2019. " $\alpha$ -Synuclein Misfolding and Aggregation: Implications in Parkinson's Disease Pathogenesis." *Biochimica et Biophysica Acta - Proteins and Proteomics* 1867(10): 890–908.
- Miklos, Andrew C. et al. 2011. "An Upper Limit for Macromolecular Crowding Effects." *BMC Biophysics* 4(1).
- Milles, Sigrid, Nicola Salvi, Martin Blackledge, and Malene Ringkjøbing Jensen. 2018. "Characterization of Intrinsically Disordered Proteins and Their Dynamic Complexes: From

- in Vitro to Cell-like Environments.” *Progress in Nuclear Magnetic Resonance Spectroscopy* 109: 79–100.
- Minton, A P. 2000. “Implications of Macromolecular Crowding for Protein Assembly.” *Current opinion in structural biology* 10(1): 34–39.
- Minton, Allen P. 2005. “Influence of Macromolecular Crowding upon the Stability and State of Association of Proteins: Predictions and Observations.” *Journal of Pharmaceutical Sciences* 94(8): 1668–75.
- Mirsky, A. E., and Linus Pauling. 1936. “On the Structure of Native, Denatured, and Coagulated Proteins.” *Proceedings of the National Academy of Sciences* 22(7): 439–47.
- Morar, Artemiza S., Alina Olteanu, Gregory B. Young, and Gary J. Pielak. 2008. “Solvent-Induced Collapse of  $\alpha$ -Synuclein and Acid-Denatured Cytochrome c.” *Protein Science* 10(11): 2195–99.
- Munishkina, L., A. Fink, and V. Uversky. 2009. “Accelerated Fibrillation of Alpha-Synuclein Induced by the Combined Action of Macromolecular Crowding and Factors Inducing Partial Folding.” *Current Alzheimer Research* 6(3): 252–60.
- Munishkina, Larissa A., Elisa M. Cooper, Vladimir N. Uversky, and Anthony L. Fink. 2004. “The Effect of Macromolecular Crowding on Protein Aggregation and Amyloid Fibril Formation.” In *Journal of Molecular Recognition*, , 456–64.
- Munishkina, Larissa, Anthony Fink, and Vladimir Uversky. 2008. “Concerted Action of Metals and Macromolecular Crowding on the Fibrillation of Alpha-Synuclein.” *Protein & Peptide Letters* 15(10): 1079–85.
- Nakajo, Shigeo et al. 1990. “Purification and Characterization of a Novel Brain-Specific 14-KDa Protein.”

- Nakajo, Shigeo et al. 1993. “A New Brain-specific 14-kDa Protein Is a Phosphoprotein: Its Complete Amino Acid Sequence and Evidence for Phosphorylation.” *European Journal of Biochemistry* 217(3): 1057–63.
- Nelson, Gordon L. 2008. “What Does It Mean to Be Green?” *Standardization News* 36(6): 2–12.
- Nuscher, Brigitte et al. 2004. “ $\alpha$ -Synuclein Has a High Affinity for Packing Defects in a Bilayer Membrane: A Thermodynamics Study.” *Journal of Biological Chemistry* 279(21): 21966–75.
- Ohta-Lino, Satoko et al. 2001. “Fast Lipid Disorientation at the Onset of Membrane Fusion Revealed by Molecular Dynamics Simulations.” *Biophysical Journal* 81(1): 217–24.
- Oldfield, Christopher J. et al. 2005. “Comparing and Combining Predictors of Mostly Disordered Proteins.” *Biochemistry* 44(6): 1989–2000.
- Oldfield, Christopher J., and A. Keith Dunker. 2014. “Intrinsically Disordered Proteins and Intrinsically Disordered Protein Regions.” *Annual Review of Biochemistry* 83: 553–84.
- De Oliveira, Guilherme A.P. et al. 2016. “Structural Basis for the Dissociation of  $\alpha$ -Synuclein Fibrils Triggered by Pressure Perturbation of the Hydrophobic Core.” *Scientific Reports* 6(November): 1–15.
- Ow, Sian Yang, and Dave E. Dunstan. 2014. “A Brief Overview of Amyloids and Alzheimer’s Disease.” *Protein Science* 23(10): 1315–31.
- Peng, Zhenling et al. 2014. “Exceptionally Abundant Exceptions: Comprehensive Characterization of Intrinsic Disorder in All Domains of Life.” *Cellular and Molecular Life Sciences* 72(1): 137–51.
- Pinet, Louise, Nadine Assrir, and Carine van Heijenoort. 2021. “Expanding the Disorder-Function Paradigm in the C-Terminal Tails of Erbbs.” *Biomolecules* 11(11).

- Polymeropoulos, M H et al. 1997. “Mutation in the Alpha-Synuclein Gene Identified in Families with Parkinson’s Disease.” *Science (New York, N.Y.)* 276(5321): 2045–47.
- Predeus, Alexander V., Seref Gul, Srinivasa M. Gopal, and Michael Feig. 2012. “Conformational Sampling of Peptides in the Presence of Protein Crowders from AA/CG-Multiscale Simulations.” *Journal of Physical Chemistry B* 116(29): 8610–20.
- Radivojac, Predrag et al. 2007. “Intrinsic Disorder and Functional Proteomics.” *Biophysical Journal* 92(5): 1439–56.
- Ralston, G. B. 1990. “Effects of ‘Crowding’ in Protein Solutions.” *Journal of Chemical Education* 67(10): 857–60.
- Ranganathan, Venketesh Thrithamara et al. 2022. “Is Ficoll a Colloid or Polymer? A Multitechnique Study of a Prototypical Excluded-Volume Macromolecular Crowder.” *Macromolecules* 55(20): 9103–12.
- Rivas, Germán, and Allen P Minton. 2016. “Macromolecular Crowding In Vitro, In Vivo, and In Between.” *Trends in Biochemical Sciences* 41(11): 970–81.
- Roberts, Christopher J. 2014. “Protein Aggregation and Its Impact on Product Quality.” *Current Opinion in Biotechnology* 30: 211–17.
- Roberts, Rosalind F., Richard Wade-Martins, and Javier Alegre-Abarrategui. 2015. “Direct Visualization of Alpha-Synuclein Oligomers Reveals Previously Undetected Pathology in Parkinson’s Disease Brain.” *Brain* 138(6): 1642–57.
- Romero, Pedro et al. 2001. “Sequence Complexity of Disordered Protein.” *Proteins: Structure, Function and Genetics* 42(1): 38–48.
- Sahni, Nidhi et al. 2015. “Widespread Macromolecular Interaction Perturbations in Human Genetic Disorders.” *Cell* 161(3): 647–60.

- Sakai, Tomomi et al. 2006. “In-Cell NMR Spectroscopy of Proteins inside *Xenopus Laevis* Oocytes.” *Journal of Biomolecular NMR* 36(3): 179–88.
- Saluja, Atul et al. 2014. “Significance of Unfolding Thermodynamics for Predicting Aggregation Kinetics: A Case Study on High Concentration Solutions of a Multi-Domain Protein.” *Pharmaceutical Research* 31(6): 1575–87.
- Sarkar, Mohona, Conggang Li, and Gary J Pielak. 2013. “Soft Interactions and Crowding.” : 187–94.
- Sasahara, Kenji, Peter McPhie, and Allen P. Minton. 2003. “Effect of Dextran on Protein Stability and Conformation Attributed to Macromolecular Crowding.” *Journal of Molecular Biology* 326(4): 1227–37.
- Schell, H., T. Hasegawa, M. Neumann, and P. J. Kahle. 2009. “Nuclear and Neuritic Distribution of Serine-129 Phosphorylated  $\alpha$ -Synuclein in Transgenic Mice.” *Neuroscience* 160(4): 796–804.
- Selenko, Philipp et al. 2006. “Quantitative NMR Analysis of the Protein G B1 Domain in *Xenopus Laevis* Egg Extracts and Intact Oocytes.” *Proceedings of the National Academy of Sciences of the United States of America* 103(32): 11904–9.
- Senske, Michael et al. 2014. “Protein Stabilization by Macromolecular Crowding through Enthalpy Rather than Entropy.” *Journal of the American Chemical Society* 136(25): 9036–41.
- Serber, Z., A. T. Keatinge-Clay, et al. 2001. “High-Resolution Macromolecular NMR Spectroscopy inside Living Cells.” *Journal of the American Chemical Society* 123(10): 2446–47.

- Serber, Z., R. Ledwidge, S. M. Miller, and V. Dötsch. 2001. "Evaluation of Parameters Critical to Observing Proteins inside Living Escherichia Coli by In-Cell NMR Spectroscopy." *Journal of the American Chemical Society* 123(37): 8895–8901.
- Serber, Zach, and Volker Dtsch. 2001. "In-Cell NMR Spectroscopy." *Changes* 40(48).
- Shin, Kyungsoo, Muzaddid Sarker, Shuya K. Huang, and Jan K. Rainey. 2017. "Apelin Conformational and Binding Equilibria upon Micelle Interaction Primarily Depend on Membrane-Mimetic Headgroup." *Scientific Reports* 7(1): 1–13.  
<http://dx.doi.org/10.1038/s41598-017-14784-0>.
- Shirai, Nobu C., and MacOto Kikuchi. 2016. "The Interplay of Intrinsic Disorder and Macromolecular Crowding on  $\alpha$ -Synuclein Fibril Formation." *Journal of Chemical Physics* 144(5).
- Shtilerman, Mark D., Tomas T. Ding, and Peter T. Lansbury. 2002. "Molecular Crowding Accelerates Fibrillization of  $\alpha$ -Synuclein: Could an Increase in the Cytoplasmic Protein Concentration Induce Parkinson's Disease?" *Biochemistry* 41(12): 3855–60.
- Sickmeier, Megan et al. 2007. "DisProt: The Database of Disordered Proteins." *Nucleic Acids Research* 35(SUPPL. 1): 786–93.
- Singleton, A. B. et al. 2003. " $\alpha$ -Synuclein Locus Triplication Causes Parkinson's Disease." *Science* 302(5646): 841.
- Sipe, Jean D. 1992. "Jean D. Sipe."
- Sivanesam, K. et al. 2015. "Binding Interactions of Agents That Alter  $\alpha$ -Synuclein Aggregation." *RSC Advances* 5(15): 11577–90.
- Skinner, Simon P. et al. 2016. "CcpNmr AnalysisAssign: A Flexible Platform for Integrated NMR Analysis." *Journal of Biomolecular NMR* 66(2): 111–24.

- Smith, Austin E., Zeting Zhang, Gary J. Pielak, and Conggang Li. 2015. “NMR Studies of Protein Folding and Binding in Cells and Cell-like Environments.” *Current Opinion in Structural Biology* 30: 7–16.
- Sulzer, David, and Robert H. Edwards. 2019. “The Physiological Role of  $\alpha$ -Synuclein and Its Relationship to Parkinson’s Disease.” *Journal of Neurochemistry* 150(5): 475–86.
- Theillet, Francois Xavier et al. 2016. “Structural Disorder of Monomeric  $\alpha$ -Synuclein Persists in Mammalian Cells.” *Nature* 530(7588): 45–50.
- Tompa, Peter. 2003. “Intrinsically Unstructured Proteins Evolve by Repeat Expansion.” *BioEssays* 25(9): 847–55.
- Trivedi, Rakesh, and Hampapthalu Adimurthy Nagarajaram. 2022. “Intrinsically Disordered Proteins.” *International Journal of Molecular Sciences* 65(8): 64–65.
- Trosel, Yanitza, Gregory Liam Patrick, Valerie Booth, and Anand Yethiraj. 2023. “Diffusion NMR and Rheology of a Model Polymer in Bacterial Cell Lysate Crowders.” *Biomacromolecules*.
- Turoverov, Konstantin K., Irina M. Kuznetsova, and Vladimir N. Uversky. 2010. “The Protein Kingdom Extended: Ordered and Intrinsically Disordered Proteins, Their Folding, Supramolecular Complex Formation, and Aggregation.” *Progress in Biophysics and Molecular Biology* 102(2–3): 73–84.
- Tycko, Robert. 2006. “Molecular Structure of Amyloid Fibrils: Insights from Solid-State NMR.” *Quarterly Reviews of Biophysics* 39(1): 1–55.
- Tysnes, Ole Bjørn, and Anette Storstein. 2017. “Epidemiology of Parkinson’s Disease.” *Journal of Neural Transmission* 124(8): 901–5.

- Ueda, K. et al. 1993. "Molecular Cloning of CDNA Encoding an Unrecognized Component of Amyloid in Alzheimer Disease." *Proceedings of the National Academy of Sciences of the United States of America* 90(23): 11282–86.
- Ueda, Kenji et al. 1993. 90 *Molecular Cloning of CDNA Encoding an Unrecognized Component of Amyloid in Alzheimer Disease (Neurodegeneration/Chaperone/Amyloid P/A4 Protein/Neuritic Plaque)*.
- Ulmer, Tobias S., Ad Bax, Nelson B. Cole, and Robert L. Nussbaum. 2005. "Structure and Dynamics of Micelle-Bound Human  $\alpha$ -Synuclein." *Journal of Biological Chemistry* 280(10): 9595–9603.
- Uversky, Vladimir. 2008. "Amyloidogenesis of Natively Unfolded Proteins." *Current Alzheimer Research* 5(3): 260–87.
- Uversky, Vladimir N. et al. 2007. "Folding and Misfolding of  $\alpha$ -Synuclein." (January 2006): 1–30.
- Uversky, Vladimir N. et al. 2010. "The Mysterious Unfoldome: Structureless, Underappreciated, yet Vital Part of Any given Proteome." *Journal of Biomedicine and Biotechnology* 2010.
- Uversky, Vladimir N. et al. 2013. "A Decade and a Half of Protein Intrinsic Disorder: Biology Still Waits for Physics." *Protein Science* 22(6): 693–724.
- Uversky, Vladimir N. et al. 2019. "Intrinsically Disordered Proteins and Their 'Mysterious' (Meta)Physics." *Frontiers in Physics* 7(FEB): 8–23.
- Uversky, Vladimir N., and Anthony L. Fink. 2004. "Conformational Constraints for Amyloid Fibrillation: The Importance of Being Unfolded." *Biochimica et Biophysica Acta - Proteins and Proteomics* 1698(2): 131–53.

- Uversky, Vladimir N., Joel R. Gillespie, and Anthony L. Fink. 2000. "Why Are 'natively Unfolded' Proteins Unstructured under Physiologic Conditions?" *Proteins: Structure, Function and Genetics* 41(3): 415–27.
- Uversky, Vladimir N., Christopher J. Oldfield, and A. Keith Dunker. 2008. "Intrinsically Disordered Proteins in Human Diseases: Introducing the D<sup>2</sup> Concept." *Annual Review of Biophysics* 37: 215–46.
- Villar-Piqué, Anna, Tomás Lopes da Fonseca, and Tiago Fleming Outeiro. 2016. "Structure, Function and Toxicity of Alpha-Synuclein: The Bermuda Triangle in Synucleinopathies." *Journal of Neurochemistry* 139: 240–55.
- Vitorge, Bruno, and Damien Jeannerat. 2006. "Erratum: NMR Diffusion Measurements in Complex Mixtures Using Constant-Time-HSQC-IDOSY and Computer-Optimized Spectral Aliasing for High Resolution in the Carbon Dimension (*Analytical Chemistry* (2006) 78 (5601-5606))." *Analytical Chemistry* 78(21): 7601.
- Wagner, Gerhard. 1993. "NMR Relaxation and Protein Mobility." *Current Opinion in Structural Biology* 3(5): 748–54.
- Walter, RH, and MR Murphy. 2009. "Examining Polyglutamine Peptide Length: A Connection between Collapsed Conformations and Increased Aggregation." *Journal of mole* 393(4): 978–92.
- Wang, Wei et al. 2011. "A Soluble  $\alpha$ -Synuclein Construct Forms a Dynamic Tetramer." *Proceedings of the National Academy of Sciences of the United States of America* 108(43): 17797–802.

- Wang, Wei, and Christopher J. Roberts. 2018. "Protein Aggregation – Mechanisms, Detection, and Control." *International Journal of Pharmaceutics* 550(1–2): 251–68.  
<https://doi.org/10.1016/j.ijpharm.2018.08.043>.
- Wang, Xiaoyan, Dima Moualla, Josephine A. Wright, and David R. Brown. 2010. "Copper Binding Regulates Intracellular Alpha-Synuclein Localisation, Aggregation and Toxicity." *Journal of Neurochemistry* 113(3): 704–14.
- Wang, Yaqiang, Laura A. Benton, Vishavpreet Singh, and Gary J. Pielak. 2012. "Disordered Protein Diffusion under Crowded Conditions." *Journal of Physical Chemistry Letters* 3(18): 2703–6.
- Ward, J. J. et al. 2004a. "Prediction and Functional Analysis of Native Disorder in Proteins from the Three Kingdoms of Life." *Journal of Molecular Biology* 337(3): 635–45.
- Waudby, Christopher A. et al. 2013. "In-Cell NMR Characterization of the Secondary Structure Populations of a Disordered Conformation of  $\alpha$ -Synuclein within E. Coli Cells." *PLoS ONE* 8(8).
- Weinreb, Paul H. et al. 1996. "NACP, a Protein Implicated in Alzheimer's Disease and Learning, Is Natively Unfolded." *Biochemistry* 35(43): 13709–15.
- Williams, Dudley H. et al. 1991. "Toward the Semiquantitative Estimation of Binding Constants. Guides for Peptide-Peptide Binding in Aqueous Solution." *Journal of the American Chemical Society* 113(18): 7020–30.
- Williams, R. M. et al. 2001. "The Protein Non-Folding Problem: Amino Acid Determinants of Intrinsic Order and Disorder." *Pacific Symposium on Biocomputing. Pacific Symposium on Biocomputing* 100: 89–100.

- Wright, Peter E., and H. Jane Dyson. 1999. "Intrinsically Unstructured Proteins: Re-Assessing the Protein Structure-Function Paradigm." *Journal of Molecular Biology* 293(2): 321–31.
- Wu, Hsien. 1995. "Studies on Denaturation of Proteins. XIII. A Theory of Denaturation. 1931. *Advances in Protein Chemistry.*" 46: 6–5.
- Wu, Kuen Phon, and Jean Baum. 2011. "Backbone Assignment and Dynamics of Human  $\alpha$ -Synuclein in Viscous 2 M Glucose Solution." *Biomolecular NMR Assignments* 5(1): 43–46.
- Xu, Shengli et al. 2006. "Oxidative Stress Induces Nuclear Translocation of C-Terminus of  $\alpha$ -Synuclein in Dopaminergic Cells." *Biochemical and Biophysical Research Communications* 342(1): 330–35.
- Xue, Bin, A. Keith Dunker, and Vladimir N. Uversky. 2012. "Orderly Order in Protein Intrinsic Disorder Distribution: Disorder in 3500 Proteomes from Viruses and the Three Domains of Life." *Journal of Biomolecular Structure and Dynamics* 30(2): 137–49.
- Zarranz, Juan J et al. 2004. "The New Mutation, E46K, of Alpha-Synuclein Causes Parkinson and Lewy Body Dementia." *Annals of neurology* 55(2): 164–73.
- Zhai, Jiali, Tzong Hsien Lee, David H. Small, and Marie Isabel Aguilar. 2012. "Characterization of Early Stage Intermediates in the Nucleation Phase of A $\beta$  Aggregation." *Biochemistry* 51(6): 1070–78.
- Zhou, Huan Xiang, Germán Rivas, and Allen P. Minton. 2008. "Macromolecular Crowding and Confinement: Biochemical, Biophysical, and Potential Physiological Consequences." *Annual Review of Biophysics* 37: 375–97.
- Zhou, Zheng et al. 2009. "Crowded Cell-like Environment Accelerates the Nucleation Step of Amyloidogenic Protein Misfolding." *Journal of Biological Chemistry* 284(44): 30148–58.

Zigoneanu, Imola G., and Gary J. Pielak. 2012. "Interaction of  $\alpha$ -Synuclein and a Cell Penetrating Fusion Peptide with Higher Eukaryotic Cell Membranes Assessed by 19F NMR." *Molecular Pharmaceutics* 9(4): 1024–29.

Zimmerman, Steven B, and Allen P Minton. 1993. "MACROMOLECULAR." : 27–65.

Zimmerman, Steven B, and Stefan Trach. 1991. "Estimation of Macromolecule Concentrations and Excluded Volume Effects for the Cytoplasm of Escherichia Coli."

**Appendix I**  
**Supplemental information**

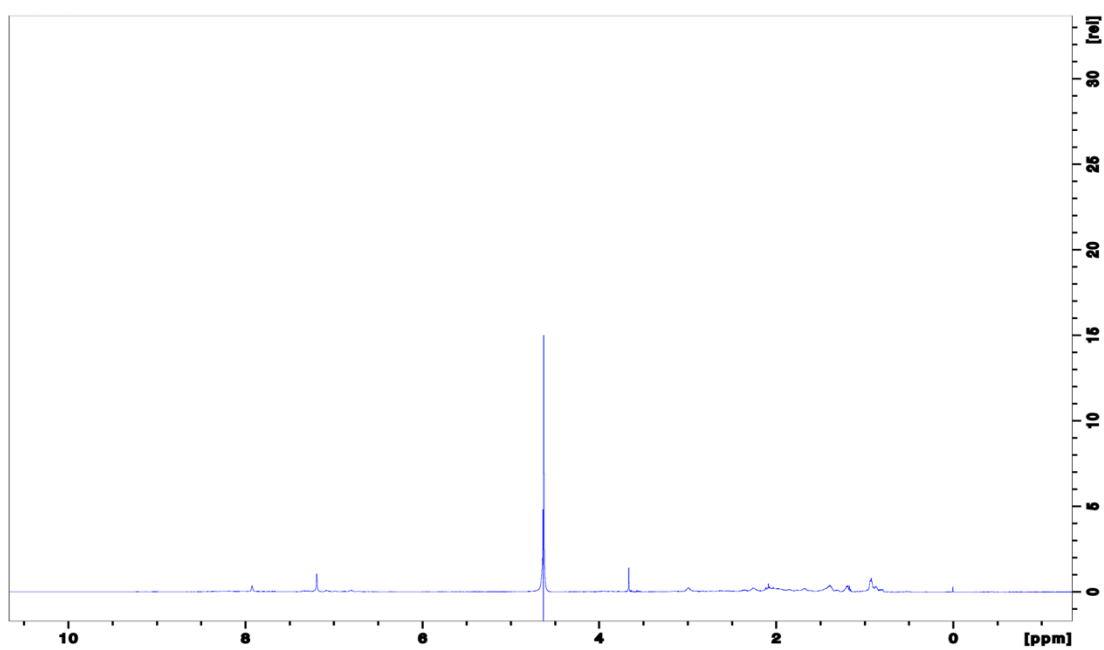


Figure S1) 1D<sup>1</sup>H with water suppression spectrum of 0.2 mM  $\alpha$ -synuclein at 25 °C and pH 7 on NMR 600 MHz.

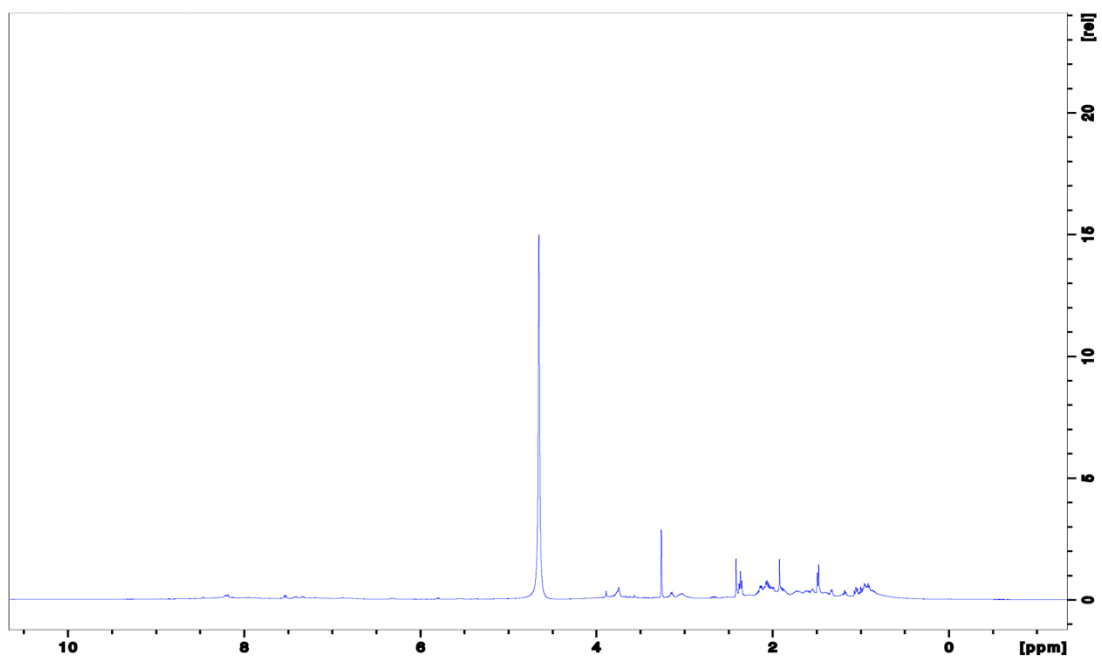


Figure S2) 1D<sup>1</sup>H with water suppression spectrum of 0.2 mM  $\alpha$ -synuclein in 200 mg/mL bacterial cell lysate at 25 °C and pH 7 on NMR 600 MHz.

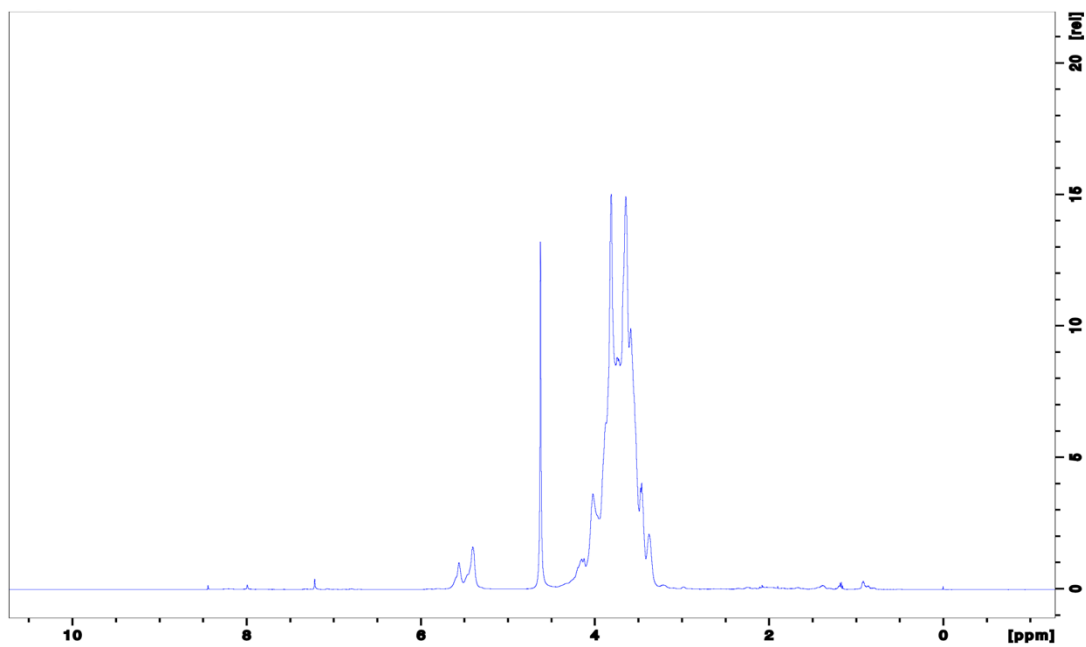


Figure S3) 1D<sup>1</sup>H with water suppression spectrum of 0.2 mM  $\alpha$ -synuclein in 200 mg/mL Ficoll70 at 25 °C and pH 7 on NMR 600 MHz.

Table S1) Characteristics of  $\alpha$ -synuclein sequence.

**1**MDVFMKGLSKAKEGVVAAAEEKTKQGVAEAAGKTKEGVLYVGSKTKEGVVHGVAATVAEKT**61**EQVTNVG  
 GAVVTGVTAVAQKTVEGAGSIAAATGFV**96**KKDQLGKNEEGAPQEGILEDMPVDPDNEAYEMPSEEGYQD  
 YEPEA**141**.

Region	Residue	Number	Hydrophobic residue	Negative residue	Positive residue	Polar residue	GRAVY index
N terminal (1-60)	G	8	32 residues (out of 60 amino acids) = 53%	7 residues (out of 60 amino acids)= 12%	12 residues (out of 60 amino acids) = 20%	9 residues (out of 60 amino acids) = 15%	-0.19
	L	2					
	M	2					
	A	9					
	V	10					
	K	11					
	E	6					
	Q	1					
	D	1					
	F	1					
	S	2					
	T	5					
	Y	1					
H	1						
NAC (61-95)	G	6	23 residues (out of 35 amino acids) = 66%	2 residues (out of 35 amino acids) = 6%	1 residues (out of 35 amino acids) = 3%	9 residues (out of 35 amino acids) = 26%	+0.85
	A	7					
	V	8					
	K	1					
	E	2					
	Q	2					
	F	1					
	S	1					
	T	5					
	I	1					
N	1						
C terminal (96-140)	G	4	18 residues (out of 45 amino acids) = 40%	15 residues (out of 45 amino acids) = 33%	3 residues (out of 45 amino acids) = 7%	9 residues (out of 45 amino acids) = 20%	-1.57
	L	2					
	M	2					
	A	3					
	V	1					
	K	3					
	E	10					
	Q	3					
	D	5					
	S	1					
	I	1					
	N	2					
	Y	3					
P	5						

## Appendix II

### BioRender's publication license

Figure S4) Publication permission for Figure 1.1.



49 Spadina Ave. Suite 200  
Toronto ON M5V 2J1 Canada  
www.biorender.com

### Confirmation of Publication and Licensing Rights

May 15th, 2023  
Science Suite Inc.

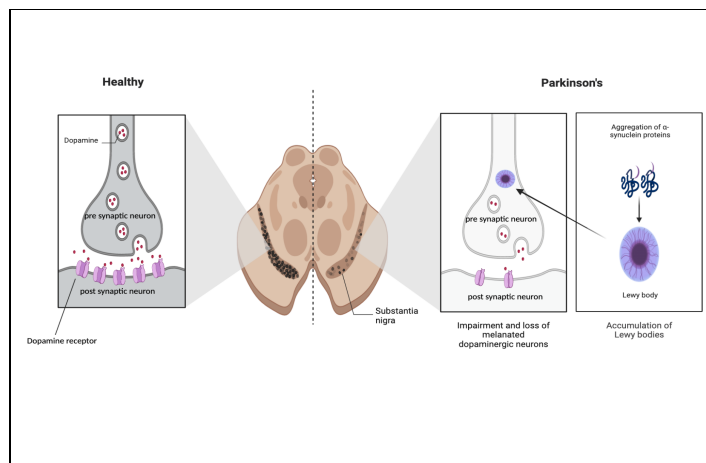
**Subscription:** Institution  
**Agreement number:** ND25DA9ZB7  
**Journal name:** M.Sc. Thesis

To whom this may concern,

This document is to confirm that Sina Heravi has been granted a license to use the BioRender content, including icons, templates and other original artwork, appearing in the attached completed graphic pursuant to BioRender's [Academic License Terms](#). This license permits BioRender content to be sublicensed for use in journal publications.

All rights and ownership of BioRender content are reserved by BioRender. All completed graphics must be accompanied by the following citation: "Created with BioRender.com".

BioRender content included in the completed graphic is not licensed for any commercial uses beyond publication in a journal. For any commercial use of this figure, users may, if allowed, recreate it in BioRender under an Industry BioRender Plan.



For any questions regarding this document, or other questions about publishing with BioRender refer to our [BioRender Publication Guide](#), or contact BioRender Support at [support@biorender.com](mailto:support@biorender.com).

Figure S5) Publication permission for Figure 1.2.



49 Spadina Ave. Suite 200  
Toronto ON M5V 2J1 Canada  
www.biorender.com

## Confirmation of Publication and Licensing Rights

May 16th, 2023  
Science Suite Inc.

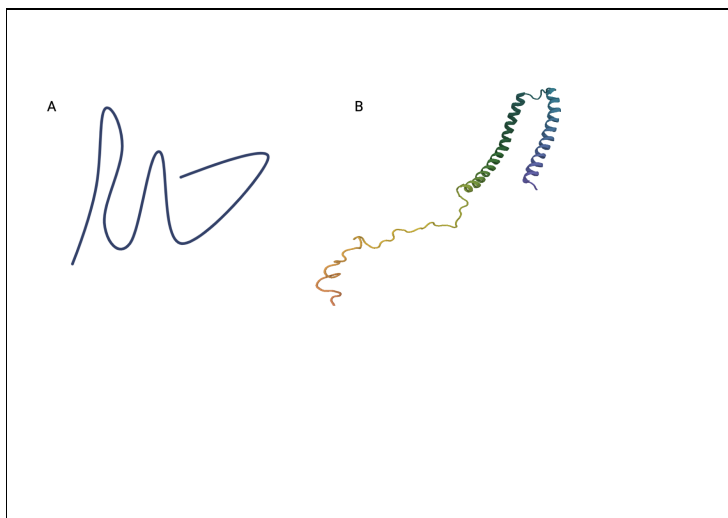
<b>Subscription:</b>	<i>Institution</i>
<b>Agreement number:</b>	<i>NV25DGROX6</i>
<b>Journal name:</b>	<i>Memorial University of Newfoundland, M.Sc. thesis</i>

To whom this may concern,

This document is to confirm that Sina Heravi has been granted a license to use the BioRender content, including icons, templates and other original artwork, appearing in the attached completed graphic pursuant to BioRender's [Academic License Terms](#). This license permits BioRender content to be sublicensed for use in journal publications.

All rights and ownership of BioRender content are reserved by BioRender. All completed graphics must be accompanied by the following citation: "Created with BioRender.com".

BioRender content included in the completed graphic is not licensed for any commercial uses beyond publication in a journal. For any commercial use of this figure, users may, if allowed, recreate it in BioRender under an Industry BioRender Plan.



For any questions regarding this document, or other questions about publishing with BioRender refer to our [BioRender Publication Guide](#), or contact BioRender Support at [support@biorender.com](mailto:support@biorender.com).

Figure S6) Publication permission for Figure 1.3.



49 Spadina Ave. Suite 200  
Toronto ON M5V 2J1 Canada  
www.biorender.com

## Confirmation of Publication and Licensing Rights

May 16th, 2023  
Science Suite Inc.

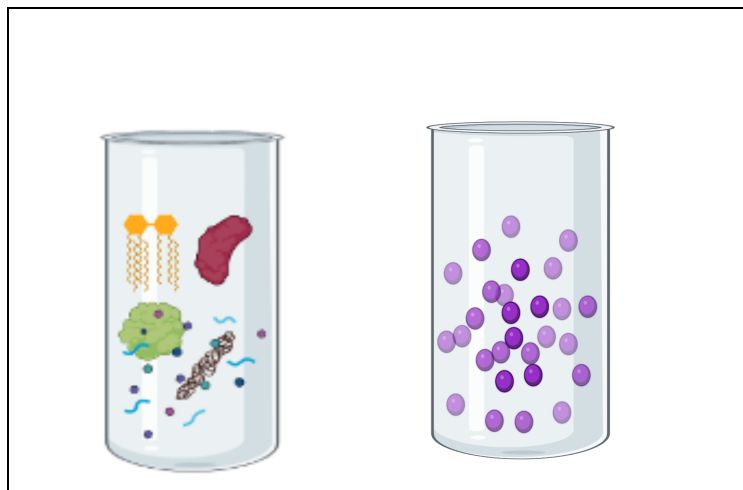
<b>Subscription:</b>	<i>Institution</i>
<b>Agreement number:</b>	<i>FR25DGFRHL</i>
<b>Journal name:</b>	<i>Memorial University of Newfoundland (M.Sc. thesis)</i>

To whom this may concern,

This document is to confirm that Sina Heravi has been granted a license to use the BioRender content, including icons, templates and other original artwork, appearing in the attached completed graphic pursuant to BioRender's [Academic License Terms](#). This license permits BioRender content to be sublicensed for use in journal publications.

All rights and ownership of BioRender content are reserved by BioRender. All completed graphics must be accompanied by the following citation: "Created with BioRender.com".

BioRender content included in the completed graphic is not licensed for any commercial uses beyond publication in a journal. For any commercial use of this figure, users may, if allowed, recreate it in BioRender under an Industry BioRender Plan.



For any questions regarding this document, or other questions about publishing with BioRender refer to our [BioRender Publication Guide](#), or contact BioRender Support at [support@biorender.com](mailto:support@biorender.com).

Figure S7) Publication permission for Figure 1.4.



49 Spadina Ave. Suite 200  
Toronto ON M5V 2J1 Canada  
www.biorender.com

## Confirmation of Publication and Licensing Rights

May 16th, 2023  
Science Suite Inc.

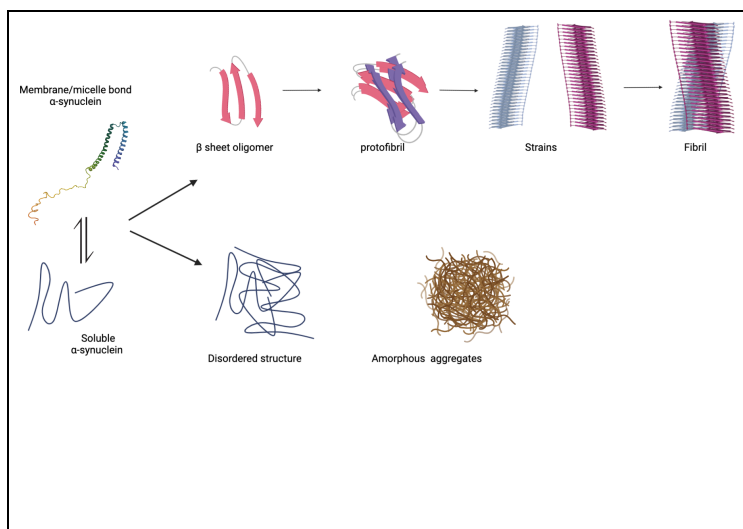
**Subscription:** *Institution*  
**Agreement number:** *VX25DGS44C*  
**Journal name:** *Memorial University of Newfoundland, M.Sc. thesis*

To whom this may concern,

This document is to confirm that Sina Heravi has been granted a license to use the BioRender content, including icons, templates and other original artwork, appearing in the attached completed graphic pursuant to BioRender's [Academic License Terms](#). This license permits BioRender content to be sublicensed for use in journal publications.

All rights and ownership of BioRender content are reserved by BioRender. All completed graphics must be accompanied by the following citation: "Created with BioRender.com".

BioRender content included in the completed graphic is not licensed for any commercial uses beyond publication in a journal. For any commercial use of this figure, users may, if allowed, recreate it in BioRender under an Industry BioRender Plan.



For any questions regarding this document, or other questions about publishing with BioRender refer to our [BioRender Publication Guide](#), or contact BioRender Support at [support@biorender.com](mailto:support@biorender.com).